



Title	Metal Porphyrinoids Having Reaction Scaffolds toward Methyl-coenzyme M Reductase Models and an Active Metal Template System for Rotaxane
Author(s)	宮崎, 雄大
Citation	大阪大学, 2020, 博士論文
Version Type	VoR
URL	<a href="https://doi.org/10.18910/76522">https://doi.org/10.18910/76522</a>
rights	
Note	

*The University of Osaka Institutional Knowledge Archive : OUKA*

<https://ir.library.osaka-u.ac.jp/>

The University of Osaka

Doctoral Dissertation

**Metal Porphyrinoids Having Reaction Scaffolds  
toward Methyl-coenzyme M Reductase Models  
and an Active Metal Template System for Rotaxane**

(金属ポルフィリノイドとその周辺の反応場を有したメチル補酵素 M 還元酵素モデル  
およびロタキサンアクティブメタルテンプレートシステムの構築)

January 2020

Yuta Miyazaki

Graduate School of Engineering,  
Osaka University



# Contents

<b>General Introduction</b>	1
<b>Chapter 1</b>	
<i>Methane generation from an external methyl donor using reconstituted myoglobin with nickel tetrahydrocorrin</i>	
1-1. Introduction	18
1-2. Results and discussion	19
1-3. Summary	27
1-4. Experimental section	28
Reference and notes	35
<b>Chapter 2</b>	
<i>Methane generation via intraprotein C–S bond cleavage in reconstituted cytochrome <math>b_{562}</math> with nickel didehydrocorrin</i>	
2-1. Introduction	37
2-2. Results and discussion	39
2-3. Summary	45
2-4. Experimental section	46
Reference and notes	51
<b>Chapter 3</b>	
<i>Synthesis of rotaxane using the ditopic strapped porphyrin based on the active metal template method</i>	
3-1. Introduction	54
3-2. Results and discussion	55
3-3. Summary	61
3-4. Experimental section	62
Reference and notes	71
<b>Conclusion</b>	73
<b>Acknowledgements</b>	76

## General introduction

### Metal porphyrinoid

A large number of important physiological events are performed by tetrapyrrole compounds, including porphyrins and their structural analogues called porphyrinoids. Porphyrin, an  $18\pi$ -conjugated tetrapyrrole compound, works as a dianionic ligand for a metal center (Fig. 1a). Heme, iron protoporphyrin IX, is an abundant and well-known porphyrin metal complex in nature, widely involved in ranging from oxygen transfer, storage, and activation to electron transfer.<sup>1</sup> Corrin and hydrocorphine, representative examples of porphyrinoid found in nature, have highly saturated tetrapyrrole frameworks which act as monoanionic ligands for metal centers. The corrin framework which has a directly connected structure at the C1- and C19-positions provides a cobalt complex, cobalamin, performing transmethylation and radical rearrangement reaction (Fig. 1b).<sup>2</sup> F430, a nickel hydrocorphine complex, is responsible for biological methane generation and degradation (Fig. 1c).<sup>3</sup> Thus, metal porphyrinoids play key roles of active centers showing unique properties and reactivities to achieve important physiological events.

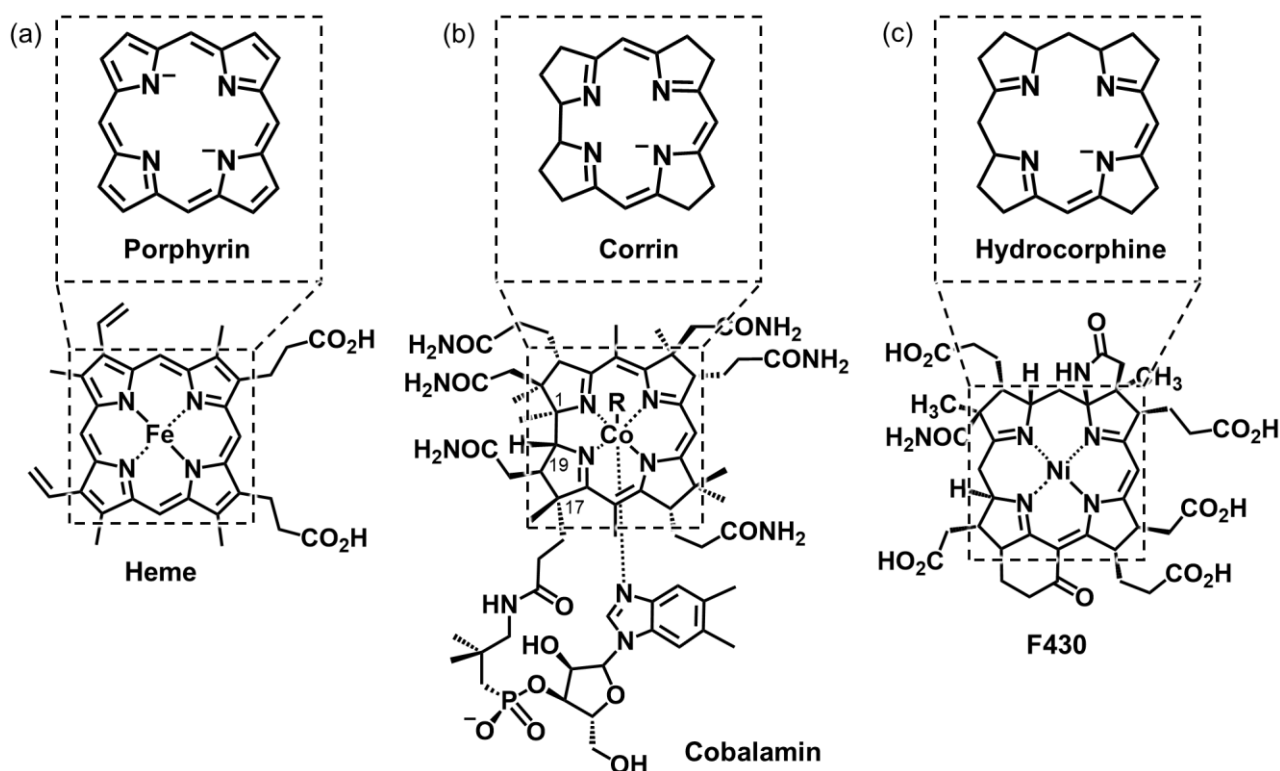


**Figure 1.** Chemical structures of (a) heme having a porphyrin framework, (b) cobalamin having a corrin framework, and (c) F430 having a hydrocorphine framework.

### Metalloprotein containing metal porphyrinoid

A metal porphyrinoid is incorporated into an appropriate cofactor binding site in a protein matrix to form a metalloprotein, performing physiological events (Fig. 2a). Representative metalloproteins containing metal porphyrinoids are shown in Fig. 2b-d.

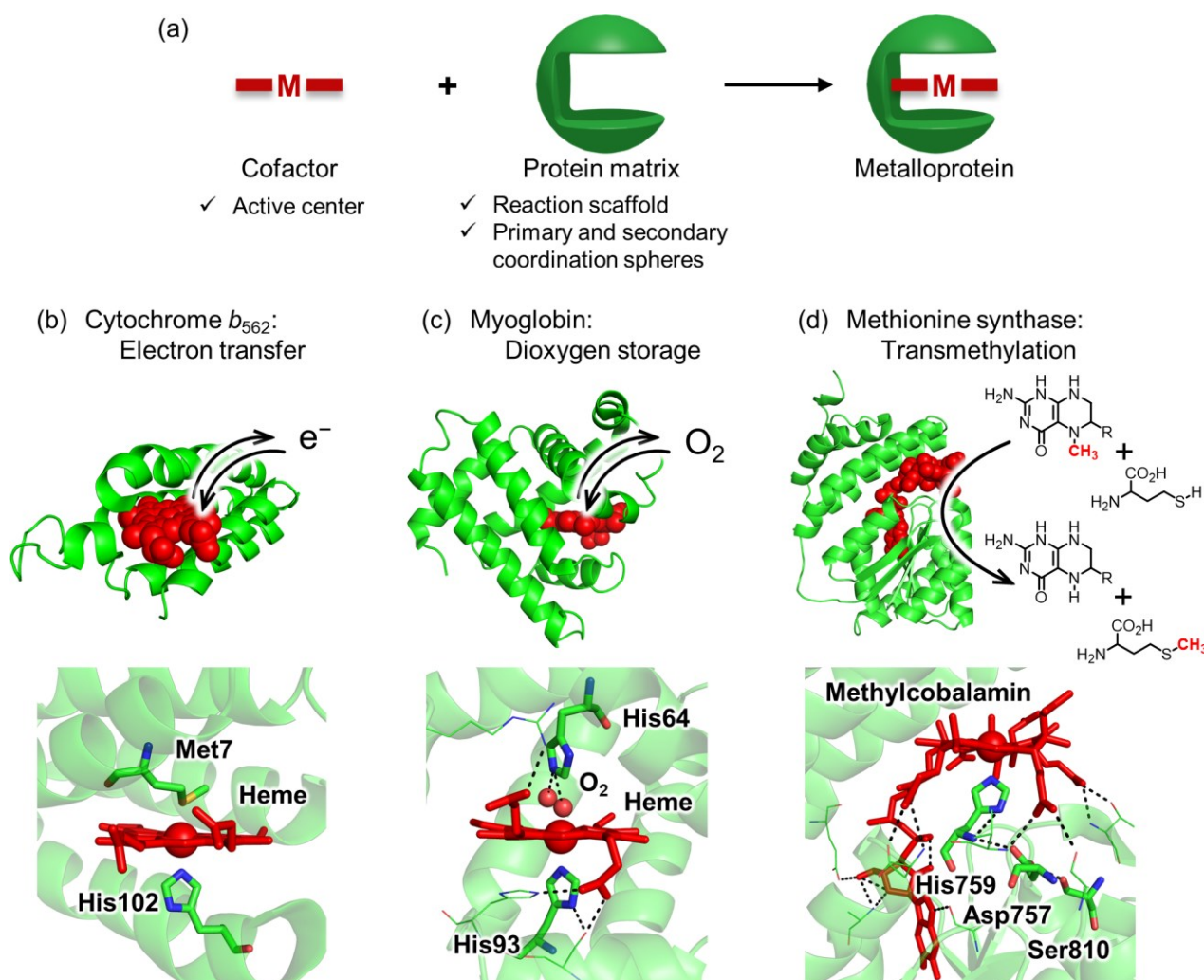


**Figure 2.** (a) Schematic representation of components of metalloprotein and their roles. Crystal structures and functions of (b) cytochrome  $b_{562}$  (PDB ID: 1QPU), (c) myoglobin (PDB ID: 1MBN), and (d) cofactor binding domain of methionine synthase (PDB ID: 1BMT). Black dashed line shows hydrogen bonding interaction.

Cytochrome  $b_{562}$  (Cyt  $b_{562}$ ), one of the hemoproteins responsible for electron transfer in *E. coli*, contains a heme cofactor and 106 amino acid residues, forming a four-helix bundle structure (Fig. 2b). Iron center of heme has a hexa-coordinated structure with His102 and Met7, resulting in a high binding affinity (ca.  $10^8 \text{ M}^{-1}$ ) and stability against heating, pH shift, and chemical treatment.<sup>4</sup> The relationship between redox property for the  $\text{Fe}^{\text{III}}/\text{Fe}^{\text{II}}$  process and amino acid residues surrounding active center has been investigated using mutagenesis technique. For instance, the bis-methionine ligating Cyt  $b_{562}$  mutant including the substitution of His102 with Met102 was found to show a positively shifted redox potential at 0.24 V vs. the normal hydrogen electrode (NHE) compared to that of native Cyt  $b_{562}$  at 0.17 V, whereas the bis-histidine ligating Cyt  $b_{562}$  mutant including the substitution of Met7 with His7 showed a negatively shifted potential at  $-0.07 \text{ V}$ .<sup>5</sup> In addition, mutations in peripherally existing and non-coordinating residues can adjust the redox potentials ranging from 0 V to 0.17 V.<sup>6</sup> These results indicate properly surrounding environment of the active center is essential for determination of the redox potential and the efficient electron transfer.

Myoglobin (Mb), a hemoprotein responsible for oxygen binding in muscle tissue, is composed with a heme

cofactor and 153 amino acid residues to form a globular structure with eight  $\alpha$ -helices (Fig. 2c).<sup>7</sup> Binding affinity of heme for apoMb is ca.  $10^{14} \text{ M}^{-1}$  in the case of sperm whale Mb contributed by coordination, hydrophobic interaction, and salt bridge between heme and the protein matrix.<sup>8</sup> In general, Mb reversibly takes a penta-coordinated structure with proximal His93 in deoxy-form and a hexa-coordinated structure with dioxygen and proximal His93 in oxy-form upon binding of dioxygen with binding affinity of ca.  $10^6 \text{ M}^{-1}$ . The bound dioxygen in oxy-form is stabilized by hydrogen bonding interaction with distal His64 as supported with the fact that substitution of His64 with other apolar amino acid residues dramatically decrease affinity.<sup>7</sup> Moreover, proximal His93 also contributes to decreasing dissociation rate of dioxygen because electron-donating histidine ligation stabilizes the  $\text{Fe(III)-O}_2^-$  state, charge separation species, according to model studies.<sup>9</sup>

Methionine synthase, one of the cobalamin-dependent enzymes, is composed of four distinct domains and it catalyzes transmethylation from *N*-methyltetrahydrofolate to homocysteine producing methionine and tetrahydrofolate in Prokaryota and Eukaryota (Fig. 2d). Each domain has specific binding site for cobalamin, *N*-methyltetrahydrofolate, and homocysteine, respectively. Cobalt center of the cobalamin has a penta-coordinated structure with His759 in the resting state containing a Co(II) species. In this mode, 6,7-dimethoxybenzimidazole moiety, peripherally-attached substituent at the C17-position, is bound in an extended conformation by salt bridge and multiple hydrogen bonding interactions. Investigation of the reaction mechanism revealed the two-step reaction. At first, a highly nucleophilic Co(I) species is methylated by the reaction with *N*-methyltetrahydrofolate to produce methylcobalamin, a methylated Co(III) species, and tetrahydrofolate. Then, methylcobalamin transfers the methyl group to homocysteine to afford a Co(I) species and methionine. The first and second steps proceed 35-million-fold and 6-million-fold faster, respectively, than those with model reactions using the cobalamin complex without the protein matrix.<sup>10</sup> Moreover, the catalytic cycle is supposed to be assisted by three conserved amino acid residues, His759, Ser810, and Asp757 by modulating the protonation of His759, resulting in control of the histidine ligation to cobalt center.<sup>11</sup>

In all cases, cofactors have specifically coordinated structures with axial amino acid residues. Additionally, amino acid residues surrounding cofactors are interacted with external substrate and/or cofactor by noncovalent fashions to keep each component at precise arrangement and modulate physicochemical properties and reactivities for sophisticated functions. In other words, protein matrices provide axial ligands and specific secondary coordination spheres as “reaction scaffolds” to active centers, resulting in regulation and expansion of functions expressed by metal porphyrinoids.

## **Synthetic and biological approaches for construction of reaction scaffolds**

In order to reproduce a reaction scaffold provided by a protein matrix and to apply various functions of metalloproteins to artificial systems, synthetic and biological approaches have been investigated. In principle, a three-dimensional substituent has been introduced to a metal porphyrinoid to generate a reaction scaffold on a porphyrinoid plane in synthetic approach. The property of reaction scaffold can be finely tuned by changing the functional group of substituent. For instance, noncovalent interactions such as ionic, hydrogen bonding, and hydrophobic interactions between a substituent and a substrate provide an appropriate access of substrate. At the beginning of investigation,

Collman and coworkers reported dioxygen binding property of picket-fence iron porphyrin as a synthetic model of myoglobin and hemoglobin (Fig. 3a).<sup>12</sup> Moreover, effects of substituents, capable of hydrogen bonding interactions, for dioxygen binding affinity and stability of oxygenated-state were evaluated.<sup>13</sup> Subsequently, a series of picket-fence metal porphyrins have been investigated as hemoprotein models and demonstrated binding of CO,<sup>12b</sup> NO/NO<sub>x</sub>,<sup>14</sup> and HS<sup>-</sup><sup>15</sup> with an iron center as seen in native hemoproteins. Metal porphyrins have also been found to catalyze widely important chemical transformations as well: direct C–H or C=C bond functionalization with metalloporphyrin-catalyzing carbene-, nitren-, and oxene-insertion reactions to synthesize natural product intermediates and pharmaceuticals. However, these purposes require high stereoselective reactions.<sup>16</sup> A metal porphyrin having three-dimensional substituent is a promising catalyst to achieve an asymmetric reaction because their substituent can regulate the orientation of substrates. In this context, various researchers have attempted metalloporphyrinoids-catalyzing asymmetric cyclopropanation of an olefin molecule with a diazoacetate reagent, a carbene source, to evaluate the reaction stereoselectivity because the product has two stereocenters.<sup>17-19</sup> Especially, highly diastereo- and enantioselective cyclopropanation of styrene with ethyl diazoacetate was achieved by Zhang and coworkers by introduction of a substituent having a chiral moiety to cobalt porphyrin (Fig. 3b).<sup>20</sup> In contrast to synthetic approach, biological approach has been investigated to directly employ a specific environment in a protein matrix as a reaction scaffold. Several groups have investigated conjugates of metal porphyrinoids with protein matrices as artificial metalloproteins and artificial metalloenzymes to achieve both of enhanced biological functions and abiological reactivities.<sup>21-25</sup> In particular, heme proteins such as cytochrome P450 and myoglobin have been engineered by conjugation with abiological metal porphyrinoid as an artificial cofactor instead of natural cofactor heme<sup>26</sup> or modification of a protein matrices providing appropriate reaction scaffolds by site directed mutagenesis,<sup>27</sup> directed evolution,<sup>28</sup> and introduction of unnatural amino acid residue.<sup>25</sup> For instance, Hayashi, Hisaeda, and coworkers reported 1,400-fold higher oxygen affinity of myoglobin reconstituted with iron porphycene than that of native myoglobin (Fig. 3c).<sup>29</sup> Hartwig and coworkers demonstrated significantly high activity for an abiological cyclopropanation of styrene with ethyl diazoacetate using reconstituted myoglobin or cytochrome P450 with iridium protoporphyrin IX (Fig. 3d).<sup>30</sup> They performed gradual increase of stereoselectivity by introduction of mutations. Several other groups also reported the cyclopropanation reactions using modified metal porphyrinoids or mutated protein matrices.<sup>31-33</sup> Taken together, construction of an artificial reaction scaffold for metal porphyrinoid by synthetic and biological approaches is expected to be a promising method to expand functions of metal porphyrinoids.

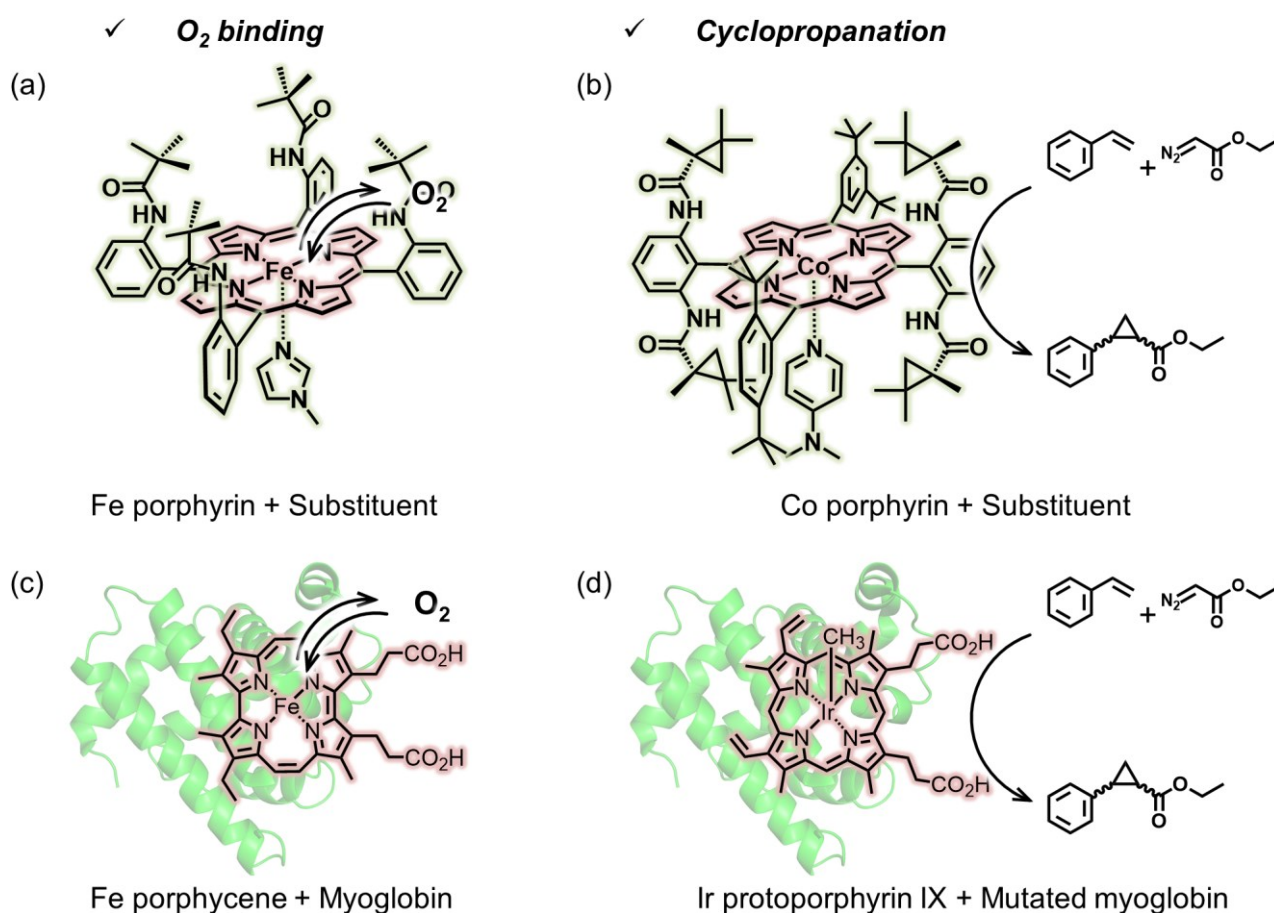


**Figure 3.** Chemical structures of modified metal porphyrinoids and functions achieved by (a), (b) the metal porphyrinoids and (c), (d) myoglobin reconstituted with the metal porphyrinoids.

### Methyl-coenzyme M reductase

Methane is the simplest hydrocarbon and it has been investigated as a greenhouse gas and alternative fuel. Most of the methane in nature is produced from H<sub>2</sub>/CO<sub>2</sub>, acetate, methylamines, and methanol by methanogens under anaerobic conditions.<sup>34</sup> Generated methane is biologically oxidized by methanotrophs. Aerobic bacteria containing two different types of methane monooxygenase (MMO), the iron enzyme sMMO and the copper enzyme pMMO, convert methane with dioxygen to carbon dioxide under aerobic conditions.<sup>35</sup> Methanotrophic archaea proceed anaerobic methane oxidation, also called reverse methanogenesis, under anaerobic conditions because the conversion of methane to carbon dioxide appears to follow the opposite enzymatic pathway of methane generation in methanogens.<sup>36</sup>

Methyl-coenzyme M reductase (MCR), which is composed of three different subunits McrA (ca. 65 kDa), McrB (ca. 45 kDa), and McrG (ca. 35 kDa) in an (αβγ)<sub>2</sub> heterohexamer, is the key enzyme in an anaerobic methane formation by methanogens and anaerobic methane oxidation by methanotrophs.<sup>3,37-39</sup> MCR was discovered in *Methanothermobacter thermoautotrophicus* by Wolfe and coworkers in 1970s.<sup>40</sup> Two F430 molecules as cofactors are involved in active centers of MCR and catalyze the reaction of methyl-coenzyme M (CH<sub>3</sub>S-CoM) with coenzyme B (HS-CoB) to produce methane and heterodisulfide (CoM-S-S-CoB) (Fig. 4). The first MCR structure was

obtained from *M. Marburgensis* containing an inactivated state of MCR and shows that F430 is located at the bottom of a funnel-shaped and substrate binding channel. F430 is also coordinated by side chain oxygen atom of Gln147 and thiolate moiety of coenzyme M in the proximal and distal sides of the hydrophobic binding cavity, respectively.<sup>41</sup> Subsequent crystal structures were found to show inactivated states containing product or substrate analogues.<sup>42-44</sup> Moreover, Shima and coworkers reported the crystal structure showing the methyl–Ni(III) state upon addition of methyl iodide to the conjugate of an active state of MCR and substrate analogues.<sup>45</sup> Furthermore, it is known that five post-translationally modified amino acids such as 1-*N*-methylhistidine ( $\alpha$ 257), 5-methylarginine ( $\alpha$ 271), 2-methylglutamine ( $\alpha$ 400), *S*-methylcysteine ( $\alpha$ 452), and thioglycine ( $\alpha$ 445) are contained within the substrate binding channel.<sup>41</sup> In all crystal structures, F430 and substrates or products are precisely located within the protein matrix by noncovalent interactions (e.g. hydrogen bonding and hydrophobic interactions and salt bridge).

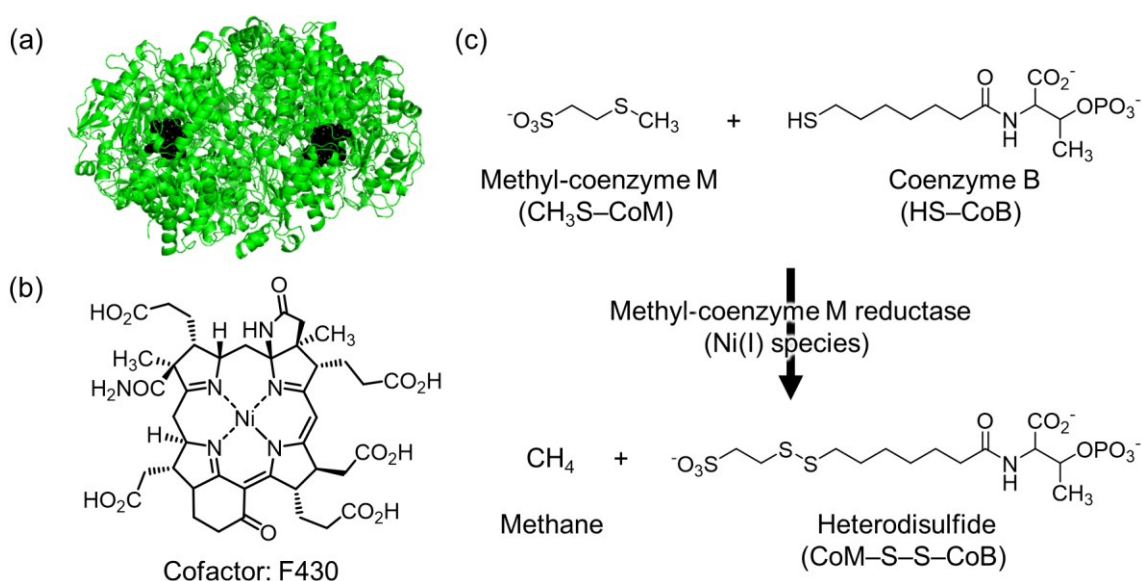


**Figure 4.** (a) Structure of methyl-coenzyme M reductase (PDB ID: 1MRO). (b) Chemical structure of F430. (c) Methane generation catalyzed by methyl-coenzyme M reductase in methanogenic archaea.

F430 was isolated as a nickel-containing and non-fluorescent compound in 1980.<sup>46,47</sup> Pentamethylester of F430, F430M, has often been employed to evaluate physicochemical properties and reactivities because of the solubility and stability. The Ni(II) form without protein matrix shows yellow color with absorption maxima at 274 nm and 430 nm, whereas the Ni(I) state shows green color with absorption maxima at 383 nm and 759 nm. The structure of F430 was revealed using NMR and X-ray crystal structural analysis in 1991.<sup>48</sup> Now, F430 is only known as a natural metal porphyrinoid that binds nickel ion and has the most reduced tetrapyrrole framework called hydrocorphine. This highly saturated framework represents the yellow color compared to the red color of porphyrin. The redox potential corresponding to the Ni<sup>II</sup>/Ni<sup>I</sup> process of F430M was determined to be  $-0.65$  V vs. NHE in a basic buffer<sup>49</sup> and  $-0.50$  V in dimethylformamide,<sup>50</sup> whereas the redox potential due to the Ni<sup>III</sup>/Ni<sup>II</sup> process was determined to be  $1.45$  V in acetonitrile.<sup>51</sup> The redox potentials of F430 bound in MCR have not been determined and expected to have lower potentials compared to those of the free F430 cofactor. Oxidation state of nickel in F430M is analyzed particularly by EPR spectroscopic measurements: EPR-active Ni(I) and Ni(III) states and EPR-silent Ni(II) state.

Ni(I) species of F430M generated by the electrochemical<sup>52</sup> or chemical reduction by NaHg in tetrahydrofuran<sup>50</sup> and Ti(III) citrate in a buffer under a basic condition<sup>49</sup> show axial EPR spectra ( $g_{\perp} = 2.065, 2.074$  and  $g_{\parallel} = 2.25$ ) with superhyperfine splitting due to the coupling with nitrogen atoms of tetrapyrrole.<sup>52</sup> The spectra with  $g_{\perp} < g_{\parallel}$  indicates  $d^9$  metal complexes ( $S = 1/2$ ) with a predominant  $d_{x^2-y^2}$  configuration of the nickel ion orbital. Ni(III) state of F430M was also electrochemically prepared to give axial EPR spectrum ( $g_{\perp} = 2.211$  and  $g_{\parallel} = 2.020$ ), showing a predominant  $d_z^2$  configuration of the nickel ion.<sup>51</sup> Because EPR spectrum reflects not only the electronic state of metal center but also the geometry of metal complex, MCR is divided into several states, resulting in active  $MCR_{red1}$  and active  $MCR_{red2}$  with Ni(I) species, inactive  $MCR_{silent}$  and  $MCR_{ox1-silent}$  with Ni(II) species, and  $MCR_{ox1}$  with Ni(III) species.<sup>3c</sup>

## Reaction mechanisms of MCR

According to the mechanistic studies, representative mechanisms including three different intermediates of methyl–Ni(III) species (mechanism I), methyl radical (mechanism II), and methyl anion (mechanism III) are shown in Fig. 5. Mechanism I proposes that nucleophilic attack of Ni(I) species to the methyl group of methyl-coenzyme M in an  $S_N2$ -type manner generates methyl–Ni(III) intermediate at first step (Fig. 5a). Electron transfer from coenzyme M to the methyl–Ni(III) yields the methyl–Ni(II) and coenzyme M radical species, followed by the formation of methane. Finally, disulfide anion radical generated by the reaction of coenzyme B thiolate and coenzyme M thyl radical provides one electron to the Ni(II) species to yield the original Ni(I) species and disulfide compound. This mechanism is based on the mechanistic studies using F430 model complexes<sup>53-56</sup> and mechanistic and crystallographic studies on the active Ni(I) enzyme with activated alkyl reagents including alkyl halides that show generation of alkyl–Ni(III) species.<sup>41,43,45,55,57-61</sup> In mechanism II, Ni(I) species promotes the homolytic cleavage of the C–S bond of methyl-coenzyme M to form transient methyl radical and Ni(II)–thiolate intermediate (Fig. 5b). Then, methyl radical abstracts the hydrogen atom from coenzyme B, followed by the generation of methane and coenzyme B thyl radical. Finally, the coenzyme B thyl radical reacts with the Ni(II)–thiolate intermediate to generate the Ni(II)–disulfide anion radical intermediate, transferring one electron to form the original Ni(I) species and disulfide compound. This mechanism is based on the calculation studies using density functional theory<sup>62</sup> and mechanistic studies using single turnover reaction of the active Ni(I) enzyme with natural substrate analogues.<sup>63</sup> Mechanism III is similar to the mechanism II: Ni(I) species attacks to the sulfur atom of methyl-coenzyme M to directly generate methyl anion as a transient intermediate and Ni(III)–thiolate intermediate (Fig. 5c). Then, methyl anion accepts the proton from coenzyme B to accomplish the generation of methane. Electron transfer from coenzyme B thiolate to the Ni(III)–thiolate intermediate generates the Ni(II)–disulfide anion radical intermediate in two steps. Transferring one electron to the Ni(II) center affords the original Ni(I) species and disulfide compound. However, generation of important intermediates, methyl–Ni(III) species (mechanism I), methyl radical (mechanism II), and methyl anion (mechanism III), are predominantly expected based on spectroscopic analyses under specific conditions. Therefore, the details of the active center and the reaction mechanism have not been completely elucidated.

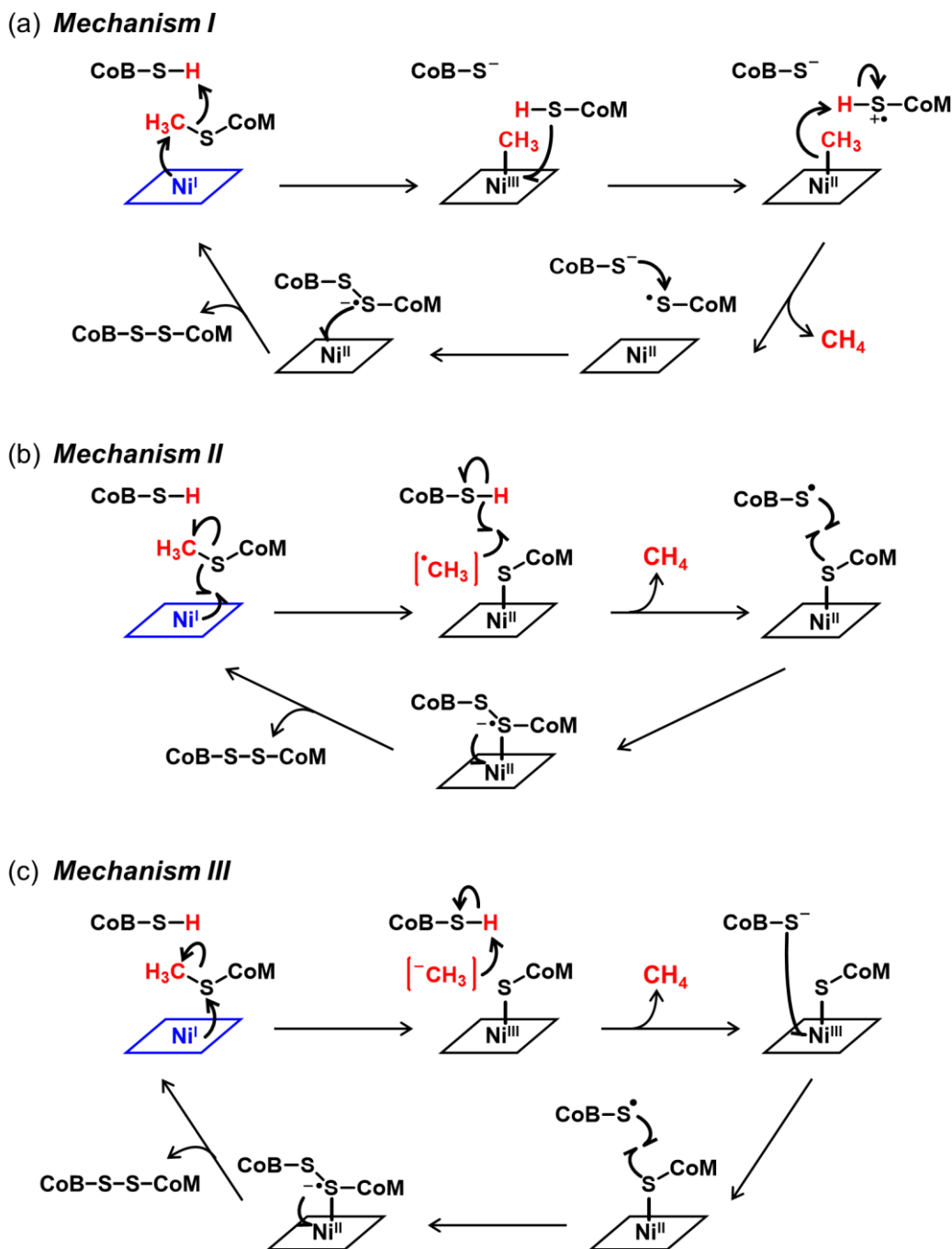


**Figure 5.** Representative reaction mechanisms of methane generation through (a) methyl-nickel intermediate, (b) methyl radical intermediate, and (c) methyl anion intermediate.

## Model studies of MCR

To elucidate the reaction mechanism of MCR, various F430 model complexes have been investigated.<sup>53-55,64-66</sup> Stolzenberg and coworkers reported nickel(II) octaethylisobacteriochlorin as a model complex of F430 and stoichiometric methane generation from methyl iodide in organic solvent upon reduction of Ni(II) species with NaHg (Fig. 6a).<sup>53</sup> They also examined various reduction and dehalogenation of alkyl or aryl halides using the model

complex.<sup>54</sup> Meyerstein and coworkers employed nickel(II) tetramethylcyclam or F430M and demonstrated the formation and isolation of methyl–Ni(II) products which show the specific peaks of methyl group in NMR spectra upon addition of dimethylmagnesium in organic solvent (Fig. 6b).<sup>55</sup> Moreover, they firstly performed methane generation (~10% yield) from methyl-coenzyme M in an aqueous solution upon reduction of nickel(II) decamethylcyclam or nickel(II) 1,3,6,10,12,15-hexaazatricyclo[13.3.1.1]eicosane by radiolysis (Fig. 6c).<sup>56</sup> Meanwhile, the reaction mechanism containing the activation of the C–S bond in methyl-coenzyme M by the reaction with a thiyl radical and formation of a sulfuranyl intermediate followed by methyl transfer to give a methyl-Ni(II) or a Ni(III) intermediate was suggested in an early mechanistic studies.<sup>51,67,68</sup> Pfaltz and coworkers examined the reaction mechanism using Ni(II) complex with a thiolate-thioether ligand, bis{1-[2-(methylthio)ethyl]cyclohexanethiolato}nickel, and demonstrated the methane formation (~50% yield) upon photoirradiation in the presence of a thiol-thioether substrate, 1-[2-(methylthio)ethyl]cyclohexanethiol, showing the formation of a sulfuranyl intermediate and cleavage of the C–S bond. However, Ni(I) species could not be identified and the reaction mechanism is unclear (Fig.6d).<sup>64</sup> Recently, Tatsumi and coworkers have reported series of F430 model complexes using azacyclam ligands having H<sub>3</sub>C–S moieties. They revealed crystal structures of Ni(I) species and demonstrated methane generation *via* intramolecular cleavage of the C–S bond (Fig. 6e).<sup>65</sup> Moreover, Zelder and coworkers achieved the synthesis of a cobalamin-based F430 model complex which has a modified and reduced corrin framework, showing similar physicochemical properties to F430 (Fig. 6f).<sup>66</sup>

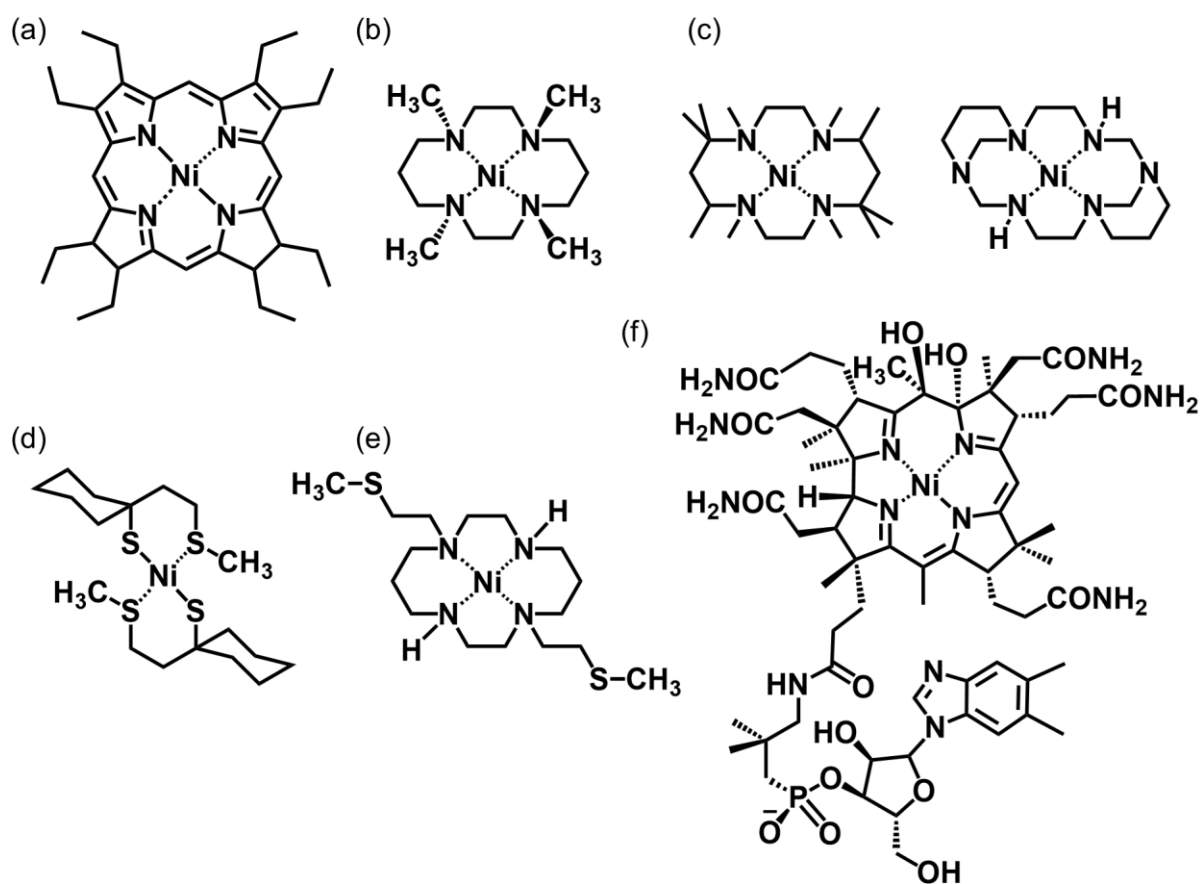


**Figure 6.** Chemical structures of F430 model complexes reported by (a) Stolzenberg,<sup>53,54</sup> (b) and (c) Meyerstein,<sup>55,56</sup> (d) Pfaltz,<sup>64</sup> (e) Tatsumi,<sup>65</sup> and (f) Zelder.<sup>66</sup>

Although various model complexes have achieved methane generation from external methyl donor or *via* the C–S bond cleavage of the ligands and provide essential insights into understanding the enzymatic reaction mechanism, reaction conditions are completely different compared to that for the native enzyme. Moreover, there is no functional model featuring the protein matrix of the enzyme. In this context, a functional model which combines a model complex and an important factor of the protein matrix of the enzyme should be promising for elucidation of the reaction mechanism and the effect of the protein matrix in the enzymatic reaction.

### **Active metal template method for mechanically interlocked compound**

Interlocked molecules such as catenanes and rotaxanes having mechanical bond have been synthesized on the investigation toward the construction of complexed architectures.<sup>69</sup> The first example of catenane was obtained by Wasserman and coworkers in 1960 with the statistical synthesis (~ 1% yield).<sup>70</sup> After that, Schill, Luttringhaus, and coworkers employed a covalently templated precursor to synthesize a catenane in high yield through 22-step synthesis in total.<sup>71</sup> Although these results suffered from low yield or multi-step synthesis, they have been bases for construction of mechanically interlocked molecules. An efficient synthetic approach “metal template method” was reported by Sauvage and coworkers in 1983. They employed Cu(I) ion as a template to assemble simple molecular units followed by the reaction with other molecules to complete an interlocked structure.<sup>72</sup> Introduction of a transition metal ion for orienting and forming a molecular assembly demonstrates applicability to employ noncovalent interactions for the formation of interlocked molecules. Subsequently, efficient synthesis of an interlocked molecule employing noncovalent interaction was reported by Stoddart and coworkers using electron deficient and electron rich  $\pi$ - $\pi$  interaction.<sup>73</sup> The same strategy was shown by Leigh and coworkers using hydrogen bonding interaction.<sup>74</sup> These efficient syntheses of interlocked molecules opened the door for wide range of applications including “molecular machine”.

Rotaxane synthesis based on the metal template method is classified in two different approaches “Stoppering” and “Clipping” (Fig. 7a). The former utilizes the reaction of an assembly including a metal ion, a macrocyclic molecule, and a thread molecule with stoppering molecules to produce a rotaxane structure. The latter employs the reaction of an assembly including a metal ion, a dumbbell molecule, and a part of macrocyclic molecule with the other part of a macrocyclic molecule to generate a rotaxane structure. In 2006, Leigh and coworkers reported “Active metal template method” based on the metal template method to fully utilize ability of metal ion including catalytic performance.<sup>75</sup> They used a macrocyclic molecule containing a pyridine moiety and achieved efficient rotaxane synthesis through formation of a molecular assembly with Cu(I) ion, alkyne, and azide units followed by azide–alkyne Huisgen cycloaddition, so called copper-catalysed azide–alkyne cycloaddition or click reaction. Goldup and coworkers also demonstrated rotaxane synthesis in extremely high yield using a macrocycle containing a bipyridine ligand for click reaction system.<sup>76</sup> Thus, a metal ion promotes not only an assembly of molecular units but also efficient formation of mechanical bond in the active template method (Fig. 7b). This new concept overcomes synthetic difficulties of interlocked molecules as seen with original metal template method and provides rapid access to highly complexed architectures.

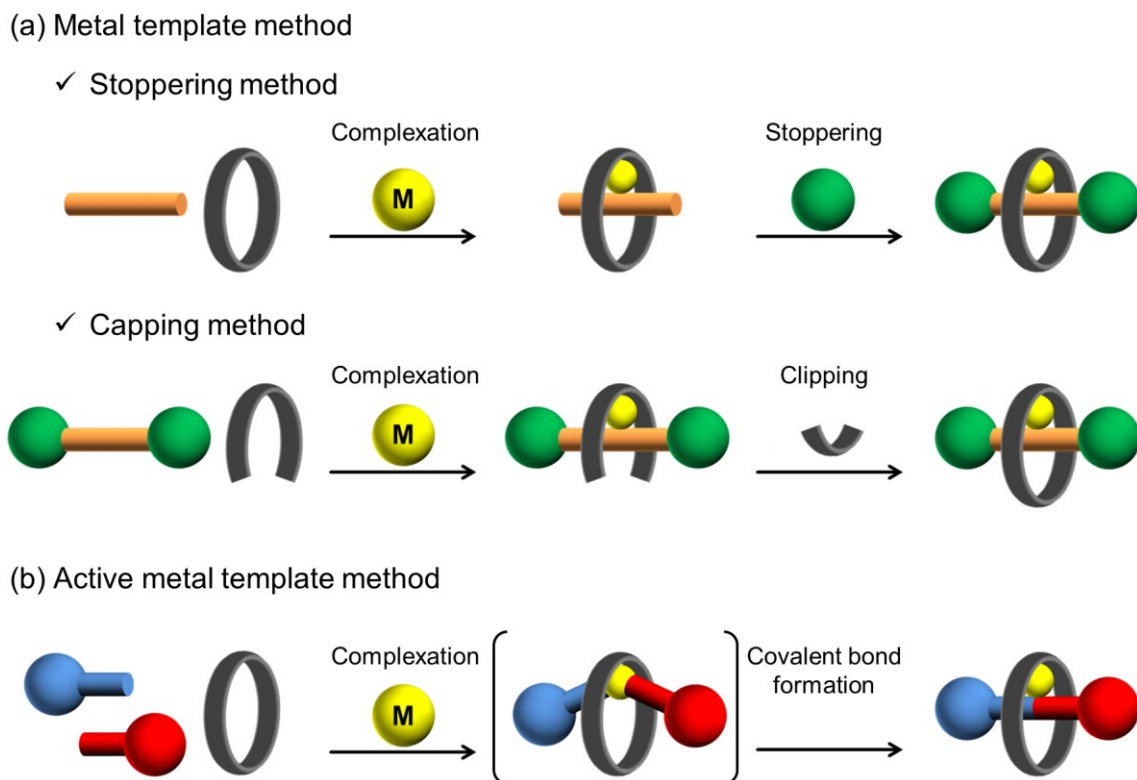


**Figure 7.** Schematic representation of (a) the metal template method by stoppering or clipping approaches and (b) the active metal template method for synthesis of rotaxane.

## Strapped porphyrin

Metal porphyrins bearing three-dimensional substituents such as strap,<sup>77</sup> cap,<sup>78</sup> and basket-handle<sup>79</sup> which cover one or both faces of porphyrin plane have been investigated as model systems of hemoproteins, because their metal porphyrin planes and substituents construct specifically covered reaction scaffolds. In particular, a metal porphyrin derivative with a metal-coordinative substituent<sup>80,81</sup> is suitable for modeling cytochrome *c* oxidase (CcO),<sup>82</sup> which is a mitochondrial membrane protein and contains a heme/copper hetero-dinuclear active site catalyzing oxygen reduction reaction. In this context, phenanthroline-strapped porphyrin (Fig. 8), which can bind metal ions at the phenanthroline and porphyrin moieties to form a hetero-dinuclear reaction scaffold, has been investigated as a model of CcO by Weiss and coworkers. They have prepared a series of phenanthroline-strapped porphyrins containing iron atom in the porphyrin moieties and evaluated their electrocatalytic properties for oxygen reduction reaction in the presence and absence of copper ion and axial ligands.<sup>83</sup> Moreover, they also reported that an imidazole molecule perfectly fits to the cavity of the phenanthroline-strapped zinc porphyrin by coordination of the imidazole nitrogen atom (N<sup>3</sup>) to the zinc center and hydrogen bonding interaction between the nitrogen atom (N<sup>1</sup>) and the phenanthroline.<sup>84</sup> This specific coordination structure has been applied to the construction of self-assembled structures forming organized nano-objects and showing energy transfer properties.<sup>85</sup> Thus, a metal-coordinated cavity in the phenanthroline-strapped porphyrin is a powerful tool to realize a bimetallic system which expresses both of the catalytic ability and molecular recognition ability.

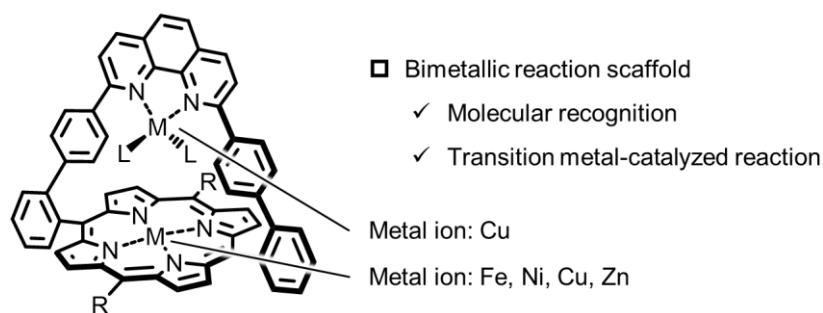
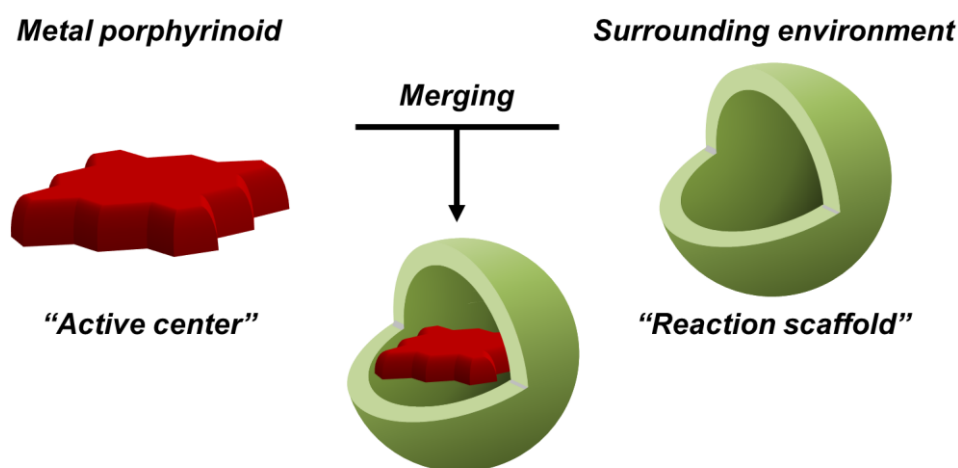


**Figure 8.** Chemical structure of phenanthroline-strapped porphyrin and its expected functions.

### System designs of metal porphyrinoids having reaction scaffolds in this thesis

Construction of an artificial reaction scaffold to a metal porphyrinoid should contribute to expanding its function. In this context, the author focused on the construction of two-type reaction scaffolds surrounding metal porphyrinoids toward modeling an enzymatic system and construction of a mechanically complexed architecture (Fig. 9). At first, regarding an investigation of a natural enzyme, a functional model featuring the protein matrix of the natural enzyme should be promising for elucidation of the reaction mechanism and the effect of the protein matrix in the enzymatic reaction. To this end, the author prepared hemoprotein-based MCR functional models containing active centers and reaction scaffolds by reconstitution method<sup>26</sup> in which a natural heme cofactor of hemoprotein is replaced with an artificial cofactor. Furthermore, the functional models demonstrated catalytic methane generation from an external methyl donor (Chapter 1) and methane generation *via* intraprotein C–S bond cleavage (Chapter 2). On the other hand, a metal-coordinated cavity in a phenanthroline-strapped porphyrin, having catalytic ability and molecular recognition ability, is attractive for construction of a mechanically complexed architecture. In this context, the author employed the complex in which Cu(I) ion and Zn(II) ion are bound to the phenanthroline and porphyrin moieties, respectively, as a platform for rotaxane synthesis based on the active metal template method (Chapter 3).



**Toward... Modeling enzymatic reaction (Chapters 1 and 2)**

**Construction of mechanically interlocked molecule (Chapter 3)**

**Figure 9.** Schematic representation of system designs in this thesis.

## **Outline of this thesis**

The author constructed an appropriate reaction scaffold which gives primary and second coordination spheres to metal porphyrinoids by synthetic and biological approaches to employ complexes as protein-based functional models of MCR (Chapters 1 and 2) and platform for rotaxane synthesis based on the active metal template method (Chapter 3).

### **Chapter 1: Methane generation from an external methyl donor using reconstituted myoglobin with nickel tetrahydrocorrin**

Reconstituted myoglobin (reconstituted Mb) with nickel(I) tetrahydrocorrin ( $\text{Ni}^{\text{I}}(\text{TDHC})$ ) was investigated as a protein-based functional model of MCR.  $\text{Ni}^{\text{II}}(\text{TDHC})$ , which has a monoanionic tetrapyrrole ligand to stabilize a low valent nickel species, was synthesized as a model complex of F430 and successfully reduced by dithionite in a buffer solution. Then, reconstituted Mb produced by conjugation of  $\text{Ni}^{\text{I}}(\text{TDHC})$  with apomyoglobin showed catalytic methane generation from methyl iodide, whereas  $\text{Ni}^{\text{I}}(\text{TDHC})$  does not generate methane. Furthermore, the effect of the protein matrix in the catalytic reaction was elucidated by spectroscopic measurements for the  $\text{Ni}^{\text{II}}/\text{Ni}^{\text{I}}$  process.

### **Chapter 2: Methane generation *via* intraprotein C–S bond cleavage in reconstituted cytochrome $b_{562}$ with nickel didehydrocorrin**

Cytochrome  $b_{562}$  (Cyt  $b_{562}$ ) reconstituted with nickel(II) didehydrocorrin ( $\text{Ni}^{\text{II}}(\text{DDHC})$ ) as a protein-based functional model of MCR was investigated to demonstrate methane generation *via* intraprotein C–S bond cleavage.  $\text{Ni}^{\text{II}}(\text{DDHC})$ , which has more saturated ligand than  $\text{Ni}^{\text{I}}(\text{TDHC})$ , was synthesized to enhance the reactivity of Ni(I) species. Photoirradiation of reconstituted Cyt  $b_{562}$  reduced the nickel center, followed by methane generation from the  $\text{H}_3\text{C}$ –S group of the methionine residue in the presence of tris(2,2'-bipyridine)ruthenium(II) chloride as a photosensitizer and sodium ascorbate as a sacrificial reagent. Further experiment using mutated Cyt  $b_{562}$  suggested the importance of precise arrangement of the active center and substrates in the protein matrix for the reaction.

### **Chapter 3: Synthesis of rotaxane using the ditopic strapped porphyrin based on the active metal template method**

Synthesis of rotaxane employing molecular recognition and catalytic ability of a metal complex of strapped porphyrin having a ditopic ligand was investigated. The successful covalent bond formation yielding rotaxane by copper-catalyzed azide–alkyne cycloaddition was observed in the presence of a Cu(I) ion bound to the phenanthroline moiety and a coordinatively unsaturated metal ion in the porphyrin moiety. Moreover, structural control of a rotaxane by introduction of a metal ion to the porphyrin moiety was achieved.

## References

1. (a) T. L. Poulos, *Chem. Rev.* **2014**, *114*, 3919–3962. (b) T. Shimizu, A. Lengalova, V. Martínek, M. Martínková, *Chem. Soc. Rev.* **2019**, *48*, 5624–5657.
2. (a) R. Banerjee, S. W. Ragsdale, *Annu. Rev. Biochem.* **2003**, *72*, 209–247. (b) K. Gruber, B. Pufferb, B. Kräutler, *Chem. Soc. Rev.* **2011**, *40*, 4346–4363.
3. (a) U. Ermler, *Dalton Trans.* **2005**, 3451–3458. (b) S. W. Ragsdale, S. Raugei, B. Ginovska, T. Wongnate, Biochemistry of methyl-coenzyme M reductase. In *Biological Chemistry of Nickel* (Eds.: D. Zamble, M. Rowinska-Zyrek, H. Koslowski), **2017**, Chapter 8, 149–169, Royal Society of Chemistry, Cambridge, (c) R. K. Thauer, *Biochemistry* **2019**, *58*, 5198–5220.
4. C. R. Robinson, Y. Liu, J. A. Thomson, J. M. Sturtevant, S. G. Sligar, *Biochemistry* **1997**, *36*, 16141–16146.
5. (a) P. D. Barker, E. P. Nerou, M. R. Cheesman, A. J. Thomson, P. de Oliveira, H. A. O. Hill, *Biochemistry* **1996**, *35*, 13618–13626. (b) S. Hay, T. Wydrzynski, *Biochemistry* **2005**, *44*, 431–439.
6. (a) S. L. Springs, S. E. Bass, G. L. McLendon, *Biochemistry* **2000**, *39*, 6075–6082. (b) S. L. Springs, S. E. Bass, G. Bowman, I. Nodelman, C. E. Schutt, G. L. McLendon, *Biochemistry* **2002**, *41*, 4321–4328.
7. B. A. Springer, S. G. Sligar, J. S. Olson, G. N. Phillips, *Chem. Rev.* **1994**, *94*, 699–714.
8. M. S. Hargrove, D. Barrick, J. S. Olson, *Biochemistry* **1996**, *35*, 11293–11299.
9. T. G. Traylor, D. K. White, D. H. Campbell, A. P. Berzinis, *J. Am. Chem. Soc.* **1981**, *103*, 4932–4936.
10. R. G. Matthews, *Acc. Chem. Res.* **2001**, *34*, 681–689.
11. H. Mosimann, B. Kräutler, *Angew. Chem. Int. Ed.* **2000**, *39*, 393–395.
12. (a) J. P. Collman, R. R. Gagne, T. R. Halbert, J. C. Marchon, C. A. Reed, *J. Am. Chem. Soc.* **1973**, *95*, 7868–7870. (b) J. P. Collman, R. R. Gagne, C. Reed, T. R. Halbert, G. Lang, W. T. Robinson, *J. Am. Chem. Soc.* **1975**, *97*, 1427–1439.
13. G. E. Wuenschell, C. Tetreau, D. Lavalette, C. A. Reed, *J. Am. Chem. Soc.* **1992**, *114*, 3346–3355.
14. M. D. Lim, I. M. Lorkovic, P. C. Ford, *J. Inorg. Biochem.* **2005**, *99*, 151–165.
15. M. D. Hartle, J. S. Prell, M. D. Pluth, *Dalton Trans.* **2016**, *45*, 4843–4853.
16. O. F. Brandenburg, R. Fasan, F. H. Arnold. *Curr. Opin. Biotechnol.* **2017**, *47*, 102–111.
17. M. P. Doyle, *Angew. Chem. Int. Ed.* **2009**, *48*, 850–852.
18. S.-F. Zhu, Q.-L. Zhou, *Natl. Sci. Rev.* **2014**, *1*, 580–603.
19. D. Inriieri, D. M. Carminati, E. Gallo, *Dalton Trans.* **2016**, *45*, 15746–15761.
20. (a) Y. Chen, K. B. Fields, X. P. Zhang, *J. Am. Chem. Soc.* **2004**, *126*, 14718–14719. (b) S. Zhu, J. A. Perman, X. P. Zhang, *Angew. Chem. Int. Ed.* **2008**, *47*, 8460–8463.
21. F. H. Arnold, *Angew. Chem. Int. Ed.* **2018**, *57*, 4143–4148.
22. S. N. Natoli, J. F. Hartwig, *Acc. Chem. Res.* **2019**, *52*, 326–335.
23. O. Shoji, Y. Aiba, Y. Watanabe, *Acc. Chem. Res.* **2019**, *52*, 925–934.
24. E. N. Mirts, A. Bhagi-Damodaran, Y. Lu, *Acc. Chem. Res.* **2019**, *52*, 935–944.
25. K. Oohora, A. Onoda, T. Hayashi, *Acc. Chem. Res.* **2019**, *52*, 945–954.
26. K. Oohora, T. Hayashi, *Methods Enzymol.* **2016**, *580*, 439–454.
27. P. Carter, *Biochem. J.* **1986**, *237*, 1–7.

28. C. Zeymer, D. Hilvert, *Annu. Rev. Biochem.* **2018**, *87*, 131–157.
29. T. Hayashi, H. Dejjima, T. Matsuo, H. Sato, D. Murata, Y. Hisaeda, *J. Am. Chem. Soc.* **2002**, *124*, 11226–11227.
30. (a) H. M. Key, P. Dydio, D. S. Clark, J. F. Hartwig, *Nature* **2016**, *534*, 534–537. (b) H. M. Key, P. Dydio, Z. Liu, J. Y.-E. Rha, A. Nazarenko, V. Seyedkazemi, D. S. Clark, J. F. Hartwig, *ACS Cent. Sci.* **2017**, *3*, 302–308.
31. P. S. Coelho, E. M. Brustad, A. Kannan<sup>1</sup>, F. H. Arnold, *Science* **2013**, *339*, 307–310.
32. M. Bordeaux, V. Tyagi, R. Fasan, *Angew. Chem. Int. Ed.* **2015**, *54*, 1744–1748.
33. K. Oohora, H. Meichin, L. Zhao, M. W. Wolf, A. Nakayama, J. Hasegawa, N. Lehnert, T. Hayashi, *J. Am. Chem. Soc.* **2017**, *139*, 17265–17268.
34. P. N. Evans, J. A. Boyd, A. O. Leu, B. J. Woodcroft, D. H. Parks, P. Hugenholtz, G. W. Tyson, *Nat. Rev. Microbiol.* **2019**, *17*, 219–232.
35. S. Friedle, E. Reisner, S. J. Lippard, *Chem. Soc. Rev.* **2010**, *39*, 2768–2779.
36. G. Borrel, P. S. Adam, L. J. McKay, L.-X. Chen, I. N. Sierra-García, C. M. K. Sieber, Q. Letourneur, A. Ghozlane, G. L. Andersen, W.-J. Li, S. J. Hallam, G. Muyzer, V. M. Oliveira, W. P. Inskeep, J. F. Banfield, S. Gribaldo, *Nat. Microbiol.* **2019**, *4*, 603–613.
37. M. Krüger, A. Meyerdierks, F. O. Glöckner, R. Amann, F. Widdel, M. Kube, R. Reinhardt, R. Kahnt, R. Böcher, R. K. Thauer, S. Shima, *Nature* **2003**, *426*, 878–881.
38. S. Scheller, M. Goenrich, R. Boecher, R. K. Thauer, B. Jaun, *Nature* **2010**, *465*, 606–608.
39. S. Shima, M. Krueger, T. Weinert, U. Demmer, J. Kahnt, R. K. Thauer, U. Ermler, *Nature* **2012**, *481*, 98–101.
40. R. P. Gunsalus, R. S. Wolfe, *J. Biol. Chem.* **1980**, *255*, 1891–1895.
41. U. Ermler, W. Grabarse, S. Shima, M. Goubeaud, R. K. Thauer, *Science* **1997**, *278*, 1457–1462.
42. W. Grabarse, F. Mahlert, S. Shima, R. K. Thauer, U. Ermler, *J. Mol. Biol.* **2000**, *303*, 329–344.
43. W. Grabarse, F. Mahlert, E. C. Duin, M. Goubeaud, S. Shima, R. K. Thauer, V. Lamzin, U. Ermler, *J. Mol. Biol.* **2001**, *309*, 315–330.
44. P. E. Cedervall, M. Dey, A. R. Pearson, S. W. Ragsdale, C. M. Wilmot, *Biochemistry* **2010**, *49*, 7683–7693.
45. E. Cedervall, M. Dey, X. Li, R. Sarangi, B. Hedman, S. W. Ragsdale, C. M. Wilmot, *J. Am. Chem. Soc.* **2011**, *133*, 5626–5628.
46. W. B. Whitman, R. S. Wolfe, *Biochem. Biophys. Res. Commun.* **1980**, *92*, 1196–1201.
47. G. Diekert, B. Klee, R. K. Thauer, *Microbiol.* **1980**, *124*, 103–106.
48. G. Färber, W. Keller, C. Kratky, B. Jaun, A. Pfaltz, C. Spinner, A. Kobelt, A. Eschenmoser, *Helv. Chim. Acta* **1991**, *74*, 697–716.
49. C. Holliger, A. J. Pierik, E. J. Reijerse, W. R. Hagen, *J. Am. Chem. Soc.* **1993**, *115*, 5651–5656.
50. B. Jaun, A. Pfaltz, *J. Chem. Soc., Chem. Commun.* **1986**, 1327–1329.
51. B. Jaun, *Helv. Chim. Acta* **1990**, *73*, 2209–2217.
52. R. Piskorski, B. Jaun, *J. Am. Chem. Soc.* **2003**, *125*, 13120–13125.
53. G. K. Lahiri, L. J. Schussel, A. M. Stolzenberg, *Inorg. Chem.* **1992**, *31*, 4991–5000.
54. G. K. Lahiri, A. M. Stolzenberg, *Inorg. Chem.* **1993**, *32*, 4409–4413.
55. S.-K. Lin, B. Jaun, *Helv. Chim. Acta* **1991**, *74*, 1725–1738.
56. I. Zilbermann, G. Golub, H. Cohen, D. Meyerstein, *Inorg. Chim. Acta* **1994**, *227*, 1–3.

57. B. Jaun, A. Pfaltz, *J. Chem. Soc., Chem. Commun.* **1988**, 293–294.
58. M. Dey, R. C. Kunz, D. M. Lyons, S. W. Ragsdale, *Biochemistry* **2007**, *46*, 11969–11978.
59. M. Dey, J. Telser, R. C. Kunz, N. S. Lees, S. W. Ragsdale, B. M. Hoffman, *J. Am. Chem. Soc.* **2007**, *129*, 11030–11032.
60. N. Yang, M. Reiher, M. Wang, J. Harmer, E. C. Duin, *J. Am. Chem. Soc.* **2007**, *129*, 11028–11029.
61. R. Sarangi, M. Dey, S. W. Ragsdale, *Biochemistry* **2009**, *48*, 3146–3156.
62. (a) V. Pelmeshnikov, M. R. A. Blomberg, P. E. M. Siegbahn, R. H. Crabtree, *J. Am. Chem. Soc.* **2002**, *124*, 4039–4049. (b) V. Pelmeshnikov, P. E. M. Siegbahn, *J. Biol. Inorg. Chem.* **2003**, *8*, 653–662. (c) S.-L. Chen, M. R. A. Blomberg, P. E. M. Siegbahn, *Chem. Eur. J.* **2012**, *18*, 6309–6315. (d) S.-L. Chen, M. R. A. Blomberg, P. E. M. Siegbahn, *Phys. Chem. Chem. Phys.* **2014**, *16*, 14029–14035.
63. T. Wongnate, D. Sliwa, B. Ginovska, D. Smith, M. W. Wolf, N. Lehnert, S. Raugei, S. W. Ragsdale, *Science* **2016**, *352*, 953–958.
64. L. Signor, C. Knuppe, R. Hug, B. Schweizer, A. Pfaltz, B. Jaun, *Chem. Eur. J.* **2000**, *6*, 3508–3516.
65. (a) J. Nishigaki, T. Matsumoto, K. Tatsumi, *Eur. J. Inorg. Chem.* **2010**, 5011–5017. (b) J. Nishigaki, T. Matsumoto, K. Tatsumi, *Inorg. Chem.* **2012**, *51*, 3690–3697. (c) J. Nishigaki, T. Matsumoto, K. Tatsumi, *Inorg. Chem.* **2012**, *51*, 5173–5187.
66. C. Brenig, L. Prieto, R. Oetterli, F. Zelder, *Angew. Chem. Int. Ed.* **2018**, *57*, 16308–16312.
67. A. Berkessel, *Bioorg. Chem.* **1991**, *19*, 101–115.
68. M. Tada, Y. Masuzawa, *Chem. Commun.* **1997**, *22*, 2161–2162.
69. (a) D. B. Amabilino, J. F. Stoddart, *Chem. Rev.* **1995**, *95*, 2725–2828. (b) J. D. Crowley, S. M. Goldup, A.-L. Lee, D. A. Leigh, R. T. McBurney, *Chem. Soc. Rev.* **2009**, *38*, 1530–1541. (c) M. Denis, S. M. Goldup, *Nat. Rev. Chem.* **2017**, *1*, 0061.
70. E. Wasserman, *J. Am. Chem. Soc.* **1960**, *82*, 4433–4434.
71. G. Schill, A. Lüttringhaus, *Angew. Chem. Int. Ed.* **1964**, *3*, 546–547.
72. C. O. Dietrich-Buchecker, J.-P. Sauvage, J. P. Kintzinger, *Tetrahedron Lett.* **1983**, *24*, 5095–5098.
73. P. R. Ashton, T. T. Goodnow, A. E. Kaifer, M. V. Reddington, A. M. Z. Slawin, N. Spencer, J. F. Stoddart, C. Vicent, D. J. Williams, *Angew. Chem. Int. Ed.* **1989**, *28*, 1396–1399.
74. A. G. Johnston, D. A. Leigh, R. J. Pritchard, M. D. Deegan, *Angew. Chem., Int. Ed.* **1995**, *34*, 1209–1212.
75. V. Aucagne, K. D. Hänni, D. A. Leigh, P. J. Lusby, D. B. Walker, *J. Am. Chem. Soc.* **2006**, *128*, 2186–2187.
76. H. Lahlali, K. Jobe, M. Watkinson, S. M. Goldup, *Angew. Chem. Int. Ed.* **2011**, *50*, 4151–4155.
77. J. Almog, J. E. Baldwin, R. L. Dyer, M. Peters, *J. Am. Chem. Soc.* **1975**, *97*, 226–227.
78. J. E. Baldwin, T. Klose, M. Peters, *J. Chem. Soc., Chem. Commun.* **1976**, 881–883.
79. J. P. Coliman, J. I. Brauman, J. P. Fitzgerald, P. D. Hampton, Y. Naruta, J. W. Sparapany, J. A. Ibers, *J. Am. Chem. Soc.* **1988**, *110*, 3477–3486.
80. S. M. Adam, G. B. Wijeratne, P. J. Rogler, D. E. Diaz, D. A. Quist, J. J. Liu, K. D. Karlin, *Chem. Rev.* **2018**, *118*, 10840–11022.
81. (a) T. Chishiro, Y. Shimazaki, F. Tani, Y. Tachi, Y. Naruta, S. Karasawa, S. Hayami, Y. Maeda, *Angew. Chem. Int. Ed.* **2003**, *42*, 2788–2791. (b) J. P. Collman, N. K. Devaraj, R. A. Decréau, Y. Yang, Y.-L. Yan, W. Ebina, T. A.

- Eberspacher, C. E. D. Chidsey, *Science* **2007**, *315*, 1565–1568. (c) H. Kitagishi, D. Shimoji, T. Ohta, R. Kamiya, Y. Kudo, A. Onoda, T. Hayashi, J. Weiss, J. A. Wytko, K. Kano, *Chem. Sci.* **2018**, *9*, 1989–1995.
82. S. Yoshikawa, A. Shimada, *Chem. Rev.* **2015**, *115*, 1936–1989.
83. (a) F. Melin, S. Choua, M. Bernard, P. Turek, J. Weiss, *Inorg. Chem.* **2006**, *45*, 10750–10757. (b) F. Melin, C. Boudon, M. Lo, K. J. Schenk, M. Bonin, P. Ochsenbein, M. Gross, J. Weiss, *J. Porphyr. Phthalocyanines* **2007**, *11*, 212–221. (c) F. Melin, A. Trivella, M. Lo, C. Ruzié, I. Hijazi, N. Oueslati, J. A. Wytko, B. Boitrel, C. Boudon, P. Hellwig, J. Weiss, *J. Inorg. Biochem.* **2012**, *108*, 196–202.
84. D. Paul, F. Melin, C. Hirtz, J. Wytko, P. Ochsenbein, M. Bonin, K. Schenk, P. Maltese, J. Weiss, *Inorg. Chem.* **2003**, *42*, 3779–3787.
85. C. Kahlfuss, J. A. Wytko, J. Weiss, *ChemPlusChem* **2017**, *82*, 584–594.
86. (a) I. Leray, D. Paul, E. Regnier, M. Koepf, J. A. Wytko, C. Boudon, J. Weiss, *Photochem. Photobiol. Sci.* **2005**, *4*, 280–286. (b) D. Paul, J. A. Wytko, M. Koepf, J. Weiss, *Inorg. Chem.* **2002**, *41*, 3699–3704. (c) M. Koepf, A. Trabolsi, M. Elhabiri, J. A. Wytko, D. Paul, A. M. Albrecht-Gary, J. Weiss, *Org. Lett.* **2005**, *7*, 1279–1282.
87. (a) M. Koepf, J. A. Wytko, J.-P. Bucher, J. Weiss, *J. Am. Chem. Soc.* **2008**, *130*, 9994–10001. (b) V. Rauch, J. A. Wytko, M. Takahashi, Y. Kikkawa, M. Kanosato, J. Weiss, *Org. Lett.* **2012**, *14*, 1998–2001. (c) V. Rauch, Y. Kikkawa, M. Koepf, I. Hijazi, J. A. Wytko, S. Campidelli, A. Goujon, M. Kanosato, J. Weiss, *Chem. Eur. J.* **2015**, *21*, 13437–13444.

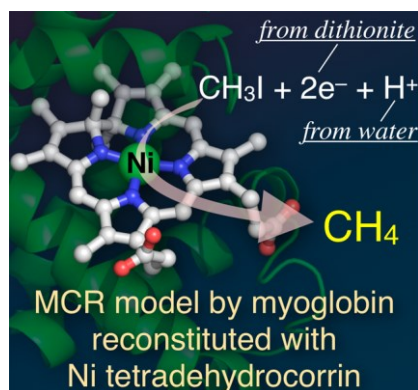
# Chapter 1

## Methane generation from an external methyl donor using reconstituted myoglobin with nickel tetradehydrocorrin

Reproduced in part with permission from [*Angew. Chem. Int. Ed.* **2019**, *58*, 13813–13817.]

DOI: 10.1002/anie.201907584

License number: 4733440350443



### 1-1. Introduction

Methyl-coenzyme M reductase (MCR), which contains F430 as a cofactor, is the key enzyme for methane generation in the final step of methanogenesis in methanogenic archaea.<sup>1-3</sup> The cofactor, a Ni complex with a reduced tetrapyrrole ligand with monoanionic character, converts methyl-coenzyme M ( $\text{CH}_3\text{S-CoM}$ ) and coenzyme B ( $\text{HS-CoB}$ ) to methane and a heterodisulfide ( $\text{CoM-S-S-CoB}$ ) compound *via* a reactive Ni(I) intermediate in the protein. Although, the enzymatic reaction has been investigated in experimental and theoretical studies,<sup>3-13</sup> the large and complex structure of MCR complicates the elucidation of the reaction mechanism. Two different plausible pathways through a methyl–Ni(III) intermediate or a transient methyl radical species and Ni(II) intermediate have been proposed.<sup>3</sup> Acceptable evidence for the latter mechanism has been provided by recent single turnover experiments.<sup>8</sup> Although methane generation by the F430 and its model complexes were demonstrated,<sup>14-17</sup> much stronger reductants, such as Ti(III) citrate and NaHg were found to be required relative to the thiol-based reductant employed by native MCR.<sup>18</sup> In this context, the author has designed and prepared Ni(TDHC) (TDHC = 8,12-dicarboxyethyl-1,2,3,7,13,17,18,19-octamethyltetradehydrocorrin; Fig. 1-1a), because the low valent nickel species was expected to be stabilized by the monoanionic TDHC ligand as seen in the Co(TDHC) complex.<sup>19,20</sup> In support of my strategy, a nickel-substituted vitamin B12 derivative having a monoanionic ligand has been recently reported as a model with spectroscopic characteristics similar to those of F430.<sup>21</sup> Furthermore, the author have focused on the effect of the protein matrix on physicochemical property and reactivity of the nickel model complex. For example, myoglobin (Mb), an oxygen-binding hemoprotein, is found to provide a simple and useful scaffold for a hydrophobic cofactor-binding cavity.<sup>22-24</sup> The study given in this chapter demonstrates methane generation from an external methyl donor by the Ni(TDHC) complex within a Mb matrix using a mild reductant (Fig. 1-1b).

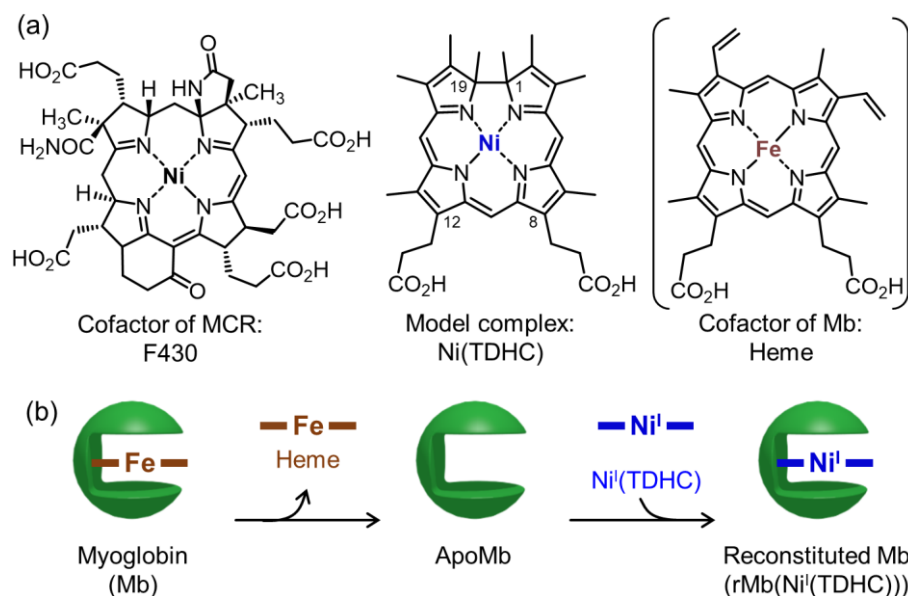


**Figure 1-1.** Molecular structures of F430, Ni(TDHC), and heme. (b) Schematic representation of Mb reconstitution with Ni(TDHC).

## 1-2. Results and discussion

### Synthesis and characterization of Ni<sup>II</sup>(TDHC)

Ni<sup>II</sup>(TDHC) was synthesized by cyclization of the corresponding biladiene-*a,c* dihydrobromide derivative in the presence of Ni(OAc)<sub>2</sub>.<sup>25</sup> Two methyl substituents at the C1- and C19-positions are on opposite faces of the corrinoid ring and the compound was obtained as two enantiomers, (1*R*,19*R*)-TDHC and (1*S*,19*S*)-TDHC. Two propionate side chains are introduced at the C8- and C12-positions, as in native heme. According to the previous work using Co(TDHC),<sup>19</sup> the side chains support fixation of the cofactor in a suitable orientation *via* a hydrogen bonding network with polar amino acid residues. Following synthesis, the Ni<sup>II</sup>(TDHC) was characterized by <sup>1</sup>H and <sup>13</sup>C NMR spectroscopy, ESI-TOF mass spectrometry (found: 611.2161, calcd: 611.2163 as C<sub>33</sub>H<sub>37</sub>N<sub>4</sub>O<sub>4</sub>Ni) and X-ray crystal structural analysis. The NMR spectra indicate that the compound is the diamagnetic Ni(II) species. The UV-vis spectrum (Fig. 1-2a) has characteristic peaks at 272, 350, and 551 nm in aqueous solution, which are identical to the peaks of the reported nickel complex without propionate side chains.<sup>25</sup> Furthermore, the crystal structure of [Ni<sup>II</sup>(TDHC)]ClO<sub>4</sub> in Fig. 1-3 indicates two enantiomers, (1*R*,19*R*)-TDHC and (1*S*,19*S*)-TDHC, in a 0.55:0.45 ratio. The reported pentamethyl ester of F430, F430M, has a more ruffled crystal structure than the present structure of Ni<sup>II</sup>(TDHC).<sup>26</sup> However, the averaged bond length between nickel and nitrogen atoms in Ni<sup>II</sup>(TDHC) is shortened only by approximately 0.1 Å relative to the F430 derivative, indicating that Ni(TDHC) is a potent model complex of F430.

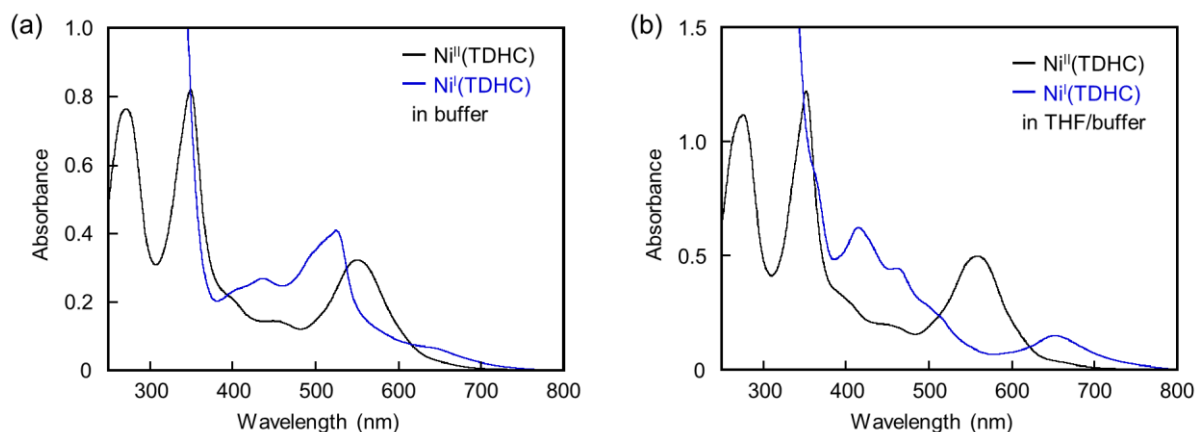


**Figure 1-2.** UV-vis absorption spectral changes of Ni<sup>II</sup>(TDHC) (black line) upon addition of dithionite (blue line) in (a) 100 mM potassium phosphate buffer (pH 7.0) and (b) THF/buffer ( $v/v = 1:1$ ) solutions.

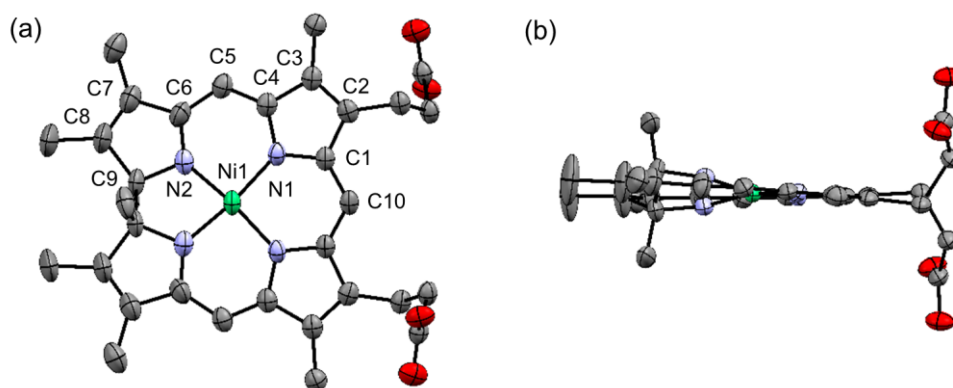


**Figure 1-3.** ORTEP representation of the crystal structure of [Ni<sup>II</sup>(TDHC)]ClO<sub>4</sub> (thermal ellipsoids shown at 50%). (a) Top view and (b) side view. Hydrogen atoms, counter anion, and solvent molecules are omitted for clarity.

### Reduction of Ni<sup>II</sup>(TDHC)

The reduction of Ni<sup>II</sup>(TDHC) with dithionite under anaerobic conditions leads to UV-vis spectral changes *via* several isosbestic points and the appearance of new peaks at 436 nm and 526 nm as well as a shoulder at 493 nm (Fig. 1-2a). Furthermore, the Ni<sup>II</sup>/Ni<sup>I</sup> redox potential in 100 mM potassium phosphate buffer at pH 7.0 was determined to be  $-0.54$  V vs. Ag|AgCl by spectroelectrochemical measurements (Fig. 1-4). The slope of the Nernst plot is 55 mV, indicating that one-electron transfer occurs in this redox event. Thus, the product obtained from the reaction with dithionite was identified as a one-electron reduced species. However, the EPR spectrum of the one-electron reduced species is silent although the Ni(I) paramagnetic species ( $d^9$ ) or ligand radical should be generated. To clarify the conflicting results, the same species was evaluated in other solvents. The UV-vis spectrum of Ni<sup>I</sup>(TDHC) in THF/buffer ( $v/v = 1:1$ ) has different peaks at 416 nm, 461 nm, and 653 nm which are not observed in the phosphate buffer solution in the absence of THF (Fig. 1-2b). Furthermore, the EPR spectrum of one-electron reduced species in THF/buffer (Fig. 1-5) has peaks at  $g_{\perp} = 2.02$  and  $g_{\parallel} = 1.96$ , indicating the Ni(I) species. This EPR spectrum is different

from that observed for native F430. In contrast to a predominant  $d_{x^2-y^2}$  configuration of the nickel ion of F430,<sup>3,18</sup> the EPR signals with  $g_{\perp} > g_{\parallel}$  observed in this work indicate a predominant  $d_{z^2}$  configuration of the nickel ion, according to the previous data.<sup>27,28</sup> This result is also supported by the data from the Evans method, indicating the presence of one unpaired electron (Fig. 1-6). These findings suggest an antiferromagnetic interaction due to the hydrophobicity-induced stacking of two Ni<sup>I</sup>(TDHC) molecules in the buffer solution. Thus, the Ni<sup>II</sup>(TDHC) complex can be reduced with dithionite, a mild reductant, to form the Ni(I) species. The Ni<sup>II</sup>/Ni<sup>I</sup> redox potential of Ni(TDHC) at  $-0.54$  V vs. Ag|AgCl is remarkably higher than the reported redox potentials of F430 derivatives ( $-0.70$  V in dimethyl formamide and  $-0.85$  V in a basic buffer),<sup>29</sup> showing that the TDHC ligand provides the thermodynamically stable Ni(I) species.

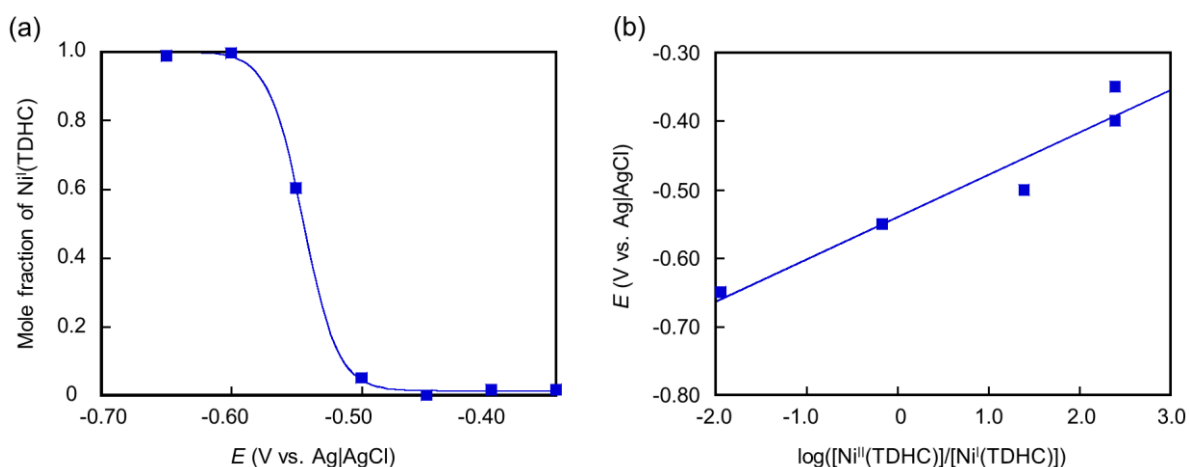


**Figure 1-4.** Nernst plots of the redox reaction of Ni(TDHC) based on  $\Delta\text{Abs}(500\text{ nm})$  values. (a) Plots with Nernst curves assuming one-electron redox process with  $E_m = -0.54$  V vs. Ag|AgCl. (b) Plots of  $E$  values against  $\log([\text{Ni}^{\text{II}}(\text{TDHC})]/[\text{Ni}^{\text{I}}(\text{TDHC})])$ . The line drawn by a least-squares fit to the plots gives a slope of 55 mV.

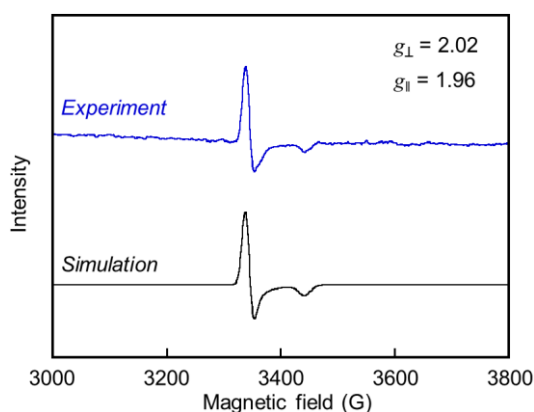


**Figure 1-5.** EPR spectrum of Ni<sup>I</sup>(TDHC) in THF/buffer ( $v/v = 1:1$ ) solution at 100 K and the simulated spectrum.

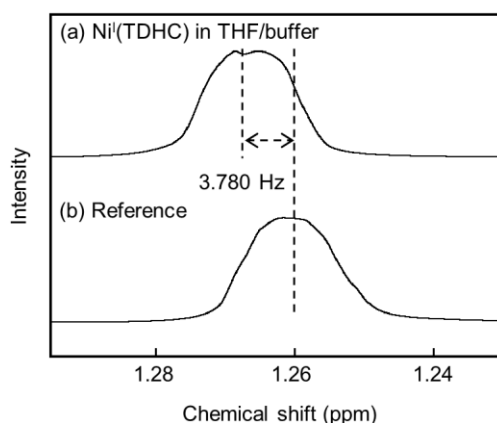


**Figure 1-6.**  $^1\text{H}$  NMR (600 MHz) spectra of *t*-butanol in a mixture of THF/buffer ( $v/v = 1:1$ ) containing 10 %  $\text{D}_2\text{O}$ : (a) with and (b) without  $\text{Ni}^{\text{I}}(\text{TDHC})$ . Conditions: Temperature = 25 °C,  $[\text{Ni}^{\text{I}}(\text{TDHC})] = 1.0$  mM,  $[t\text{-butanol}] = 320$  mM.

### Preparation and characterization of $\text{rMb}(\text{Ni}^{\text{I}}(\text{TDHC}))$

The binding of  $\text{Ni}(\text{TDHC})$  to an apo-form of Mb matrix (apoMb), which was prepared by removal of heme from Mb, was investigated (Fig. 1-1b). First, the addition of the  $\text{Ni}^{\text{II}}(\text{TDHC})$  complex into an apoMb aqueous solution does not produce significant changes in UV-vis and CD spectra under conventional conditions, indicating that the difficulty of binding. These results are possibly due to unfavorable charge repulsion and/or steric hindrance. In contrast, the addition of the  $\text{Ni}^{\text{I}}(\text{TDHC})$  complex to an aqueous solution of apoMb provides the obvious spectral changes (Fig. 1-7a) under anaerobic conditions, showing formation of the reconstituted protein,  $\text{rMb}(\text{Ni}^{\text{I}}(\text{TDHC}))$ . The UV-vis titration experiment of apoMb into the  $\text{Ni}^{\text{I}}(\text{TDHC})$  solution indicates the dissociation constant ( $K_d$ ) of 11  $\mu\text{M}$  (Fig. 1-7b). In the far-UV region of the CD spectrum, the characteristic negative Cotton effects were observed at 208 nm and 222 nm derived from the  $\alpha$ -helices of the reconstituted protein (Fig. 1-8a). Moreover, the Cotton effects corresponding to the absorption peaks derived from  $\text{Ni}^{\text{I}}(\text{TDHC})$  are observed in the visible region of the CD spectrum (Fig. 1-8b). This result clearly shows the incorporation of the nickel complex into the chiral environment of the protein matrix and successful binding of the complex to the heme pocket of Mb. Furthermore, ESI-TOF mass spectrum gives a peak at  $m/z = 2194.2$ , which is consistent with the expected value of the reconstituted protein ( $m/z = 2194.4$  ( $z = 8^-$ )). The UV-vis spectrum of  $\text{rMb}(\text{Ni}^{\text{I}}(\text{TDHC}))$  is similar to that observed for  $\text{Ni}^{\text{I}}(\text{TDHC})$  in THF/buffer containing 10% pyridine (Fig. 1-9), suggesting that His93, the intrinsic residue coordinating to heme in native Mb, works as an axial ligand in the protein matrix. Furthermore, maintenance of the Ni(I) species in the protein matrix is confirmed by the EPR spectrum and the Evans method (Fig. 1-10 and 11). Especially, the EPR spectrum of  $\text{rMb}(\text{Ni}^{\text{I}}(\text{TDHC}))$  shows the predominant  $d_{z^2}$  configuration of the nickel ion in a similar manner to  $\text{Ni}^{\text{I}}(\text{TDHC})$  in THF/buffer ( $v/v = 1:1$ ).<sup>27,28</sup> Taken together, the results indicate that  $\text{Ni}^{\text{I}}(\text{TDHC})$  is bound into the heme pocket of apoMb and stabilized by the protein matrix.

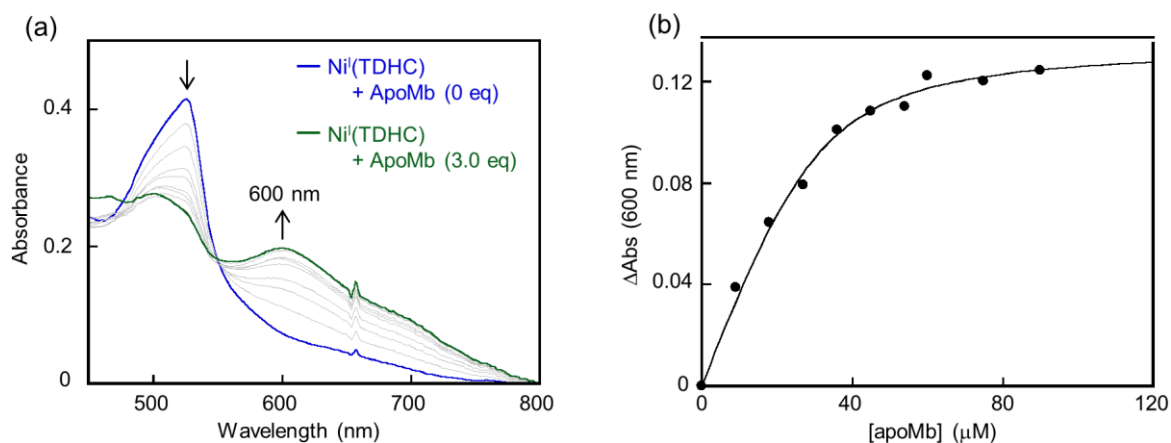


**Figure 1-7.** (a) UV-vis absorption spectral changes of Ni<sup>I</sup>(TDHC) (blue line) upon addition of apoMb (green line) in 100 mM potassium phosphate buffer (pH 7.0) at 25 °C under an N<sub>2</sub> atmosphere. (b) Plots of absorbance at 600 nm against apoMb concentration.

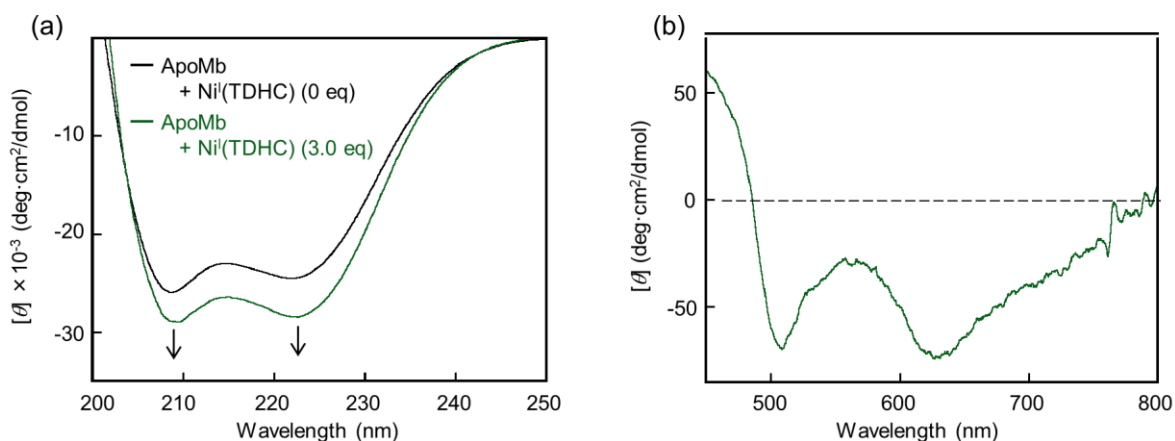


**Figure 1-8.** (a) CD spectral changes of apoMb (black line) in the ultraviolet region upon addition of Ni<sup>I</sup>(TDHC) (green color) in 100 mM potassium phosphate buffer (pH 7.0) at 25 °C under an N<sub>2</sub> atmosphere. (b) CD spectrum of rMb(Ni<sup>I</sup>(TDHC)) in the visible region.

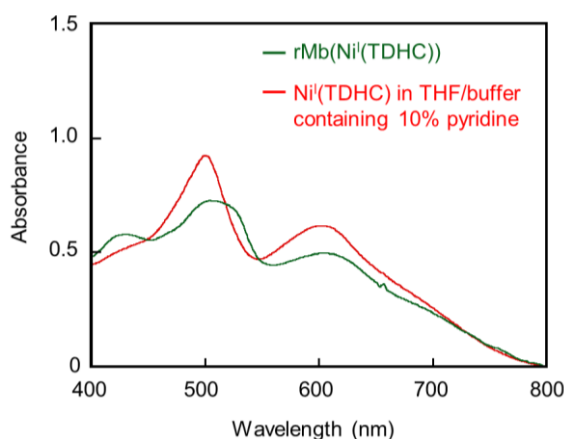


**Figure 1-9.** UV-vis spectra of rMb(Ni<sup>I</sup>(TDHC)) in 100 mM potassium phosphate buffer (pH 7.0) (green color) and Ni<sup>I</sup>(TDHC) in a mixture of THF/buffer ( $\nu/\nu = 1:1$ ) containing 10% pyridine (red color).

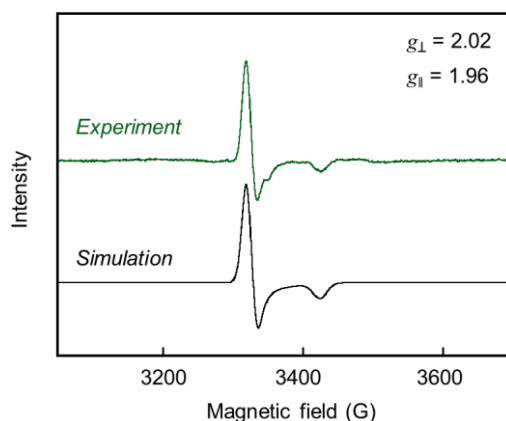


**Figure 1-10.** EPR spectrum of rMb(Ni<sup>I</sup>(TDHC)) in 100 mM potassium phosphate buffer (pH 7.0) at 20 K and the simulated spectrum.

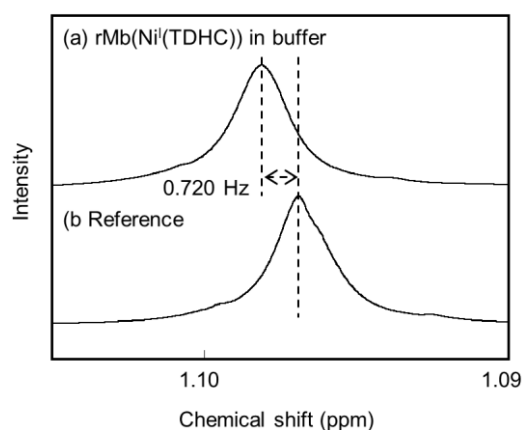


**Figure 1-11.** <sup>1</sup>H NMR (600 MHz) spectra of *t*-butanol in a 100 mM potassium phosphate buffer (pH 7.0) containing 10 % D<sub>2</sub>O: (a) with and (b) without rMb(Ni<sup>I</sup>(TDHC)). Conditions: Temperature = 25 °C, [rMb(Ni<sup>I</sup>(TDHC))] = 0.16 mM, [*t*-butanol] = 320 mM.

### Methane generation from an external methyl donor

Methane generation from methyl iodide using rMb(Ni<sup>I</sup>(TDHC))<sup>30</sup> in the presence of dithionite as a terminal reductant was carried out in buffer (pH 7.0) at 25 °C under an N<sub>2</sub> atmosphere. The GC traces and time-course plots of generated methane in the gas phase of the sealed reaction vial are shown in Fig. 1-12. Interestingly, rMb(Ni<sup>I</sup>(TDHC)) promotes generation of methane gas with an initial turnover frequency of 1.1 h<sup>-1</sup>. Methane generation was mostly complete within 1 h and other gaseous products, such as ethane, were not detected in the reaction. The protein matrix should play an important role in methane generation, because the bare Ni<sup>I</sup>(TDHC) complex generates negligible amounts of methane gas under the same conditions, apparently as a result of the significant difference in redox potentials of free Ni<sup>I</sup>(TDHC) and rMb(Ni<sup>I</sup>(TDHC)). Spectroelectrochemical measurement of rMb(Ni(TDHC)) shows the Ni<sup>II</sup>/Ni<sup>I</sup> redox potential of -0.65 V vs. Ag|AgCl (Fig. 1-13), which is negatively shifted by 0.11 V compared to that of Ni(TDHC) (Fig. 1-4). Furthermore, the author conducted the isotope-labeling experiment of the methane generation using <sup>13</sup>C-labeled methyl iodide with GC/MS (Fig. 1-14). The

quantitative isotope shift was observed in the mass analysis compared to the result using normal methyl iodide, showing the definitive evidence of the formation of the methane gas from methyl iodide. The turnover number reached 1.6 after the optimization of pH and substrate concentration (Fig. 1-15 and Table 1-1).<sup>31</sup> In the present study, the author employed methyl iodide as a methyl-group donor, which promotes the formation of the methyl–Ni(III) intermediate for ionic methane generation involving the protonation and reduction of the nickel center according to previous investigations using MCR and methyl iodide.<sup>3,6,7</sup> Thus, methane generation *via* a methyl–Ni(III) intermediate is also proposed in this study using rMb(Ni<sup>I</sup>(TDHC)) and methyl iodide. However, recent investigations of MCR propose the catalytic cycle *via* methyl radical species in the presence of the native substrates having the CH<sub>3</sub>–S group, while they clearly exclude the formation of the methyl–Ni(III) intermediate. Therefore, this work replicates the reactivity of MCR for methyl iodide.<sup>3</sup>

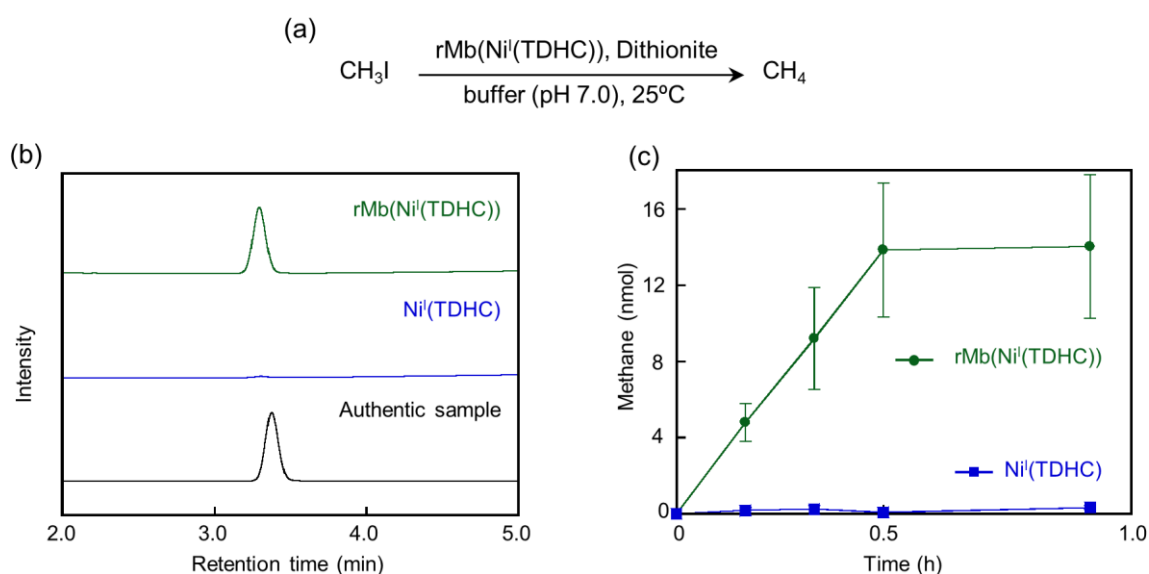


**Figure 1-12.** (a) Reaction leading to generation of methane. (b) GC traces of the reaction of methyl iodide with dithionite in the presence of rMb(Ni<sup>I</sup>(TDHC)) (green line) and free (Ni<sup>I</sup>(TDHC)) (blue line). Authentic methane gas is shown with a black line. (c) Time course plots of methane generation. Conditions: total volume = 500  $\mu\text{L}$ , [rMb(Ni<sup>I</sup>(TDHC))] or [Ni<sup>I</sup>(TDHC)] = 45  $\mu\text{M}$ , [CH<sub>3</sub>I] = 64.4 mM, [dithionite] = 1.0 mM in 100 mM potassium phosphate buffer (pH 7.0) at 25 °C under an N<sub>2</sub> atmosphere.

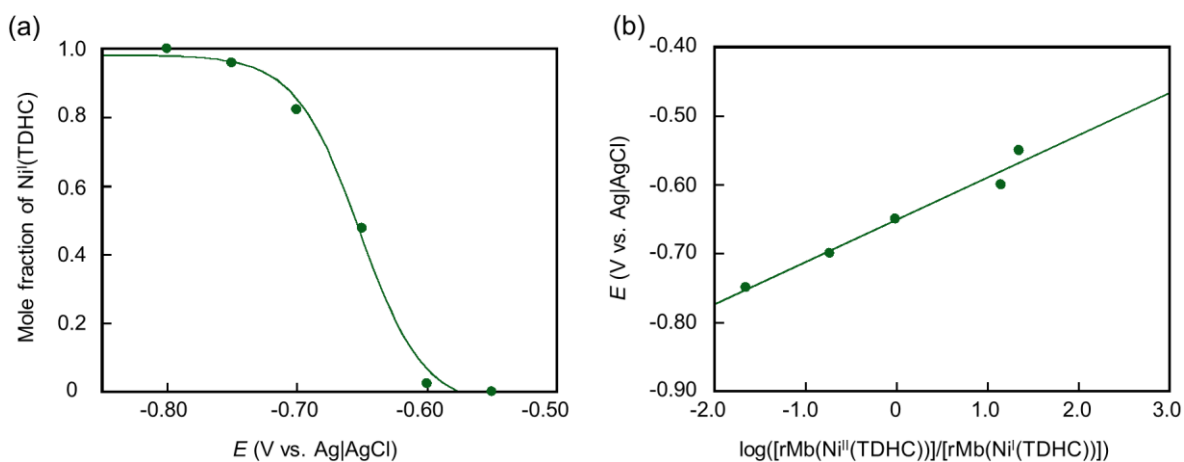


**Figure 1-13.** Nernst plots of the redox reaction of rMb(Ni(TDHC)) based on  $\Delta\text{Abs}(415 \text{ nm})$  values. (a) Plots with Nernst curves assuming one-electron redox process with  $E_m = -0.65 \text{ V vs. Ag|AgCl}$ . (b) Plots of  $E$  values against  $\log([r\text{Mb}(\text{Ni}^{\text{II}}(\text{TDHC}))]/[r\text{Mb}(\text{Ni}^{\text{I}}(\text{TDHC}))])$ . The line drawn by a least-squares fit to the plots gives a slope of 65 mV.

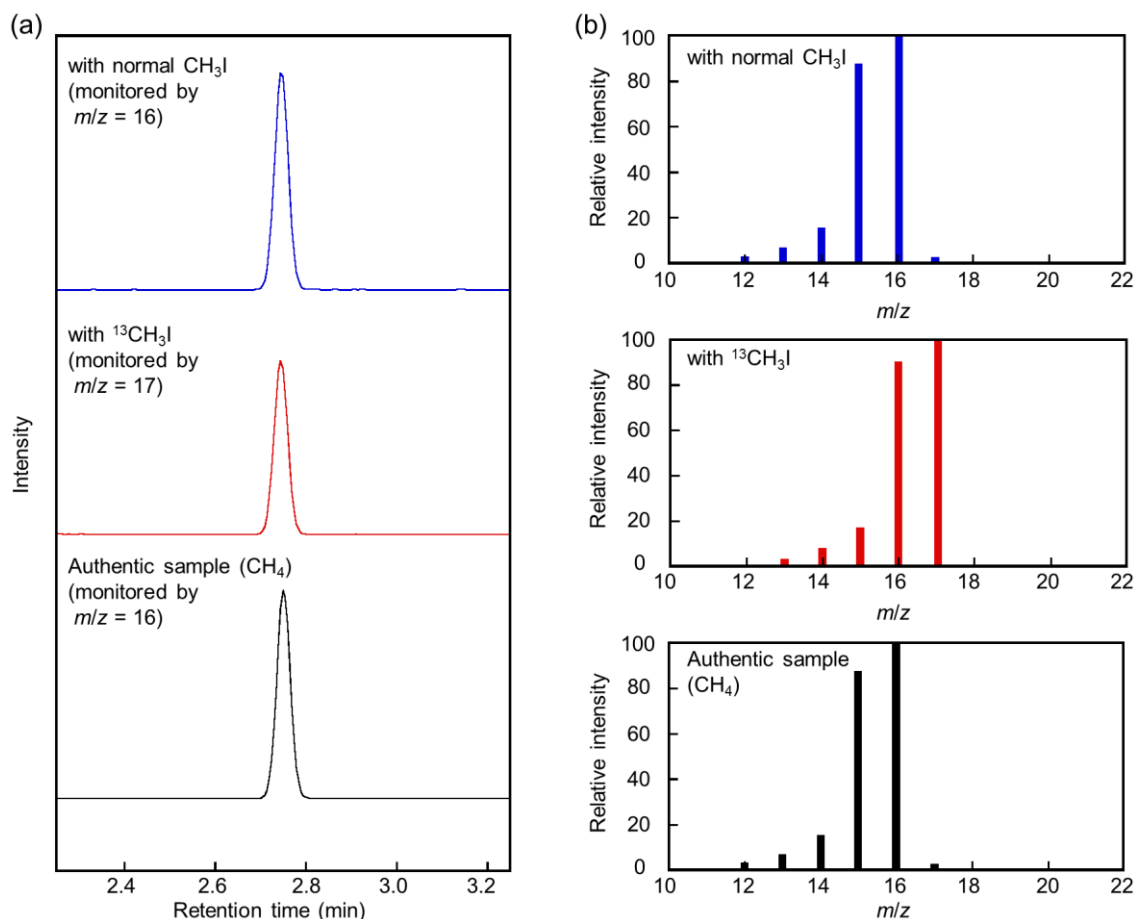


**Figure 1-14.** (a) GC/MS traces of the reaction using normal  $\text{CH}_3\text{I}$  monitoring  $^{12}\text{CH}_4$  ( $m/z = 16$ ) (top),  $^{13}\text{CH}_3\text{I}$  monitoring  $^{13}\text{CH}_4$  ( $m/z = 17$ ) (middle), and authentic gas sample monitoring  $^{12}\text{CH}_4$  ( $m/z = 16$ ) (bottom). (b) Mass spectra of  $\text{CH}_4$  generated from normal  $\text{CH}_3\text{I}$  (top) or  $^{13}\text{CH}_3\text{I}$  (middle) and of authentic gas of  $\text{CH}_4$  (bottom). Conditions: total volume = 1500  $\mu\text{L}$ ,  $[r\text{Mb}(\text{Ni}^{\text{I}}(\text{TDHC}))] = 45 \mu\text{M}$ ,  $[\text{normal } \text{CH}_3\text{I}]$  or  $[^{13}\text{CH}_3\text{I}] = 64.4 \text{ mM}$ ,  $[\text{dithionite}] = 1.0 \text{ mM}$  in 100 mM potassium phosphate buffer (pH 7.0) for 12 h at 25  $^\circ\text{C}$  under an  $\text{N}_2$  atmosphere.

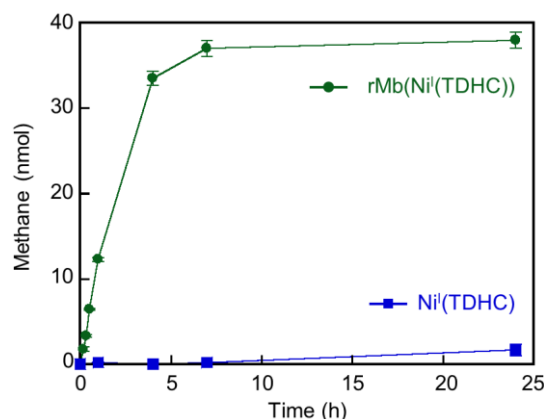


**Figure 1-15.** Time-course plots of methane generation. Conditions: total volume = 500  $\mu$ L, [rMb(Ni<sup>I</sup>(TDHC))] or [Ni<sup>I</sup>(TDHC)] = 45  $\mu$ M, [CH<sub>3</sub>I] = 20.0 mM, [dithionite] = 1.0 mM in 100 mM potassium phosphate buffer (pH 8.0) at 25 °C under an N<sub>2</sub> atmosphere.

**Table 1-1.** Turnover number (TON) in methane generation by rMb(Ni<sup>I</sup>(TDHC)) under various pH and substrate concentration conditions<sup>a</sup>

Entry	pH	[CH <sub>3</sub> I] (mM)	TON
1	6.0	64.4	0.22 $\pm$ 0.01
2	7.0	64.4	0.50 $\pm$ 0.08
3	8.0	64.4	0.65 $\pm$ 0.11
4	9.0	20.0	1.61 $\pm$ 0.04

[a] conditions: [rMb(Ni<sup>I</sup>(TDHC))] = 45  $\mu$ M, [dithionite] = 1.0 mM in 100 mM potassium phosphate buffer at 25 °C under an N<sub>2</sub> atmosphere.

### 1-3. Summary

In conclusion, reconstituted Mb with nickel tetrahydrocorrin serves as a functional model of MCR, generating methane with a relatively mild reductant. In contrast to F430 and previous model systems requiring strong reductants, such as Ti(III) citrate and NaHg, the TDHC ligand provides a complex which permits reduction by dithionite, a mild reductant.<sup>32</sup> The protein matrix, which provides a hydrophobic cavity and/or histidine ligation, appears to play an important role in shifting the redox potential, which activates the Ni(I) species to promote the methane generation. To the best of my knowledge, the present system is the first example of a protein-based functional model of MCR which generates methane using dithionite as a terminal reductant. The appreciable enhancement of methane generation compared with the control experiments in this work is important as a first step in model studies showing the essential insights into native enzymes.<sup>33,34</sup> The further improvement of the catalytic activity of the functional model will be demonstrated by mutation of the protein matrix and optimization of the synthetic cofactor. A suitable methyl group donor will be investigated to replicate the catalysis by MCR and to contribute to the elucidation of the reaction mechanism as well as the development of MCR-inspired artificial metalloenzymes.

## 1-4. Experimental section

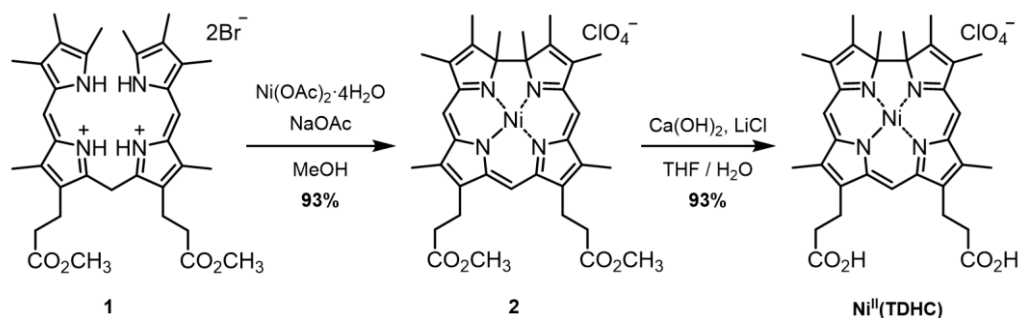
### Instruments

UV-vis spectral measurements were carried out with a UV-3150 or UV-2550 double-beam spectrophotometer (Shimadzu), a BioSpec-nano spectrometer (Shimadzu) or a V-670 spectrophotometer (JASCO). CD spectra were recorded at 25 °C on a J-820AC spectropolarimeter (JASCO). ESI-TOF MS analyses were performed with a micrOTOF-II mass spectrometer (Bruker). <sup>1</sup>H and <sup>13</sup>C NMR spectra were collected on an Avance III HD (400 MHz) spectrometer and an Avance III (600 MHz) spectrometer (Bruker). The <sup>1</sup>H NMR chemical shift values are reported in ppm relative to a residual solvent peak. EPR spectra were measured using an EMX Micro spectrophotometer (Bruker). pH measurements were made with an F-52 or F-72 pH meter (Horiba). ICP-OES was performed on an ICPS-7510 emission spectrometer (Shimadzu). Air-sensitive manipulations were performed in a UNILab glove box (MBRAUN). Methane gas generation was quantified by gas chromatography, GC-2014 (Shimadzu) equipped with a TCD detector or GC-2010 plus (Shimadzu) equipped with a BID detector. Methane gas generation using <sup>13</sup>C-labeled methyl iodide was evaluated by GCMS-QP2010 Ultra gas chromatograph mass spectrometer (Shimadzu).

### Materials and methods

All reagents of the highest guaranteed grade available were obtained from commercial sources and were used as received unless otherwise indicated. Distilled water was demineralized using a Millipore Integral 3 apparatus. 8,12-bis(2'-methoxycarbonyl)ethyl-1,2,3,7,13,17,18,19-octamethylbiladiene-*a,c* dihydrobromide **1** was synthesized according to the procedures reported in the literature.<sup>19</sup> A standard nickel solution for ICP-OES was purchased from FUJIFILM Wako Pure Chemical Corporation. Authentic CH<sub>4</sub> gas (0.408 % (v/v), balancer: argon) was purchased from GL Sciences Inc. A <sup>13</sup>C-labeled methyl iodide (99 atom % of <sup>13</sup>C) was purchased from Isotec Inc.

### Synthesis of Ni<sup>II</sup>(TDHC)



Scheme 1-1. Synthesis of Ni<sup>II</sup>(TDHC).

### 8,12-bis(2'-methoxycarbonyl)ethyl-1,2,3,7,13,17,18,19-octamethyltetradehydrocorrinatonicel(II)

**perchlorate (2).** 1,19-dimethylbiladiene-*a,c* dihydrobromide **1** (500 mg, 0.67 mmol), Ni(OAc)<sub>2</sub>·4H<sub>2</sub>O (500 mg, 2.0 mmol) and NaOAc (490 mg, 6.0 mmol) were dissolved in methanol (80 mL) and the solution was stirred for 1 h at

room temperature. The precipitate which was obtained upon addition of 150 mL of aqueous solution of  $\text{NaClO}_4 \cdot \text{H}_2\text{O}$  (6.6 g, 47 mmol) was filtered off, washed with water, and dried overnight. The product of nickel corrin derivative **2** was obtained by re-precipitation in a *n*-hexane/dichloromethane solution as a dark violet powder (46 mg, 0.62 mmol, 93% yield).  $^1\text{H}$  NMR (400 MHz,  $\text{CDCl}_3$ ):  $\delta$  7.68 (s, 1H), 7.47 (s, 2H), 3.67 (s, 6H), 3.37 (t,  $J = 7.3$  Hz, 4H), 2.83 (t,  $J = 7.3$  Hz, 4H), 2.64 (s, 6H), 2.52 (s, 6H), 2.50 (s, 6H), 0.61 (s, 6H). HRMS (ESI, positive mode,  $m/z$ ):  $[\text{M} - \text{ClO}_4]^+$  calcd. for  $\text{C}_{35}\text{H}_{41}\text{N}_4\text{O}_4\text{Ni}$ , 639.2476; found, 639.2478.

**8,12-dicarboxyethyl-1,2,3,7,13,17,18,19-octamethyltetrahydrocorrinatonicel(II) perchlorate ( $\text{Ni}^{\text{II}}(\text{TDHC})$ ).**

The dimethyl ester of the tetrahydrocorrin nickel complex **2** (400 mg, 0.54 mmol),  $\text{Ca}(\text{OH})_2$  (23 mg, 3.1 mmol) and  $\text{LiCl}$  (1.9 g, 44 mmol) were dissolved in THF (200 mL) and water (200 mL) and then stirred at 40 °C for 2 h under an  $\text{N}_2$  atmosphere. To the solution, citric acid (6.6 g, 34 mmol) was added and the solution was extracted with dichloromethane. The organic layer was washed with brine and dried over anhydrous  $\text{Na}_2\text{SO}_4$  and the solvent was evaporated under reduced pressure. The residue was re-precipitated from *n*-hexane/dichloromethane to yield tetrahydrocorrin nickel complex,  $\text{Ni}^{\text{II}}(\text{TDHC})$ , as a dark violet powder (380 mg, 0.53 mmol, 98% yield).  $^1\text{H}$  NMR (600 MHz,  $\text{CD}_2\text{Cl}_2$ ):  $\delta = 7.96$  (s, 1H), 7.36 (s, 2H), 3.34 (m, 4H), 2.84 (m, 4H), 2.59 (s, 6H), 2.47 (s, 6H), 2.45 (s, 6H), 0.58 (s, 6H).  $^{13}\text{C}$  NMR (150 MHz,  $\text{CD}_2\text{Cl}_2$ ):  $\delta$  164.12, 159.98, 157.99, 155.97, 145.14, 141.34, 135.11, 124.84, 98.87, 98.21, 92.07, 36.00, 25.38, 20.78, 13.70, 10.41, 9.98. HRMS (ESI, positive mode,  $m/z$ ):  $[\text{M} - \text{ClO}_4]^+$  calcd. for  $\text{C}_{33}\text{H}_{37}\text{N}_4\text{O}_4\text{Ni}$ , 611.2163; found, 611.2155. UV-vis ( $\text{H}_2\text{O}$ , (nm)  $\epsilon$  ( $\text{M}^{-1} \cdot \text{cm}^{-1}$ )):  $\lambda_{\text{max}} = 271.5$  (25300), 349.5 (27200), 452.5 (4590), 551.0 (11200).

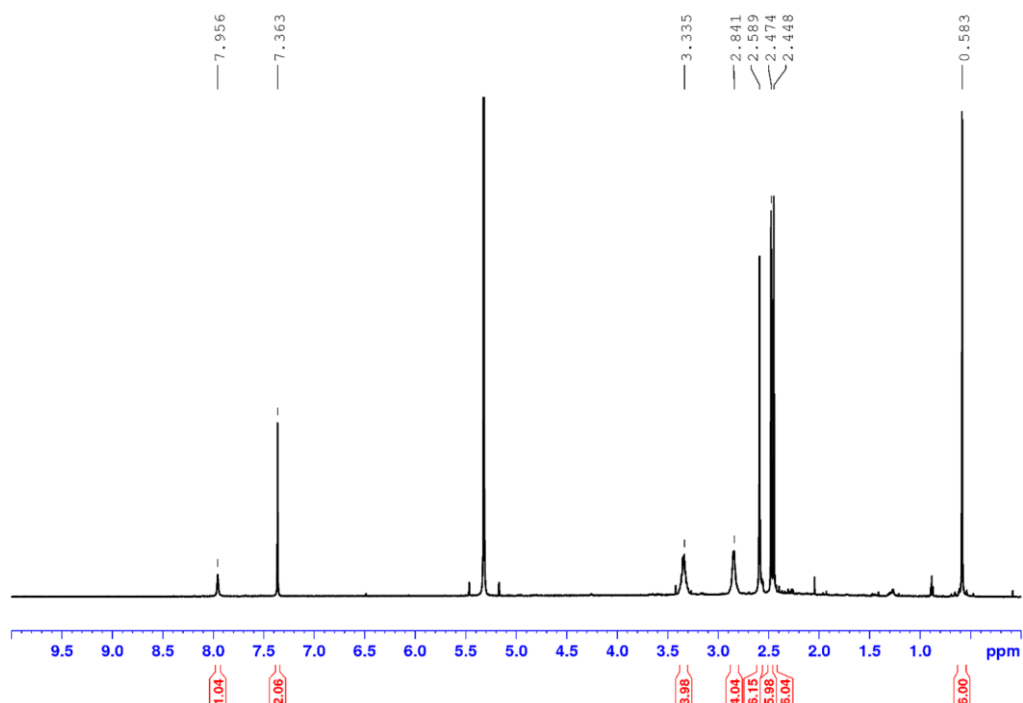


**Figure 1-16.**  $^1\text{H}$  NMR spectrum (600 MHz,  $\text{CD}_2\text{Cl}_2$ ) of  $\text{Ni}^{\text{II}}(\text{TDHC})$ .

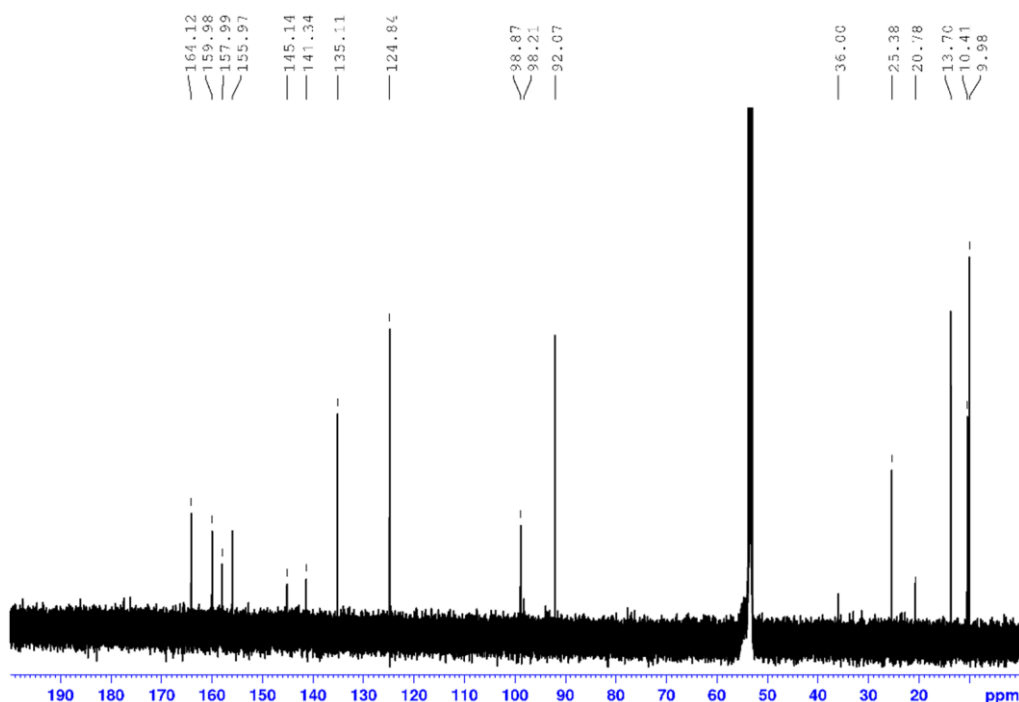


**Figure 1-17.**  $^{13}\text{C}$  NMR spectrum (150 MHz,  $\text{CD}_2\text{Cl}_2$ ) of  $\text{Ni}^{\text{II}}(\text{TDHC})$ .

### X-ray crystal structural analysis of $\text{Ni}^{\text{II}}(\text{TDHC})$

Crystals of  $\text{Ni}^{\text{II}}(\text{TDHC})$  suitable for x-ray crystallography were grown by vapor diffusion of benzene into a saturated acetone solution. The crystals were mounted on the CryoLoop (Hampton Research Corp.) with a light mineral oil and placed in an  $\text{N}_2$  stream at 113 K. All measurements were carried out on a Rigaku XtaLAB P200 diffractometer, which is equipped with a rotating anode X-ray source (Mo  $K\alpha$  radiation) and a hybrid photon counting detector (PILATUS 200K). The cell refinements were performed with a CrystalClear software package (Data Collection and Processing Software Package, Rigaku Corp.). All of the crystallographic calculations were performed using the CrystalStructure software package (Crystal Structure Analysis Software Package, Version 4.2.4, Rigaku Corp.). The structures were solved by direct method (SIR92).<sup>35</sup> Non-hydrogen atoms were refined anisotropically by full-matrix least-squares on  $F^2$  using SHELXL Version 2016/6.<sup>36</sup> The structure in the final stage of the refinement showed no movement in the atom position. Hydrogen atoms were attached at idealized positions on carbon atoms and not refined. Crystal data and structural refinement parameters were listed below (Table 1-2). The CCDC number is 1912367. This data can be obtained from The Cambridge Crystallographic Data Centre *via* [www.ccdc.cam.ac.uk/data\\_request/cif](http://www.ccdc.cam.ac.uk/data_request/cif).

**Table 1-2.** Crystal data and data collection parameters

Compounds	Ni <sup>II</sup> (TDHC)
CCDC Number	1912367
Empirical formula	C <sub>45</sub> H <sub>49</sub> ClN <sub>4</sub> NiO <sub>8</sub>
Formula weight	868.06
Temperature (K)	113(1)
Wavelength (Å)	0.71075
Crystal system	monoclinic
Space group	<i>P2/c</i> (#13)
a (Å)	12.121(2)
b (Å)	16.582(2)
c (Å)	10.8113(19)
α (deg.)	90.0000
β (deg.)	102.320(4)
γ (deg.)	90.0000
Volume (Å <sup>3</sup> )	2123.0(6)
Z	2
Density (calculated) (g/cm <sup>3</sup> )	1.358
μ[Mo-Kα], (/cm)	5.778
Crystal size (mm)	0.200 x 0.170 x 0.020
Theta range for data collection	3.099- 25.242
No. of reflections measured	26732
Unique data ( <i>R</i> <sub>int</sub> )	4875 (0.0795)
Data/restraints/parameters	4875/4/287
<i>R</i> 1 <sup>a</sup> ( <i>I</i> > 2.0σ( <i>I</i> ))	0.0649
<i>wR</i> 2 <sup>b</sup> ( <i>I</i> > 2.0σ( <i>I</i> ))	0.1895
<i>R</i> 1 <sup>a</sup> (all data)	0.0912
<i>wR</i> 2 <sup>b</sup> (all data)	0.2047
GOF on <i>F</i> <sup>2</sup>	1.011
Δρ, e/Å <sup>3</sup>	1.00, -0.81

[a]  $R1 = (\sum||F_o| - |F_c||) / (\sum|F_o|)$ , [b]  $wR2 = [\{\sum w(F_o^2 - F_c^2)^2\} / \{\sum w(F_o^4)\}]^{1/2}$

### Preparation of rMb(Ni<sup>I</sup>(TDHC))

Horse heart Mb was purchased from Sigma-Aldrich and purified by CM-Cellulose cation exchange column (FUJIFILM Wako Pure Chemical Corp.). Removal of heme from Mb was performed along with the reported procedure.<sup>37</sup> To a solution of Ni<sup>II</sup>(TDHC) (500 µL in total, final conc. 50 µM) and dithionite (final conc. 1.0 mM) in 100 mM potassium phosphate buffer (pH 7.0), an apoMb solution (final conc. 150 µM) in 100 mM potassium phosphate buffer (pH 7.0) was added under an N<sub>2</sub> atmosphere at 25 °C. The obtained rMb(Ni<sup>I</sup>(TDHC)) aqueous solution (final conc. 45 µM) was used for experiments without purification unless otherwise indicated.

### Determination of the dissociation constant of rMb(Ni<sup>I</sup>(TDHC))

Titration experiments were conducted by addition of an apoMb solution (final conc. 0 to 90 µM) in 100 mM potassium phosphate buffer (pH 7.0) to a solution (500 µL in total) of Ni<sup>II</sup>(TDHC) (final conc. 30 µM) and dithionite (final conc. 600 µM) in 100 mM potassium phosphate buffer (pH 7.0) at 25 °C under an N<sub>2</sub> atmosphere. After standing for 5 min at 25 °C under an N<sub>2</sub> atmosphere, UV-vis spectra were measured using an optical cell with a 1-cm path length (Figure 1-7a). The absorbance at 600 nm was plotted against the concentration of apoMb and fitted by non-linear least squares equation (1-1) (Figure 1-7b). According to the calculation, the dissociation constant of rMb(Ni<sup>I</sup>(TDHC)) was determined to be 11 µM.

$$\Delta A_{obs} = \frac{b \cdot \Delta \varepsilon}{2 \cdot K} \cdot \left[ 1 + K \cdot [\text{apoMb}] + K \cdot [\text{Ni(TDHC)}]_0 - \left\{ (1 + K \cdot [\text{apoMb}] + K \cdot [\text{Ni(TDHC)}]_0)^2 - 4 \cdot K^2 \cdot [\text{apoMb}] \cdot [\text{Ni(TDHC)}]_0 \right\}^{\frac{1}{2}} \right] \quad (1-1)$$

$$K_d = \frac{1}{K} \quad (1-2)$$

where  $\Delta A_{obs}$  is the differential absorbance generated by subtraction of the absorbance of free Ni<sup>I</sup>(TDHC) at 600 nm,  $b$  is the optical path length (cm),  $\Delta \varepsilon$  is the difference of absorption coefficient between rMb(Ni<sup>I</sup>(TDHC)) and free Ni<sup>I</sup>(TDHC),  $K$  is the binding constant ( $\mu\text{M}^{-1}$ ),  $K_d$  is the dissociation constant ( $\mu\text{M}$ ),  $[\text{apoMb}]$  is the concentration of apoMb ( $\mu\text{M}$ ), and  $[\text{Ni}^{\text{I}}(\text{TDHC})]_0$  is the initial concentration of Ni<sup>I</sup>(TDHC) ( $\mu\text{M}$ ).

### Determination of the concentration of rMb(Ni<sup>I</sup>(TDHC))

The concentration of rMb(Ni<sup>I</sup>(TDHC)) in an aqueous solution was calculated with equation (1-3) using the determined dissociation constant and the concentration of Ni<sup>I</sup>(TDHC) and apoMb.

$$\left[ \text{rMb} \left( \text{Ni}^{\text{I}}(\text{TDHC}) \right) \right] = \frac{([\text{Ni}^{\text{I}}(\text{TDHC})]_0 + [\text{apoMb}]_0 + K_d)}{2} - \frac{\sqrt{([\text{Ni}^{\text{I}}(\text{TDHC})]_0 + [\text{apoMb}]_0 + K_d)^2 - 4 \cdot [\text{Ni}^{\text{I}}(\text{TDHC})]_0 \cdot [\text{apoMb}]_0}}{2} \quad (1-3)$$

where  $[rMb(Ni^I(TDHC))]$  is the concentration of  $rMb(Ni^I(TDHC))$  ( $\mu M$ ),  $[Ni^I(TDHC)]_0$  is the initial concentration of  $Ni^I(TDHC)$  ( $\mu M$ ),  $[apoMb]_0$  is the initial concentration of  $apoMb$  ( $\mu M$ ), and  $K_d$  is the dissociation constant ( $\mu M$ ).

### Spectroelectrochemistry

Spectroelectrochemical measurements were carried out at 25 °C using an optically transparent thin-layer electrode cell (optical path length of 1 mm) under an Ar atmosphere. A Pt mesh working electrode and a Pt wire counter electrode were used along with an Ag|AgCl reference electrode (3 M NaCl<sub>aq.</sub>, from ALS Co., Ltd.). The potentials of these electrodes were controlled and measured with a potentiostat (CompactStat, Ivium Technologies). A solution of  $Ni(TDHC)$  (0.50 mM) and  $rMb(Ni(TDHC))$  (0.19 mM) with methyl viologen (0.40 mM) as an electron mediator was prepared in 100 mM potassium phosphate buffer (pH 7.0). At each applied potential, the electronic absorption spectra were monitored until no further spectral changes were detected. The data were fitted to the Nernst equation and the number of electrons included in the reaction was determined through its fitting curve.

### EPR measurements

EPR spectroscopic measurements were performed with an EMXmicro spectrometer (Bruker) at the X-band (9.44 GHz) microwave frequency. A solution of  $Ni^I(TDHC)$  (1.0 mM) was prepared in a mixture of THF/100 mM potassium phosphate buffer (pH 7.0) ( $v/v = 1:1$ ) and its EPR spectrum was recorded with 4.0 mW microwave power and 10 G modulation amplitude at 100 K using liquid N<sub>2</sub> vapor. A solution of  $rMb(Ni^I(TDHC))$  (0.52 mM) was prepared in 100 mM potassium phosphate buffer (pH 7.0) and its EPR spectrum was measured with 0.013 mW microwave power and 10 G of modulation amplitude at 20 K using liquid He vapor. The prepared sample was quickly frozen in a cold pentane bath chilled with liquid N<sub>2</sub>. Processing and simulation were conducted with WinEPR software package (Bruker).

### Evans method

The effective magnetic moments and the number of unpaired electrons of  $Ni^I(TDHC)$  and  $rMb(Ni^I(TDHC))$  were determined using the Evans method.<sup>38-40</sup> <sup>1</sup>H NMR spectra of 3% *t*-butanol were measured in a mixture of THF/100 mM potassium phosphate buffer (pH 7.0) ( $v/v = 1:1$ ) containing 10% D<sub>2</sub>O in the presence and absence of  $Ni^I(TDHC)$  (1.0 mM). <sup>1</sup>H NMR spectra of 3% *t*-butanol were measured in 100 mM potassium phosphate buffer (pH 7.0) containing 10% D<sub>2</sub>O in the presence and absence of  $rMb(Ni^I(TDHC))$  (0.16 mM). A sealed capillary filled with 1,4-dioxane as a reference was placed in each NMR tube containing sample solution. The difference of chemical shifts of the *t*-butanol protons between the samples in the presence and absence of nickel species was used to calculate the effective magnetic moment and the number of unpaired electrons. The equations below were used in the analysis.

$$\chi_M^{para} (m^3/mol) = \frac{3 \cdot \Delta\delta \cdot 10^{-6}}{1000 \cdot M} \quad (1-4)$$

$$\mu_{eff} = \sqrt{\frac{3 \cdot \chi_M^{para} \cdot k \cdot T \cdot \mu_0}{N_A} \cdot \frac{1}{\mu_B}} \quad (1-5)$$

$$\mu_{eff} = g \cdot \sqrt{S \cdot (S + 1)} = \sqrt{n \cdot (n + 1)} \quad (1-6)$$

where  $\chi_M^{para}$  is molar susceptibility,  $\Delta\delta$  is difference of chemical shift of *t*-butanol in ppm in the presence and absence of nickel species,  $M$  is concentration of nickel species in mol/L,  $\mu_{eff}$  is the effective magnetic moment,  $k$  is the Boltzmann constant ( $1.38 \times 10^{-23} \text{ J}\cdot\text{K}^{-1}$ ),  $T$  is temperature in K,  $N_A$  is the Avogadro constant ( $6.02 \times 10^{23} \text{ mol}^{-1}$ ),  $\mu_0$  is the magnetic permeability of a vacuum ( $4 \times \pi \times 10^{-7} \text{ T}^2 \cdot \text{m}^3 \cdot \text{J}^{-1}$ ),  $\mu_B$  is the Bohr magneton ( $9.27 \times 10^{-24} \text{ J}\cdot\text{T}^{-1}$ ),  $g$  is the  $g$  value for electron spin (2.002),  $S$  is the spin state, and  $n$  shows the number of unpaired electron.

### Methane generation reaction

In a 2.0 mL vial sealed with a silicon septum, a solution of rMb(Ni<sup>I</sup>(TDHC)) (final conc. 45  $\mu\text{M}$ ) or Ni<sup>I</sup>(TDHC) (final conc. 45  $\mu\text{M}$ ), dithionite (final conc. 1.0 mM), and methyl iodide (final conc. 20.0 mM or 64.4 mM) dissolved in 100 mM potassium phosphate buffer (pH 6.0 – 9.0) (500  $\mu\text{L}$  in total) was prepared. After stirring at 25 °C for 10 min – 24 h, the headspace-gas was analyzed by GC. The product was identified by a comparison of its retention time with that of the authentic standard sample. The amount of methane gas was determined from the area of the corresponding eluted peak using the calibration curve. Two following analytic procedures depending on GC apparatuses were used and confirmed to produce the same results.

(1) The gas sample (1000  $\mu\text{L}$ ) was carefully taken from the headspace of the vial by a gastight syringe while the same volume of water was compensated to prevent the pressure change. The gas sample was injected into a GC-2014 (Shimadzu) equipped with a TCD detector, a Chromatopac Integrator C-R8A (Shimadzu) and a 2.0 m  $\times$  3.0 mm ID packed column ACTIVATED CHARCOAL 60-80 mesh using argon as a carrier gas. Measurement conditions: injector temperature = 120 °C, detector temperature = 120 °C, column temperature = 60 °C, flow rate 50 mL/min.

(2) The gas sample (100  $\mu\text{L}$ ) was carefully taken from the headspace of the vial by a gastight syringe. Because of the small volume against the headspace (1.5 mL), the pressure change was ignored relative to the other experimental errors. The gas sample was injected into a GC-2010 plus (Shimadzu) equipped with a BID detector and a 2.0 m  $\times$  1.0 mm ID micropacked column SHINCARBON-ST 80-100 mesh using helium as a carrier gas. Measurement conditions: injector temperature = 200 °C, split ratio 5:1, detector temperature = 250 °C, column temperature = 60 °C (1 min hold) – 18 °C/min – 220 °C (2 min hold), flow rate 55.8 mL/min.

## Reference and notes

1. B. C. McBride, R. S. Wolfe, *Biochemistry* **1971**, *10*, 2317–2324.
2. D. Ankel-Fuchs, R. K. Thauer, *Eur. J. Biochem.* **1986**, *156*, 171–177.
3. R. K. Thauer, *Biochemistry* **2019**, *58*, 5198–5220.
4. S. Scheller, M. Goenrich, R. Boecher, R. K. Thauer, B. Jaun, *Nature* **2010**, *465*, 606–608.
5. M. Krüger, A. Meyerdierks, F. O. Glöckner, R. Amann, F. Widdel, M. Kube, R. Reinhardt, R. Kahnt, R. Böcher, R. K. Thauer, S. Shima, *Nature* **2003**, *426*, 878–881.
6. M. Dey, J. Telser, R. C. Kunz, N. S. Lees, S. W. Ragsdale, B. M. Hoffman, *J. Am. Chem. Soc.* **2007**, *129*, 11030–11032.
7. P. E. Cedervall, M. Dey, X. Li, R. Sarangi, B. Hedman, S. W. Ragsdale, C. M. Wilmot, *J. Am. Chem. Soc.* **2011**, *133*, 5626–5628.
8. T. Wongnate, D. Sliwa, B. Ginovska, D. Smith, M. W. Wolf, N. Lehnert, S. Raugei, S. W. Ragsdale, *Science* **2016**, *352*, 953–958.
9. V. Pelmeshikov, M. R. A. Blomberg, P. E. M. Siegbahn, R. H. Crabtree, *J. Am. Chem. Soc.* **2002**, *124*, 4039–4049.
10. S. L. Chen, M. R. A. Blomberg, P. E. M. Siegbahn, *Phys. Chem. Chem. Phys.* **2014**, *16*, 14029–14035.
11. C. Mbofana, M. Zimmer, *Inorg. Chem.* **2006**, *45*, 2598–2602.
12. E. C. Duin, M. L. Mckee, *J. Phys. Chem. B* **2008**, *112*, 2466–2482.
13. A. Ghosh, T. Wondimagegn, H. Ryeng, *Curr. Opin. Chem. Biol.* **2001**, *5*, 744–750.
14. G. K. Lahiri, L. J. Schussel, A. M. Stolzenberg, *Inorg. Chem.* **1992**, *31*, 4991–5000.
15. U. E. Krone, K. Laufer, R. K. Thauer, H. P. C. Hogenkamp, *Biochemistry* **1989**, *28*, 10061–10065.
16. J. Nishigaki, T. Matsumoto, K. Tatsumi, *Inorg. Chem.* **2012**, *51*, 5173–5187.
17. M. W. Renner, L. R. Furenlid, K. M. Barkigia, A. Forman, H. K. Shim, D. J. Simpson, K. M. Smith, J. Fajer, *J. Am. Chem. Soc.* **1991**, *113*, 6891–6898.
18. R. Piskorski, B. Jaun, *J. Am. Chem. Soc.* **2003**, *125*, 13120–13125.
19. T. Hayashi, Y. Morita, E. Mizohata, K. Oohora, J. Ohbayashi, T. Inoue, Y. Hisaeda, *Chem. Commun.* **2014**, *50*, 12560–12563.
20. Y. Morita, K. Oohora, A. Sawada, T. Kamachi, K. Yoshizawa, T. Hayashi, *Inorg. Chem.* **2017**, *56*, 1950–1955.
21. C. Brenig, L. Prieto, R. Oetterli, F. Zelder, *Angew. Chem. Int. Ed.* **2018**, *57*, 16308–16312.
22. K. Oohora, A. Onoda, T. Hayashi, *Acc. Chem. Res.* **2019**, *52*, 945–954.
23. K. Oohora, H. Meichin, L. Zhao, M. W. Wolf, A. Nakayama, J. Hasegawa, N. Lehnert, T. Hayashi, *J. Am. Chem. Soc.* **2017**, *139*, 17265–17268.
24. K. Oohora, H. Meichin, Y. Kihira, H. Sugimoto, Y. Shiro, T. Hayashi, *J. Am. Chem. Soc.* **2017**, *139*, 18460–18463.
25. R. Grigg, W. A. Johnson, R. Kenyon, B. V. Math, K. Richardson, *J. Chem. Soc. C* **1969**, 176–182.
26. G. Färber, W. Keller, C. Kratky, B. Jaun, A. Pfaltz, C. Spinner, A. Kobelt, A. Eschenmoser, *Helv. Chim. Acta* **1991**, *74*, 697–716.

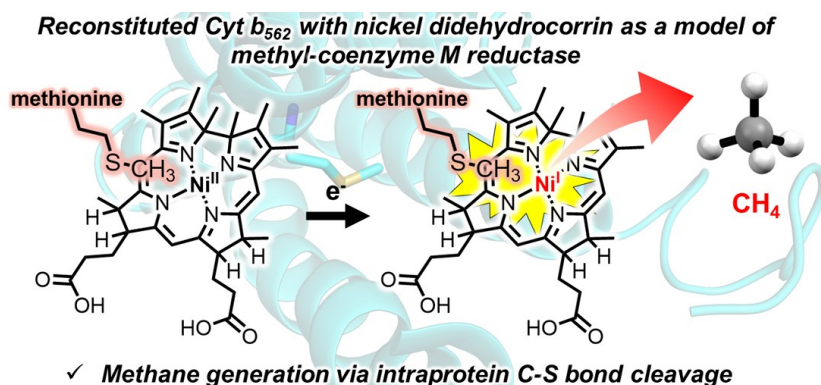
27. S. V. Kryatov, B. S. Mohanraj, V. V. Tarasov, O. P. Kryatova, E. V. Rybak-Akimova, B. Nuthakki, J. F. Rusling, R. J. Staples, A. Y. Nazarenko, *Inorg. Chem.* **2002**, *41*, 923–930.
28. There is possibility of the assignment as a Ni<sup>II</sup>(TDHC)  $\pi$ -anion radical with some Ni(I) character or a Ni(I) and Ni(II)  $\pi$ -anion radical hybrid according to previous report: K. M. Kadish, M. M. Franzen, B. C. Han, C. Araullo-McAdams, D. Sazou, *J. Am. Chem. Soc.* **1991**, *113*, 512–517.
29. C. Holliger, A. J. Pierik, E. J. Reijerse, W. R. Hagen, *J. Am. Chem. Soc.* **1993**, *115*, 5651–5656.
30. The final concentration of rMb(Ni<sup>I</sup>(TDHC)) is determined to be 45  $\mu$ M by the dissociation constant (11  $\mu$ M) and initial concentration of apoMb (150  $\mu$ M) and Ni<sup>I</sup>(TDHC) (50  $\mu$ M). The experiment of methane generation was carried out without purification of the reconstituted protein because the UV-vis spectra before and after the purification are almost identical.
31. The decrease of the concentration of methyl iodide seems to decelerate the unfavorable deactivation/decomposition of Ni(TDHC).
32. E. J. Reijerse, M. Sommerhalter, P. Hellwig, A. Quentmeier, D. Rother, C. Laurich, E. Bothe, W. Lubitz, C. G. Friedrich, *Biochemistry* **2007**, *46*, 7804–7810.
33. E. N. Mirts, A. Bhagi-Damodaran, Y. Lu, *Acc. Chem. Res.* **2019**, *52*, 935–944.
34. N. Yeung, Y.-W. Lin, Y.-G. Gao, X. Zhao, B. S. Russell, L. Lei, K. D. Miner, H. Robinson, Y. Lu, *Nature* **2009**, *462*, 1079–1082.
35. A. Altomare, G. Cascarano, C. Giacovazzo, A. Guagliardi, *J. Appl. Cryst.* **1993**, *26*, 343.
36. G. M. Sheldrick, *Acta Cryst.* **2008**, *A64*, 112–122.
37. F. W. Teale, *Biochim. Biophys. Acta* **1959**, *35*, 543.
38. D. F. Evans, *J. Chem. Soc.* **1959**, 2003–2005.
39. G. A. Bain, J. F. Berry, *J. Chem. Edu.* **2008**, *85*, 532–536.
40. S. K. Sur, *J. Magn. Reson.* **1989**, *82*, 169–173.

## Chapter 2

### Methane generation *via* intraprotein C–S bond cleavage in reconstituted cytochrome *b*<sub>562</sub> with nickel didehydrocorrin

Reproduced in part with permission from [*J. Organomet. Chem.* **2019**, *901*, 120945.]

DOI: 10.1016/j.jorganchem.2019.120945



#### 2-1. Introduction

Methane has been investigated both as an alternative fuel and a greenhouse gas. Most of the methane gas in nature is generated as a metabolite of organic compounds by archaea under anaerobic conditions.<sup>1,2</sup> Methanogenic archaea are known to have the enzyme, methyl-coenzyme M reductase (MCR), which catalyzes the rate-limiting and final step of biological methane generation.<sup>3-5</sup> This reaction is promoted by a nickel hydrocorphinoid cofactor, well known as F430, in the active site. Methyl-coenzyme M ( $\text{CH}_3\text{S-CoM}$ ) and coenzyme B ( $\text{HS-CoB}$ ) are converted to methane and the heterodisulfide compound ( $\text{CoM-S-S-CoB}$ ) by the active Ni(I) intermediate in the enzymatic reaction (Fig. 2-1).

In spite of various experimental and theoretical studies, the reaction mechanism of MCR has not yet been completely elucidated because of the complicated structures of F430 and MCR.<sup>6-27</sup> At this moment, two plausible reaction mechanisms have been proposed and they include formation of an organometallic methyl–Ni(III) intermediate or a transient methyl radical intermediate.<sup>5</sup> In the former case, the stable methyl–Ni(III) intermediate is observed in a reaction of the active MCR containing the Ni(I) species of F430 with methyl iodide.<sup>13-17</sup> The latter mechanism is more plausible according to a recent study which included a detailed analysis of single turnover reaction of MCR with substrates having the  $\text{CH}_3\text{-S}$  group, which are similar to native substrates.<sup>22</sup> In this context, an appropriate model complex of F430 has been required to properly evaluate the physicochemical property and reactivity of F430.<sup>28-32</sup> Although some model complexes achieved methane gas generation from activated methyl donors, examples of methane gas generation *via* C–S bond cleavage have been quite limited. Jaun and coworkers demonstrated that photoirradiation of a Ni(II) complex with a thiolate-thioether ligand, bis{1-[2-(methylthio)ethyl]cyclohexanethiolato}nickel, in the presence of the corresponding thiol-thioether substrate, 1-[2-(methylthio)ethyl]cyclohexanethiol, generated methane gas and the disulfide 1,2-dithiaspiro[4.5]decane *via* cleavage

of the C–S bond.<sup>30</sup> Tatsumi and coworkers also reported that chemical reduction of Ni(II) complexes using azacyclam ligands having thioether group, such as 1,8-dimethyl-4,11-bis{(2-methylthio)ethyl}-1,4,8,11-tetraaza-1,4,8,11-cyclotetradecane and 1,8-{bis(2-methylthio)ethyl}-1,4,8,11-tetraaza-1,4,8,11-cyclotetradecane, generated methane and ethane gases *via* intramolecular C–S bond cleavage. The larger amount of methane gas was generated upon addition of a thiol compound, 2,6-dimesitylbenzenethiol.<sup>31</sup> These model complexes mimicking the enzymatic system have provided important insights into the understanding of the reaction mechanism of MCR.

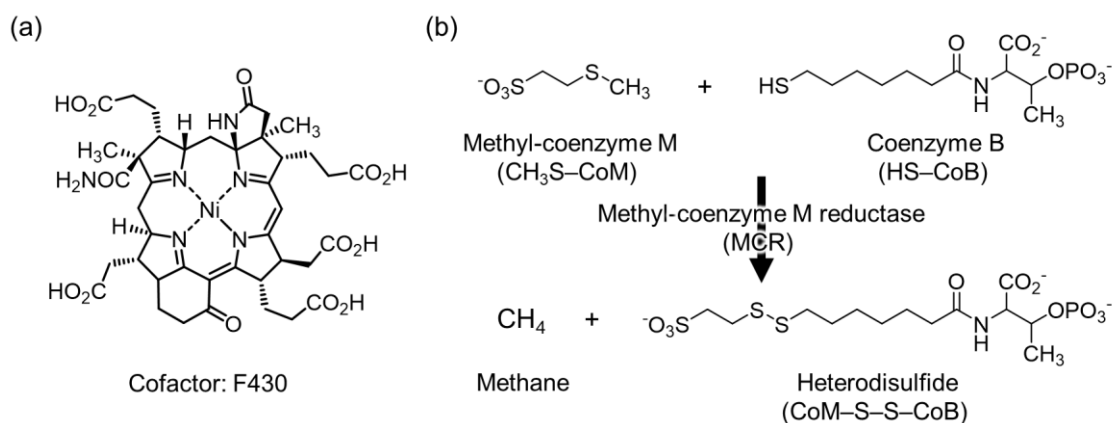


**Figure 2-1.** (a) Molecular structure of cofactor F430. (b) Methane generation catalyzed by MCR in methanogenic archaea.

In Chapter 1, the author described a protein-based functional MCR model which is prepared by myoglobin (Mb) reconstituted with nickel tetradehydrocorrin (Ni(TDHC)) as a model complex of F430.<sup>33</sup> The active Ni(I) species was identified in the presence and absence of the protein matrix of Mb. The protein-based functional model was found to promote methane gas generation from methyl iodide, whereas the bare Ni<sup>I</sup>(TDHC) complex does not generate any significant amounts of methane gas under the same condition, indicating the importance of a protein matrix. However, even the Ni(I) species in the protein matrix of Mb appears to be insufficient to activate a substrate having a CH<sub>3</sub>–S group as seen in enzymatic reaction by MCR. Thus, the author constructed a different type of protein-based functional model of MCR by conjugation of nickel didehydrocorrin (Ni(DDHC)) and the apo-form of cytochrome *b*<sub>562</sub> (Cyt *b*<sub>562</sub>) in order to enhance the reactivity of the Ni(I) species and replicate methane generation *via* C–S bond cleavage (Fig. 2-2). This is because the Ni(I) species of Ni(DDHC) is expected to be a more reactive than that of Ni(TDHC). Previous investigations have found that the nucleophilicity of the Co(I) species of cobalt didehydrocorrin (Co(DDHC)) is enhanced relative to the Co(I) species of cobalt tetradehydrocorrin (Co(TDHC)).<sup>34,35</sup> In addition, Cyt *b*<sub>562</sub> should be a suitable protein matrix because the CH<sub>3</sub>–S group of the methionine residue, Met7, is located close to the metal center in the heme pocket. In Chapter 2, methane gas generation *via* intraprotein C–S bond cleavage of Met7 is demonstrated using reconstituted Cyt *b*<sub>562</sub> upon photoreduction of the nickel center.

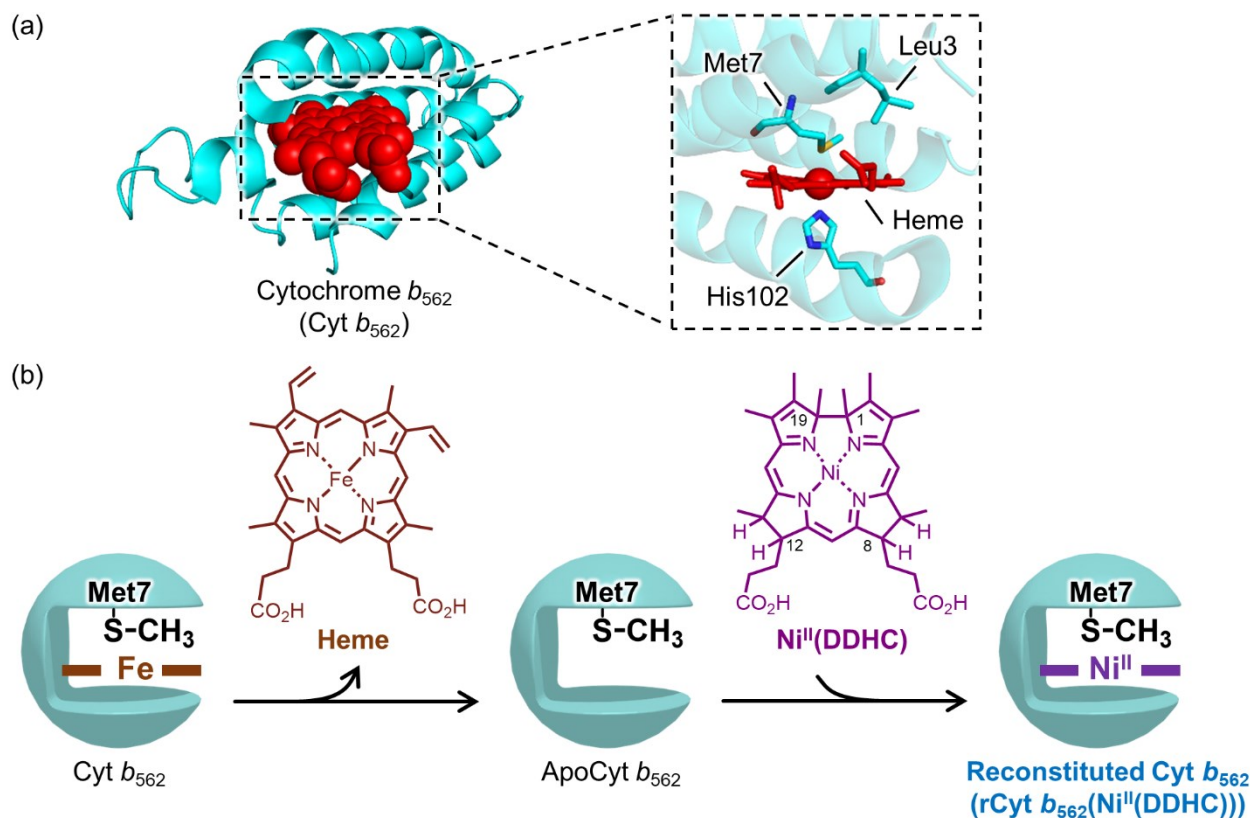


**Figure 2-2.** (a) Structure of Cyt  $b_{562}$  (PDB ID: 1QPU). (b) Schematic representation of the reconstitution of Cyt  $b_{562}$  with Ni(DDHC).

## 2-2. Results and discussion

### Synthesis and characterization of Ni<sup>II</sup>(DDHC)

The author designed a Ni(DDHC) cofactor having a monoanionic tetrapyrrole ligand and two propionate side chains at the C8- and C12-positions for the purpose of fixing the cofactor in the proper position *via* a hydrogen bonding network with polar amino acid residues in the heme binding pocket. Hydrogenation of Ni<sup>II</sup>(TDHC) with Pd/C and H<sub>2</sub> produced Ni<sup>II</sup>(DDHC). The ESI-TOF mass spectrum of Ni<sup>II</sup>(DDHC) provides a peak at  $m/z = 615.2478$  with a characteristic isotope pattern of a compound containing nickel ion, which is consistent with the calculated exact mass number for  $[\text{M}-\text{ClO}_4]^+$  (calcd.:  $m/z = 615.2476$ ). The UV-vis spectrum shows characteristic peaks at 264, 295, 321, and 453 nm in an aqueous solution (Fig. 2-3). The CV measurements revealed two reversible redox peaks at  $-0.61$  and  $0.44$  V vs. Ag|AgCl in acetonitrile as shown in Fig. 2-4. The former redox peak is assigned to the Ni<sup>II</sup>/Ni<sup>I</sup> process, which is negatively shifted by 0.16 V compared to that of Ni<sup>II</sup>(TDHC) (Fig. 2-5), indicating the enhanced reactivity of the Ni(I) species. The latter redox peak appears to be attributed to the Ni<sup>III</sup>/Ni<sup>II</sup> process, which is not observed in Ni<sup>II</sup>(TDHC). The range of redox potentials corresponding to the Ni<sup>II</sup>/Ni<sup>I</sup> process at  $-0.61$  V vs. Ag|AgCl and the Ni<sup>III</sup>/Ni<sup>II</sup> process at  $0.44$  V vs. Ag|AgCl are narrower compared to the reported potential data of the pentamethyl ester of F430 (Ni<sup>II</sup>/Ni<sup>I</sup>:  $-0.70$  V in dimethylformamide, Ni<sup>III</sup>/Ni<sup>II</sup>:  $1.25$  V in acetonitrile).<sup>6-8</sup>

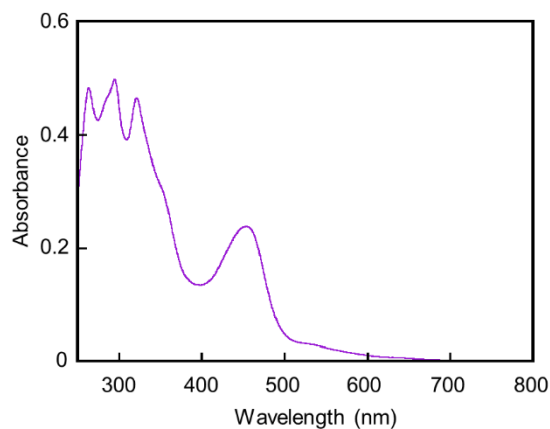


**Figure 2-3.** UV-vis spectrum of Ni<sup>II</sup>(DDHC) in 100 mM potassium phosphate buffer (pH 7.0) at 25 °C.

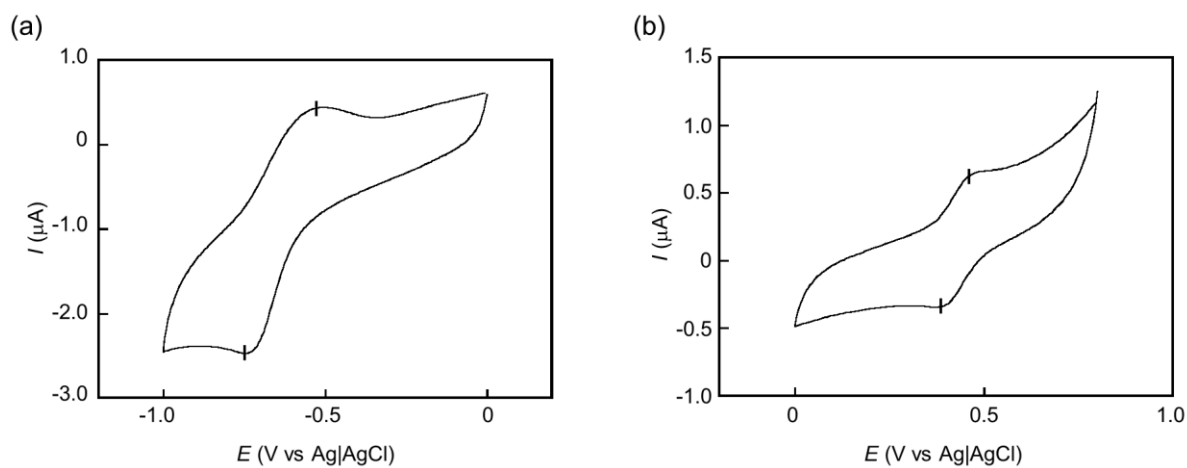


**Figure 2-4.** Cyclic voltammograms of Ni<sup>II</sup>(DDHC) in anhydrous acetonitrile with 100 mM TBAPF<sub>6</sub> with a scan rate of 100 mV/s under an N<sub>2</sub> atmosphere. Sweeping range: (a) -1.0 to 0 V, (b) 0 to 0.8 V.

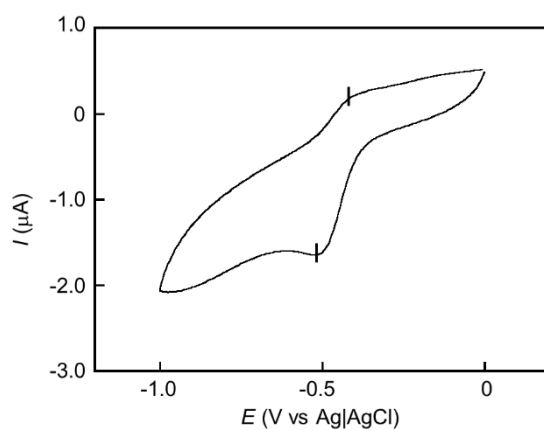


**Figure 2-5.** Cyclic voltammogram of Ni<sup>II</sup>(TDHC) in anhydrous acetonitrile with 100 mM TBAPF<sub>6</sub> with a scan rate of 100 mV/s under an N<sub>2</sub> atmosphere. Sweeping range: -1.0 to 0 V.

## Preparation and characterization of reconstituted Cyt $b_{562}$

Cyt  $b_{562}$  has the hydrophobic cofactor-binding cavity which provides a hexa-coordinated structure of the native heme with two axial ligands, His102 and Met7 (Fig. 2-2),<sup>36</sup> and the CH<sub>3</sub>-S group of Met7 side chain is expected to work as an intraprotein methyl donor. The insertion of Ni<sup>II</sup>(DDHC) into the apo-form of Cyt  $b_{562}$  (apoCyt  $b_{562}$ ) provided reconstituted Cyt  $b_{562}$ , rCyt  $b_{562}$ (Ni<sup>II</sup>(DDHC)), as a protein-based model of MCR. The UV-vis spectra do not show significant changes upon addition of apoCyt  $b_{562}$  to a Ni<sup>II</sup>(DDHC) aqueous solution (Fig. 2-6a). In contrast, the addition of Ni<sup>II</sup>(DDHC) to an apoCyt  $b_{562}$  aqueous solution exhibits stronger CD signals at 208 and 222 nm derived from  $\alpha$ -helices compared to those of apoCyt  $b_{562}$ , supporting the formation of the reconstituted protein (Fig. 2-6b). In fact, according to previous investigations of hemoprotein reconstitutions, the insertion of metal complexes into the binding pocket of the apoprotein promotes re-folding of the protein matrices, involving stronger Cotton effects in the ultraviolet region.<sup>37,38</sup> However, the binding affinity of Ni<sup>II</sup>(DDHC) to apoCyt  $b_{562}$  appears to be relatively low because the increase of CD spectral intensity in the ultraviolet region is less than the increase of CD spectral intensity caused by binding of hemin. Assuming complete refolding of the  $\alpha$ -helices upon addition of the metal complex, 27% of Cyt  $b_{562}$  is reconstituted with Ni<sup>II</sup>(DDHC) compared to Cyt  $b_{562}$  fully reconstituted with hemin, which is estimated by the intensity at 222 nm under conventional conditions. Furthermore, ESI-TOF mass spectrum gives a peak at  $m/z = 2497.5$ , which is consistent with the calculated mass number of rCyt  $b_{562}$ (Ni<sup>II</sup>(DDHC)) ( $m/z = 2497.3$  ( $z = 5+$ )) (Fig. 2-7).<sup>39</sup> The conjugation of Ni<sup>II</sup>(TDHC) and apoCyt  $b_{562}$  also produces rCyt  $b_{562}$ (Ni<sup>II</sup>(TDHC)), which is confirmed by UV-vis and CD spectral measurements (Fig. 2-8).

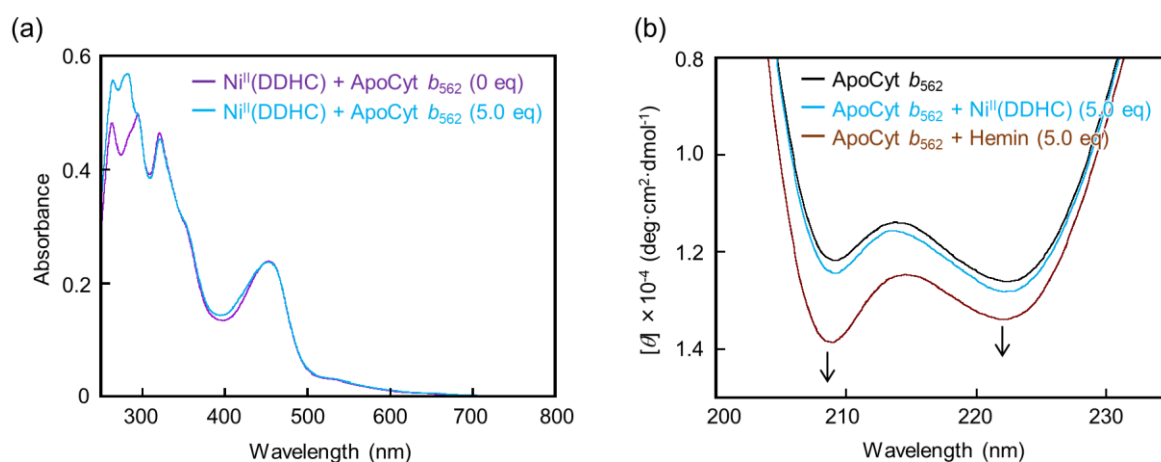


**Figure 2-6.** (a) UV-vis spectral changes of Ni<sup>II</sup>(DDHC) (purple line) upon addition of 5.0 eq of apoCyt  $b_{562}$  (cyan line) in 100 mM potassium phosphate buffer (pH 7.0) at 25 °C. (b) CD spectral changes of apoCyt  $b_{562}$  (black line) upon addition of 5.0 eq of Ni<sup>II</sup>(DDHC) (cyan line) or hemin (brown line) in 100 mM potassium phosphate buffer (pH 7.0) at 25 °C.

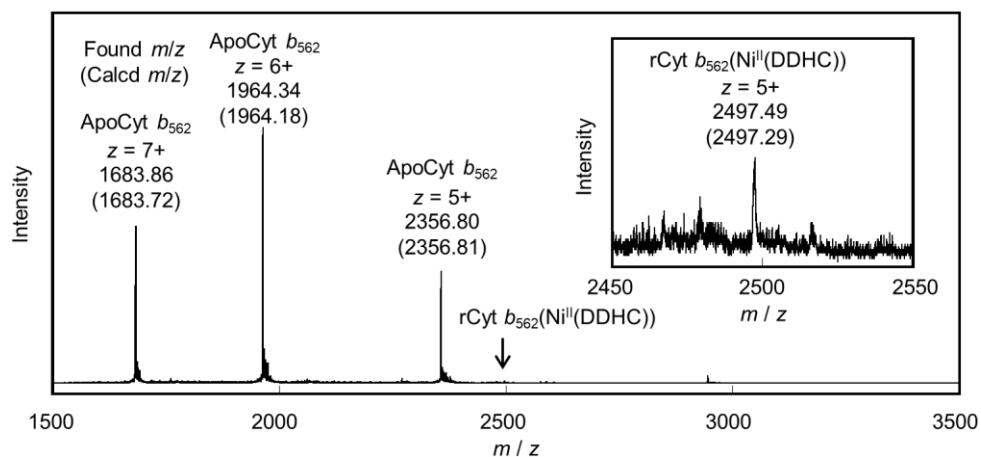


**Figure 2-7.** ESI-TOF MS for the characterization of rCyt  $b_{562}(\text{Ni}^{\text{II}}(\text{DDHC}))$ . The sample in 50 mM ammonium acetate buffer was analyzed. Inset: the peak consistent with rCyt  $b_{562}(\text{Ni}^{\text{II}}(\text{DDHC}))$ .

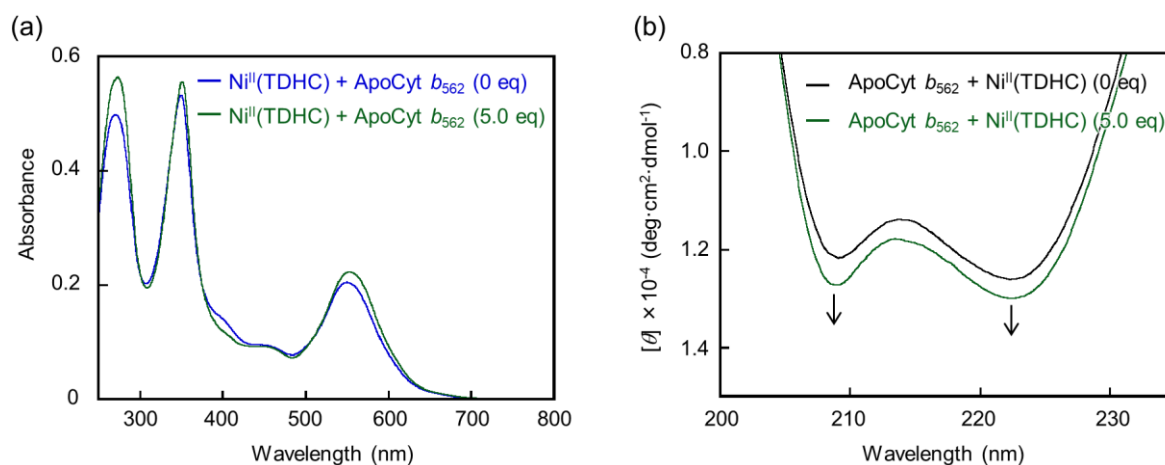


**Figure 2-8.** (a) UV-vis spectral changes of  $\text{Ni}^{\text{II}}(\text{TDHC})$  (blue line) upon addition of 5.0 eq of apoCyt  $b_{562}$  (green line) in 100 mM potassium phosphate buffer (pH 7.0) at 25 °C. (b) CD spectral changes of apoCyt  $b_{562}$  (black line) upon addition of 5.0 eq of  $\text{Ni}^{\text{II}}(\text{TDHC})$  (green line) in 100 mM potassium phosphate buffer (pH 7.0) at 25 °C.

### Photo-induced methane generation from reconstituted Cyt $b_{562}$

Methane gas generation from reconstituted Cyt  $b_{562}$  was then demonstrated in 100 mM potassium phosphate buffer (pH 7.0) at 25 °C under an  $\text{N}_2$  atmosphere. First, the author used dithionite or Ti(III) citrate to reduce  $\text{Ni}^{\text{II}}(\text{DDHC})$  in the protein matrix, but methane gas generation was not observed. Therefore, the author tried to reduce the  $\text{Ni}^{\text{II}}(\text{DDHC})$  complex with photoirradiation in the presence of tris(2,2'-bipyridine)ruthenium(II) chloride as a photosensitizer and sodium ascorbate as a sacrificial reagent. A solution of  $\text{Ni}^{\text{II}}(\text{DDHC})$  or  $\text{Ni}^{\text{II}}(\text{TDHC})$  (final conc.: 50  $\mu\text{M}$ ), apoCyt  $b_{562}$  (final conc.: 150  $\mu\text{M}$ ), tris(2,2'-bipyridine)ruthenium(II) chloride (final conc.: 100  $\mu\text{M}$ ), and sodium ascorbate (final conc.: 100 mM) dissolved in 100 mM potassium phosphate buffer (pH 7.0) (100  $\mu\text{L}$  in total) was prepared. After 2 h of photoirradiation with a Xe-lamp, gaseous products were analyzed and quantified by gas chromatography (GC). The GC traces for evaluation of the amounts of methane gas are shown in Fig. 2-9 and the

retention time of observed peaks for methane gases which are generated from the reconstituted proteins are consistent with the retention time of authentic methane gas. Other gaseous products such as ethane were not detected in the reaction. Fig. 2-10 summarizes the methane generation results produced by Ni<sup>II</sup>(DDHC), the apoprotein, and reconstituted Cyt *b*<sub>562</sub> variants. Although control experiments with Ni<sup>II</sup>(DDHC) itself or apoCyt *b*<sub>562</sub> generated negligible amounts of methane gas, a small amount of methane gas (24 pmol, yield: 0.16% based on apoCyt *b*<sub>562</sub> and turnover number (TON): 0.0049 based on Ni(TDHC)) was observed from rCyt *b*<sub>562</sub>(Ni<sup>II</sup>(TDHC)). Interestingly, a 12-fold greater amount of methane gas (290 pmol, yield: 1.9% based on apoCyt *b*<sub>562</sub> and TON: 0.057 based on Ni(DDHC)) was generated from rCyt *b*<sub>562</sub>(Ni<sup>II</sup>(DDHC)) compared to the amount of methane gas generated from rCyt *b*<sub>562</sub>(Ni<sup>II</sup>(TDHC)). The efficient methane gas generation from rCyt *b*<sub>562</sub>(Ni<sup>II</sup>(DDHC)) is likely due to the difference in the reactivity of the Ni(I) species as expected by the CV measurements. As shown in Fig. 2-4 and 5, the redox potential of Ni<sup>II</sup>(DDHC) for the Ni<sup>II</sup>/Ni<sup>I</sup> process is more negative than that of Ni<sup>II</sup>(TDHC), indicating higher reactivity of the Ni(I) species of Ni(DDHC). Furthermore, the redox potential of rCyt *b*<sub>562</sub>(Ni<sup>II</sup>(DDHC)) in a buffer solution appears to be more negative than that of rCyt *b*<sub>562</sub>(Ni<sup>II</sup>(TDHC)), as seen in the negatively shifted redox potential of Co(DDHC) compared to Co(TDHC) regardless of the presence and absence of the protein matrix.<sup>35</sup>

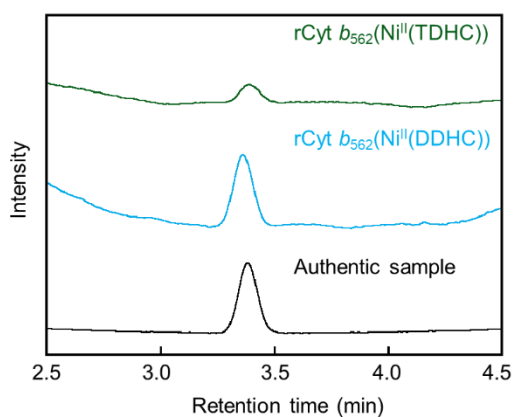


**Figure 2-9.** GC traces of the reaction with rCyt *b*<sub>562</sub>(Ni<sup>II</sup>(TDHC)) (green line) and rCyt *b*<sub>562</sub>(Ni<sup>II</sup>(DDHC)) (cyan line) in the presence of tris(2,2'-bipyridine)ruthenium(II) chloride and sodium ascorbate in 100 mM potassium phosphate buffer (pH 7.0) at 25 °C under an N<sub>2</sub> atmosphere. Authentic methane gas is shown with a black line.

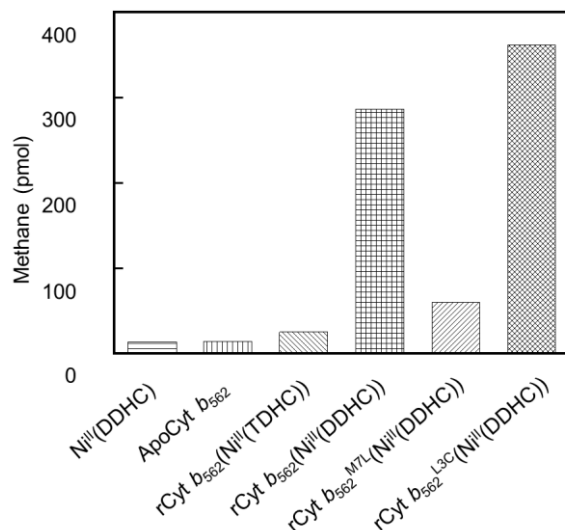


**Figure 2-10.** Generated amounts of methane from Ni<sup>II</sup>(DDHC), apoCyt *b*<sub>562</sub>, rCyt *b*<sub>562</sub>(Ni<sup>II</sup>(TDHC)), rCyt *b*<sub>562</sub>(Ni<sup>II</sup>(DDHC)), rCyt *b*<sub>562</sub><sup>M7L</sup>(Ni<sup>II</sup>(DDHC)), and rCyt *b*<sub>562</sub><sup>L3C</sup>(Ni<sup>II</sup>(DDHC)) after 2 h of photoirradiation. Conditions: Total volume 100  $\mu$ L, [Ni<sup>II</sup>(DDHC)] = 50  $\mu$ M, [ApoCyt *b*<sub>562</sub> variant] = 150  $\mu$ M, [[Ru(bpy)<sub>3</sub>]Cl<sub>2</sub>] = 100  $\mu$ M, [Sodium ascorbate] = 100 mM in 100 mM potassium phosphate buffer (pH 7.0) for 2 h at 25  $^{\circ}$ C under an N<sub>2</sub> atmosphere.

In nature, cofactor and substrates are precisely arranged within the protein matrix of MCR.<sup>11,12,27,28</sup> According to the crystal structure of MCR, methyl-coenzyme M binds to the hydrophobic pocket above F430 with a predominant electrostatic interaction between the protein matrix and its sulfonate tail, showing that the CH<sub>3</sub>-S group of methyl-coenzyme M is located close to and oriented towards the cofactor.<sup>11,12,17,25</sup> On the other hand, the thiol group of coenzyme B is found to be placed at a proper distance from methyl-coenzyme M and F430 within the funnel-shaped and substrate binding channel of MCR. These suitable arrangements of substrates and active cofactor are required to cleave the C-S bond and generate methane gas. Generally, the proximity effect promotes a reaction between an amino acid residue and an active cofactor in the protein matrix. For example, Watanabe and coworkers reported the hydroxylation of the Trp43 residue which is located close to high-valent iron(IV)-oxo complex of heme within the binding pocket of the F43W/H64L mutant of Mb.<sup>40,41</sup> Hayashi and coworkers also reported transmethylation from methylated Co(TDHC) to His64 which is located above the cofactor within Mb reconstituted with Co(TDHC).<sup>42</sup> According to these examples, the author proposes that the Ni(I) species of Ni(DDHC) activates the CH<sub>3</sub>-S group of Met7 close to the metal center within the heme-binding pocket of Cyt *b*<sub>562</sub> to produce methane gas in the present study although the detailed reaction mechanism is currently under investigation. To confirm the possibility of the CH<sub>3</sub>-S group of Met7 as an intraprotein substrate, the author employed a mutated protein matrix, Cyt *b*<sub>562</sub><sup>M7L</sup>, in which Met7 was substituted with Leu7. The significant decrease of methane gas generation was observed from rCyt *b*<sub>562</sub><sup>M7L</sup>(Ni<sup>II</sup>(DDHC)) (60 pmol, yield: 0.40% based on apoCyt *b*<sub>562</sub><sup>M7L</sup> and TON: 0.012 based on Ni(DDHC)) (Fig. 2-10). This is because the protein matrix lacks the suitable intraprotein methyl donor, the CH<sub>3</sub>-S group of Met7, in the active site. To evaluate the demethylation of the protein matrices, mass spectral analyses were

conducted after isolation and concentration of protein matrices of rCyt  $b_{562}$ (Ni<sup>II</sup>(DDHC)) and rCyt  $b_{562}^{M7L}$ (Ni<sup>II</sup>(DDHC)). The ESI-TOF mass spectrum of rCyt  $b_{562}$ (Ni<sup>II</sup>(DDHC)) after the reaction has characteristic peaks at  $m/z = 1964.42$  ( $z = 6+$ ) and  $1961.59$  ( $z = 6+$ ) as shown in Fig. 2-11a. The former peak is assigned to the protein matrix of apoCyt  $b_{562}$  (calcd.:  $m/z = 1964.18$  ( $z = 6+$ )), whereas the latter is consistent with the calculated  $m/z$  for demethylated apoCyt  $b_{562}$  where one methyl group is absent from the protein matrix (calcd.:  $m/z = 1961.84$  ( $z = 6+$ )). In contrast, the ESI-TOF mass spectrum of rCyt  $b_{562}^{M7L}$ (Ni<sup>II</sup>(DDHC)) after the reaction has a single peak at  $m/z = 1961.34$  ( $z = 6+$ ) as shown in Fig. 2-11b. This peak is attributed to the protein matrix of apoCyt  $b_{562}^{M7L}$  (calcd.:  $m/z = 1961.18$  ( $z = 6+$ )) suggesting that the demethylation of any residues in rCyt  $b_{562}^{M7L}$ (Ni<sup>II</sup>(DDHC)) is excluded. Thus, the protein matrix of rCyt  $b_{562}^{M7L}$ (Ni<sup>II</sup>(DDHC)) retains its molecular weight after the reaction. The present findings indicate that methane is clearly derived from Met7 *via* C–S bond cleavage by the active Ni(I) species of Ni(DDHC).

Cyt  $b_{562}^{L3C}$ , a Cyt  $b_{562}$  mutant in which Leu3 is substituted with Cys3, was also prepared in order to provide and fix a thiol group mimicking another native substrate, coenzyme B, close to the reaction center (Fig. 2-2a). Interestingly, the Cys3 residue clearly increases the amount of methane gas generation (360 pmol, yield: 2.4% based on apoCyt  $b_{562}^{L3C}$  and TON: 0.072 based on Ni(DDHC)) by 24% compared to rCyt  $b_{562}$ (Ni<sup>II</sup>(DDHC)) as shown in Fig. 2-10. This finding suggests that the thiol group of Cys3 promotes a hydrogen transfer to produce methane as seen in the thiol group of coenzyme B in the reaction scaffold of MCR.

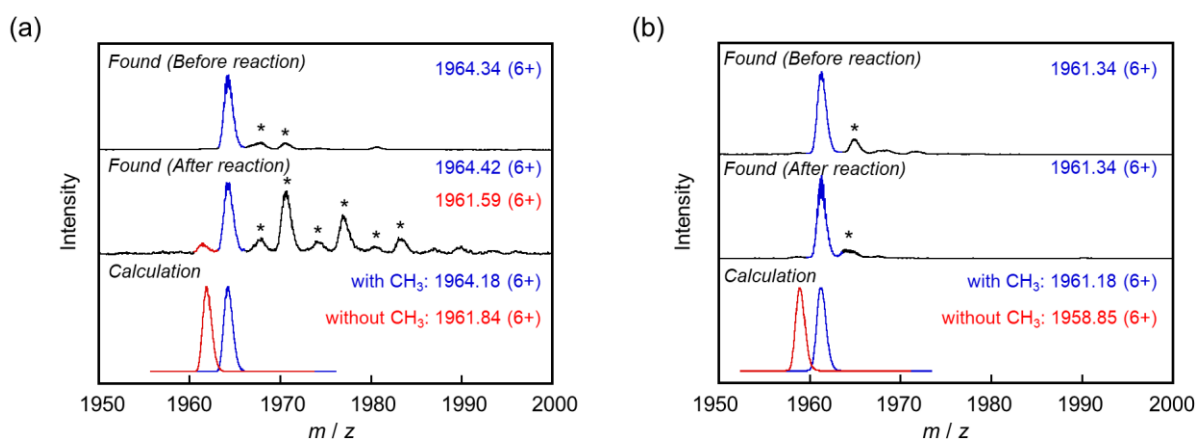


**Figure 2-11.** ESI-TOF mass spectra of protein matrices of (a) rCyt  $b_{562}$ (Ni<sup>II</sup>(DDHC)) and (b) rCyt  $b_{562}^{M7L}$ (Ni<sup>II</sup>(DDHC)). Upper and middle spectra show the results obtained before and after the reaction, respectively. Bottom profiles represent the calculated spectra showing protein matrices retaining the CH<sub>3</sub> group (blue line) and losing one CH<sub>3</sub> group (red line). The asterisks in (a) and (b) indicate potassium and sodium adducts of the protein matrices, respectively.

### 2-3. Summary

Ni<sup>II</sup>(DDHC) is an appropriate model complex of F430 compared to Ni<sup>II</sup>(TDHC), because the more negative Ni<sup>II</sup>/Ni<sup>I</sup> redox potential of Ni(DDHC) is expected to provide a highly reactive Ni(I) species compared to that of Ni(TDHC). Therefore, in the present investigation, methane gas generation was initiated with Ni<sup>I</sup>(DDHC) in the Cyt  $b_{562}$  matrix which has a thioether group derived from the methionine residue in the cofactor binding cavity.

Photoirradiation of rCyt  $b_{562}(\text{Ni}^{\text{II}}(\text{DDHC}))$  in the presence of a photosensitizer and a sacrificial reagent resulted in efficient methane generation. Furthermore, comparison of the results of methane generation and mass changes of protein matrices between rCyt  $b_{562}(\text{Ni}^{\text{II}}(\text{DDHC}))$  and rCyt  $b_{562}^{\text{M7L}}(\text{Ni}^{\text{II}}(\text{DDHC}))$  provides evidence that methane is derived from the  $\text{CH}_3\text{-S}$  group of Met7 *via* C–S bond cleavage by the reactive Ni(I) species in the protein matrix. In addition, the generation of methane gas from rCyt  $b_{562}^{\text{L}^{3\text{C}}}(\text{Ni}^{\text{II}}(\text{DDHC}))$  is found to be enhanced compared to methane generated from rCyt  $b_{562}(\text{Ni}^{\text{II}}(\text{DDHC}))$ . These results clearly indicate that precise arrangements of the thioether, the thiol, and the nickel center provide efficient methane generation *via* C–S bond cleavage in the protein matrix. Therefore, methane generation by the reconstituted protein is promoted not only by having an appropriate nickel complex but also by the precise arrangements of thiol and thioether moieties in the second coordination sphere. Two key residues, Met7 and Cys3, are regarded as substrate models of methyl-coenzyme M and coenzyme B, respectively. To the best of my knowledge, this study is the first example of methane gas generation *via* intraprotein C–S bond cleavage using a protein-based functional model of MCR. Further studies on methane gas generation *via* C–S bond cleavage within a protein matrix will contribute to the elucidation of the reaction mechanism of MCR as well as the development of artificial metalloenzymes inspired by MCR.

## 2-4. Experimental section

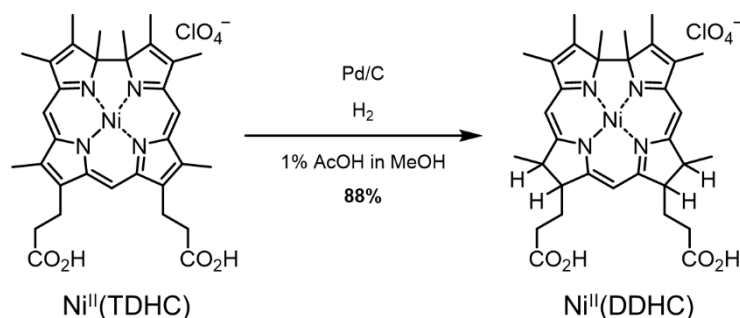
### Instruments

UV-vis spectral measurements were carried out with a BioSpec-nano spectrophotometer (Shimadzu) or a V-670 spectrophotometer (JASCO). CD spectra were recorded on a J-820AC spectropolarimeter (JASCO). ESI-TOF MS analyses were performed with a micrOTOF-II mass spectrometer (Bruker).  $^1\text{H}$  NMR spectrum was collected on an Avance III (600 MHz) spectrometer (Bruker). The  $^1\text{H}$  NMR chemical shift values are reported in ppm relative to a residual solvent peak. ICP-OES was performed on an ICPS-7510 emission spectrometer (Shimadzu). Electrochemical studies were performed using a potentiostat (CompactStat, Ivium Technologies). A single-compartment cell was used for all cyclic voltammetry (CV) experiments with a polished Pt working electrode, a Pt wire counter electrode and an Ag|AgCl (3 M  $\text{NaCl}_{\text{aq}}$ , from ALS Co., Ltd.) reference electrode. All electrochemical experiments were performed with 100 mM tetrabutylammonium hexafluorophosphate ( $\text{TBAPF}_6$ ) as a supporting electrolyte. All solutions were purged with  $\text{N}_2$  before CV measurements. Air-sensitive manipulations were performed in a UNILab glove box (MBRAUN). Purification by HPLC was conducted with a HPLC Prominence System (Shimadzu). Size exclusion chromatographic (SEC) purification was performed using an ÄKTApurifier system (GE Healthcare). The pH measurements were made with an F-72 pH meter (Horiba). Photoirradiation reaction was conducted using an Optical Modulex (USHIO Inc.) equipped with a 500 W Xe arc lamp, a cold filter (Asahi Spectra Co., Ltd.), and a 420 nm sharp cut filter (SIGMAKOKI Co., Ltd.) to produce light in the range of  $420 \leq \lambda \leq 750$  nm for 2 h at 25 °C in a cryostat (CoolSpeK, UNISOKU Co., Ltd.) under an  $\text{N}_2$  atmosphere. Methane gas was quantified by gas chromatography, GC-2010 plus (Shimadzu) equipped with a BID detector.

## Materials and methods

All reagents of the highest guaranteed grade available were obtained from commercial sources and were used as received unless otherwise indicated. A standard nickel solution for ICP-OES was purchased from FUJIFILM Wako Pure Chemical Corporation. TBAPF<sub>6</sub> (>98% purity) was purchased from Tokyo Chemical Industry Co., Ltd., and recrystallized from heated ethanol and dried under vacuum before use. Authentic methane gas (0.408 % (v/v), balancer: Ar) was purchased from GL Sciences Inc. Distilled water was demineralized using a Millipore Integral 3 apparatus. Nickel tetradehydrocorrin (Ni(TDHC)) was prepared according to the procedures explained in Chapter 1.<sup>33</sup> Apo-forms of Cyt *b*<sub>562</sub> and Cyt *b*<sub>562</sub><sup>M7L</sup> were prepared by acidification followed by extraction of heme with 2-butanone (Teale's conventional method).<sup>42</sup> Apo-form of Cyt *b*<sub>562</sub><sup>L3C</sup> was prepared by dialysis against 50 mM potassium phosphate buffer (pH 7.0) containing 0.1 % sodium dodecyl sulfate and 1% 2-mercaptoethanol at 30 °C for 20 h followed by further dialysis against 100 mM potassium phosphate buffer (pH 7.0) as reported in the literature.<sup>43</sup>

## Synthesis of Ni<sup>II</sup>(DDHC)



**Scheme 2-1.** Synthesis of Ni<sup>II</sup>(DDHC).

In a two-necked flask, 10% palladium on carbon (24 mg) was added into a solution of Ni<sup>II</sup>(TDHC) (20 mg, 28 μmol) in methanol (8 mL) containing 1% (v/v) acetic acid and hydrogenation was performed under 0.1 MPa of H<sub>2</sub> atmosphere at 65 °C for 3.5 h. The reaction solution was filtered and evaporated under reduced pressure. After the residue was dissolved in dichloromethane (50 mL), the solution was washed with brine (30 mL) and water (30 mL) for three times and dried with Na<sub>2</sub>SO<sub>4</sub>. This crude product was purified by reverse phase HPLC (acetonitrile/H<sub>2</sub>O eluent, C18 column). The desired fraction was collected and evaporated under reduced pressure. After evaporation, Ni<sup>II</sup>(DDHC) (18 mg, 25 μmol, 88% yield) was obtained as yellow powder. Although the <sup>1</sup>H NMR spectrum of purified Ni<sup>II</sup>(DDHC) in CD<sub>2</sub>Cl<sub>2</sub> was measured, each peak is difficult to be assigned because of the existence of two diastereomers and their conformers (Fig. 2-12 and 13). HRMS (ESI, positive mode, *m/z*): [M - ClO<sub>4</sub>]<sup>+</sup> calcd. for C<sub>33</sub>H<sub>41</sub>N<sub>4</sub>O<sub>4</sub>Ni, 615.2476; found, 615.2478. UV-Vis (H<sub>2</sub>O, (nm) ε (M<sup>-1</sup>·cm<sup>-1</sup>)): λ<sub>max</sub> = 264 (20800), 295 (22800), 321 (21500), 453 (11400).

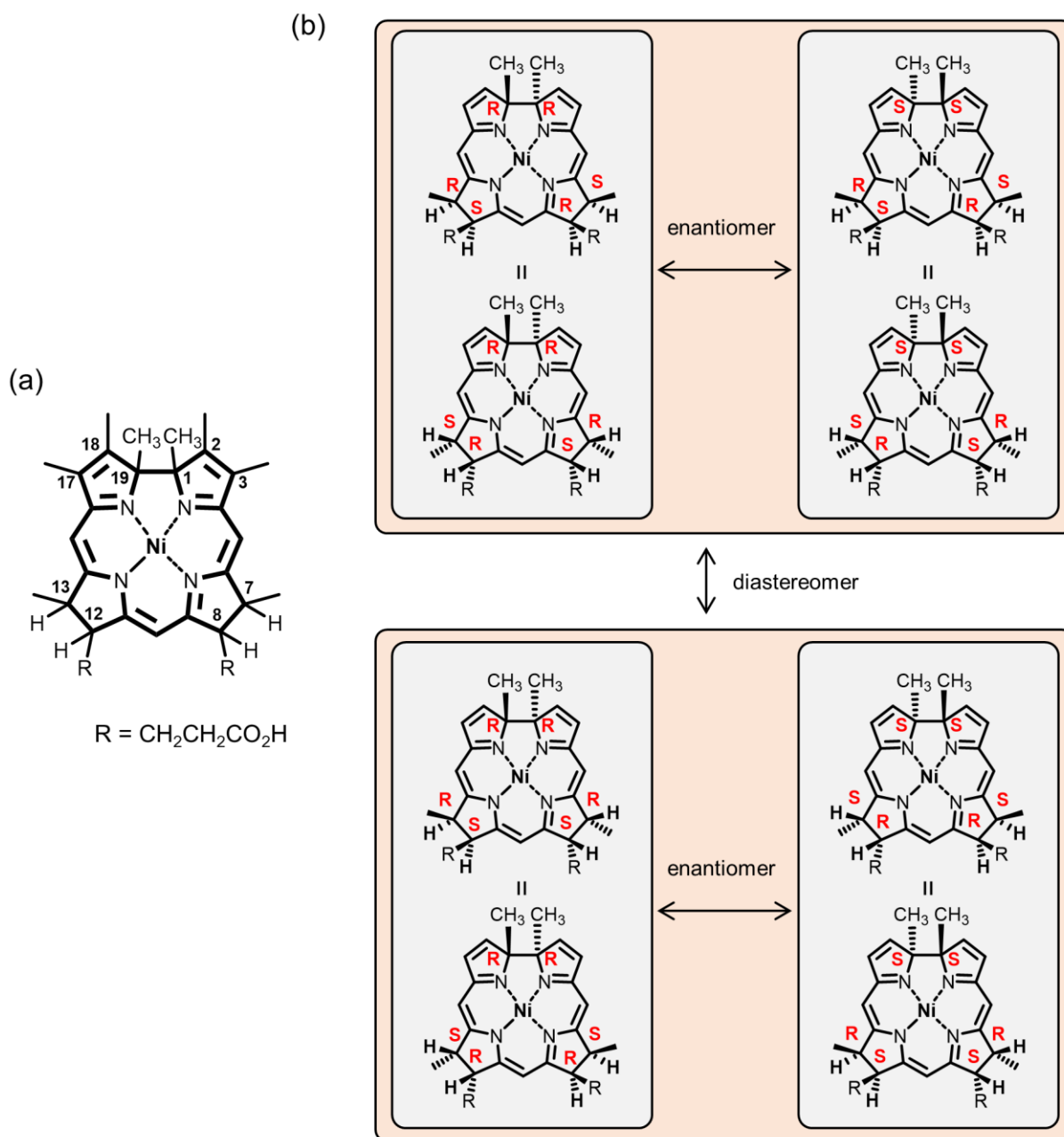


**Figure 2-12.** (a) Molecular structure of Ni<sup>II</sup>(DDHC). (b) The expected stereoisomers of Ni<sup>II</sup>(DDHC). Methyl groups at C2-, C3-, C17-, and C18-positions are omitted for clarity. Ni<sup>II</sup>(TDHC) is exist as a mixture of two enantiomers due to the methyl groups at C1- and C19-positions. Hydrogenation of two pyrroles of Ni<sup>II</sup>(TDHC) with Pd/C and H<sub>2</sub> occurs with syn-stereoselectivity. Moreover, steric repulsion caused by substituents at “C7- and C8-” and “C12- and C13-” positions of Ni<sup>II</sup>(DDHC) will induce sterically distorted structures. Thus, Ni<sup>II</sup>(DDHC) is obtained as a mixture of diastereomers, enantiomers, and conformers.

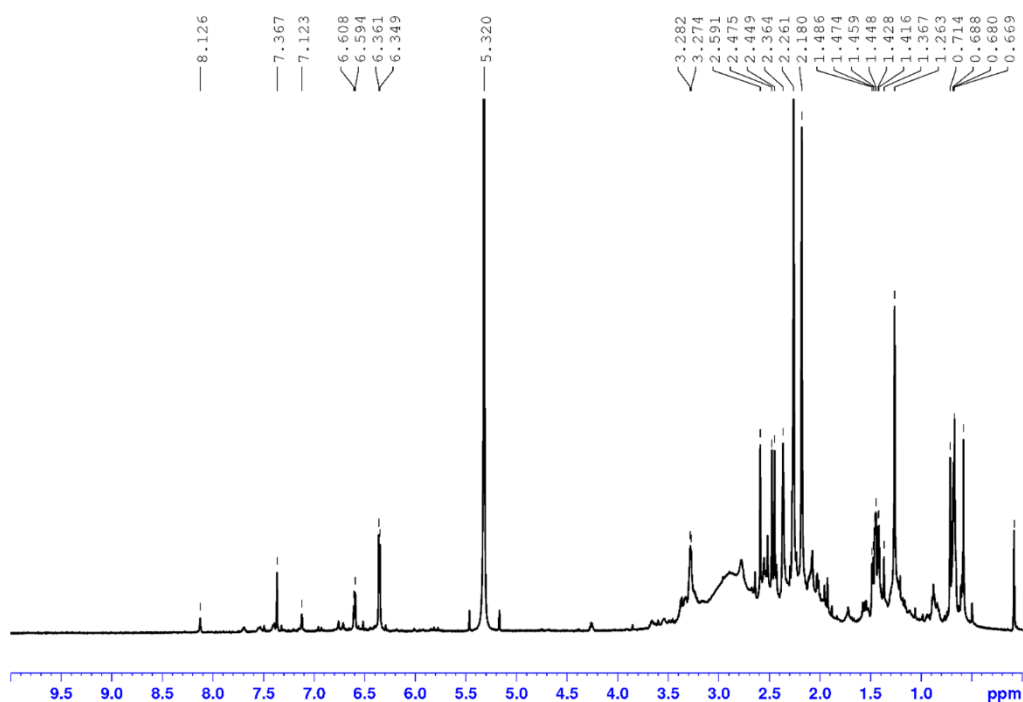


**Figure 2-13.**  $^1\text{H}$  NMR spectrum (600 MHz,  $\text{CD}_2\text{Cl}_2$ ) of  $\text{Ni}^{\text{II}}(\text{DDHC})$ .

### Protein sequence of Cyt $b_{562}$ and its mutants

Cyt  $b_{562}$

ADLEDNMETLNDNLKVIEKADNAAQVKDALTKMRAAALDAQKATPPKLEDKSPDSEPMKDFRHGFDILV  
GQIDDALKLANEGKVKEAQAAAEQLKTTRNAYHQKYR

Cyt  $b_{562}^{\text{M7L}}$

ADLEDNLETLNDNLKVIEKADNAAQVKDALTKMRAAALDAQKATPPKLEDKSPDSEPMKDFRHGFDILV  
GQIDDALKLANEGKVKEAQAAAEQLKTTRNAYHQKYR

Cyt  $b_{562}^{\text{L3C}}$

ADCEDNMETLNDNLKVIEKADNAAQVKDALTKMRAAALDAQKATPPKLEDKSPDSEPMKDFRHGFDILV  
GQIDDALKLANEGKVKEAQAAAEQLKTTRNAYHQKYR

### Expression and purification of Cyt $b_{562}$ and its mutants

The gene expression systems used to obtain wild type Cyt  $b_{562}$  was reported in previous paper.<sup>44</sup> Site-directed mutagenesis was performed by the polymerase chain reaction (PCR) using the KOD-Plus-Neo kit (Toyobo Life Science) according to the protocol of the manufacturer. The wild type Cyt  $b_{562}$  gene cloned into pUC118 was used as a template to introduce M7L and L3C single mutation into the Cyt  $b_{562}$  matrix. The primer sequences used to generate each mutant were:

M7L: (5'-CGTTTGCCGCTGATCTTGAAGACAATCTGGAAACCCTCAACGAC-3') and the complementary primer;

L3C: (5'-CTGCGTCGTTTGCCGCTGATTGCGAAGACAATATGGAAACCCTC-3') and the complementary primer.

After PCR, the template DNA plasmids were digested with Dpn I (Thermo Fisher Scientific). *E. coli* DH5 $\alpha$  competent cells were transformed with the PCR products. After the cultivation, the plasmids were purified using the NucleoSpin Plasmid EasyPure (Takara). DNA sequencing was performed to verify each correct mutation in the gene sequence. The resulting expression plasmid was used to transform *E. coli* strain TG1. YT medium (6 L) containing ampicillin (600 mg) was inoculated with 150 mL of the culture (OD = 0.5) of the transformed cells. After the cells were grown aerobically with vigorous shaking at 37 °C for 12 h, the cells were harvested by centrifugation. The harvested cells from 6 L of culture were re-suspended in ca. 100 mL of a 10 mM Tris-HCl buffer (pH 8.0) and lysed by the addition of chloroform (ca. 2 mL). After stirring for 1 h at 4 °C, 10 mM Tris-HCl (pH 8.0) (ca. 200 mL) was added to the lysate. Then, the lysate was stirred for 1 h at 4 °C again and centrifuged to collect supernatant. The pH value of the supernatant was adjusted to 4.5 by the addition of 1 M HCl. After stirring for 1 h at 4 °C, the precipitate was removed by centrifugation. In the case of the M7L mutant, excess amount of hemin (final conc.: ca. 30  $\mu$ M) was added before acidification by 1 M HCl to convert the apo-form to the holo-form. The supernatant was loaded onto a CM-52 cellulose (FUJIFILM Wako Pure Chemical Corporation) cation-exchange column pre-equilibrated with 50 mM KH<sub>2</sub>PO<sub>4</sub> containing 0.1 mM EDTA (pH 4.5). The fraction of the target protein was collected by an eluent gradiented with (A) 50 mM KH<sub>2</sub>PO<sub>4</sub> containing 0.1 mM EDTA and 50 mM KCl (pH 4.5) and (B) 50 mM KH<sub>2</sub>PO<sub>4</sub> containing 0.1 mM EDTA and 150 mM KCl (pH 4.5). The obtained solution was concentrated using an Amicon stirred cell equipped with a 5 kDa molecular weight cut-off ultrafiltration membrane (Millipore). The concentrated solution was passed through a HiPrep 16/60 Sephacryl S-200 HR column equilibrated with 100 mM potassium phosphate buffer (pH 7.0) using an ÄKTApurifier system (GE Healthcare). The fractions with  $R_z > 5$  ( $R_z$  is a ratio of absorbance values at 418 nm and 280 nm) were collected and concentrated. The obtained Cyt  $b_{562}$  mutants were characterized by SDS-PAGE and ESI-TOF MS, and stored at -80 °C.

#### **Preparation of reconstituted Cyt $b_{562}$ with Ni<sup>II</sup>(DDHC) or Ni<sup>II</sup>(TDHC)**

To a solution of Ni<sup>II</sup>(DDHC) or Ni<sup>II</sup>(TDHC) (final conc.: 50  $\mu$ M) in 100 mM potassium phosphate buffer (pH 7.0), an apoCyt  $b_{562}$  solution (final conc.: 150  $\mu$ M) in 100 mM potassium phosphate buffer (pH 7.0) was added under an N<sub>2</sub> atmosphere at 25 °C. The obtained reconstituted Cyt  $b_{562}$  (rCyt  $b_{562}$ (Ni<sup>II</sup>(DDHC)) and rCyt  $b_{562}$ (Ni<sup>II</sup>(TDHC))) aqueous solution was used for experiments without purification.

#### **Photo-induced methane generation from reconstituted Cyt $b_{562}$**

In an optical cell (pathlength: 1 mm, volume: 1000  $\mu$ L) sealed with a silicon septum, a solution of Ni<sup>II</sup>(DDHC) or Ni<sup>II</sup>(TDHC) (final conc.: 50  $\mu$ M), apoCyt  $b_{562}$  (final conc.: 150  $\mu$ M), tris(2,2'-bipyridine) ruthenium(II) chloride (final conc.: 100  $\mu$ M), sodium ascorbate (final conc.: 100 mM) dissolved in 100 mM potassium phosphate buffer (pH 7.0)

(100  $\mu$ L in total volume) was prepared. The solution was then irradiated using an Optical Modulex (USHIO Inc.) equipped with a Xe lamp and optical filters to produce visible light for 2 h at 25  $^{\circ}$ C under an  $N_2$  atmosphere. After photoirradiation, the gas sample (100  $\mu$ L) was carefully taken from the headspace of the vial by a gastight syringe and injected into a GC-2010 plus (Shimadzu) equipped with a BID detector and a 2.0 m  $\times$  1.0 mm ID micropacked column SHINCARBON-ST 80-100 mesh using He as a carrier gas. Measurement conditions: injector temperature = 200  $^{\circ}$ C, split ratio 5:1, detector temperature = 250  $^{\circ}$ C, column temperature = 60  $^{\circ}$ C (1 min hold) – 18  $^{\circ}$ C/min – 220  $^{\circ}$ C (2 min hold), column flow rate 55.8 mL/min. The product was identified by a comparison of its retention time with that of the authentic standard sample. The amount of methane gas was determined from the area of the corresponding eluted peak using the calibration curve.

### Mass spectral analysis of the protein matrix after the photoirradiation reaction

Protein matrices in reaction solutions (200  $\mu$ L) were purified using a HiTrap Desalting column (5 mL, GE Healthcare) with 50 mM ammonium acetate buffer under aerobic conditions. The obtained protein solutions were concentrated using an Amicon Ultra 0.5 mL Centrifugal Filter with a 3-kDa molecular weight cut-off membrane (Millipore). The concentrated protein solutions (50  $\mu$ L) were mixed with 0.1 % formic acid in methanol (50  $\mu$ L) and analyzed by a micrOTOF-II mass spectrometer (Bruker).

### Reference and notes

1. P. N. Evans, J. A. Boyd, A. O. Leu, B. J. Woodcroft, D. H. Parks, P. Hugenholtz, G. W. Tyson, *Nat. Rev. Microbiol.* **2019**, *17*, 219–232.
2. G. Borrel, P. S. Adam, L. J. McKay, L.-X. Chen, I. N. Sierra-García, C. M. K. Sieber, Q. Letourneur, A. Ghozlane, G. L. Andersen, W.-J. Li, S. J. Hallam, G. Muyzer, V. M. Oliveira, W. P. Inskeep, J. F. Banfield, S. Gribaldo, *Nat. Microbiol.* **2019**, *4*, 603–613.
3. B. C. McBride, R. S. Wolfe, *Biochemistry* **1971**, *10*, 2317–2324.
4. D. Ankel-Fuchs, R. K. Thauer, *Eur. J. Biochem.* **1986**, *156*, 171–177.
5. R. K. Thauer, *Biochemistry* **2019**, *58*, 5198–5220.
6. B. Jaun, A. Pfaltz, *J. Chem. Soc., Chem. Commun.* **1986**, 1327–1329.
7. B. Jaun, *Helv. Chim. Acta* **1990**, *73*, 2209–2217.
8. R. Piskorski, B. Jaun, *J. Am. Chem. Soc.* **2003**, *125*, 13120–13125.
9. B. Jaun, A. Pfaltz, *J. Chem. Soc., Chem. Commun.* **1988**, 293–294.
10. S.-K. Lin, B. Jaun, *Helv. Chim. Acta* **1991**, *74*, 1725–1738.
11. U. Ermler, W. Grabarse, S. Shima, M. Goubeaud, R. K. Thauer, *Science* **1997**, *278*, 1457–1462.
12. W. Grabarse, F. Mahlert, E. C. Duin, M. Goubeaud, S. Shima, R. K. Thauer, V. Lamzin, U. Ermler, *J. Mol. Biol.* **2001**, *309*, 315–330.
13. M. Dey, R. C. Kunz, D. M. Lyons, S. W. Ragsdale, *Biochemistry* **2007**, *46*, 11969–11978.
14. M. Dey, J. Telser, R. C. Kunz, N. S. Lees, S. W. Ragsdale, B. M. Hoffman, *J. Am. Chem. Soc.* **2007**, *129*, 11030–

11032.

15. N. Yang, M. Reiher, M. Wang, J. Harmer, E. C. Duin, *J. Am. Chem. Soc.* **2007**, *129*, 11028–11029.
16. R. Sarangi, M. Dey, S. W. Ragsdale, *Biochemistry* **2009**, *48*, 3146–3156.
17. P. E. Cedervall, M. Dey, X. Li, R. Sarangi, B. Hedman, S. W. Ragsdale, C. M. Wilmot, *J. Am. Chem. Soc.* **2011**, *133*, 5626–5628.
18. V. Pelmeshnikov, M. R. A. Blomberg, P. E. M. Siegbahn, R. H. Crabtree, *J. Am. Chem. Soc.* **2002**, *124*, 4039–4049.
19. V. Pelmeshnikov, P. E. M. Siegbahn, *J. Biol. Inorg. Chem.* **2003**, *8*, 653–662.
20. S.-L. Chen, M. R. A. Blomberg, P. E. M. Siegbahn, *Chem. Eur. J.* **2012**, *18*, 6309–6315.
21. S.-L. Chen, M. R. A. Blomberg, P. E. M. Siegbahn, *Phys. Chem. Chem. Phys.* **2014**, *16*, 14029–14035.
22. T. Wongnate, D. Sliwa, B. Ginovska, D. Smith, M. W. Wolf, N. Lehnert, S. Raugei, S. W. Ragsdale, *Science* **2016**, *352*, 953–958.
23. M. Krüger, A. Meyerdierks, F. O. Glöckner, R. Amann, F. Widdel, M. Kube, R. Reinhardt, J. Kahnt, R. Böcher, R. K. Thauer, S. Shima, *Nature* **2003**, *426*, 878–881.
24. S. Scheller, M. Goenrich, R. Boecher, R. K. Thauer, B. Jaun, *Nature* **2010**, *465*, 606–608.
25. S. Shima, M. Krueger, T. Weinert, U. Demmer, J. Kahnt, R. K. Thauer, U. Ermler, *Nature* **2012**, *481*, 98–101.
26. P. E. Cedervall, M. Dey, A. R. Pearson, S. W. Ragsdale, C. M. Wilmot, *Biochemistry* **2010**, *49*, 7683–7693.
27. S. Ebner, B. Jaun, M. Goenrich, R. K. Thauer, J. Harmer, *J. Am. Chem. Soc.* **2010**, *132*, 567–575.
28. M. W. Renner, L. R. Furenlid, K. M. Barkigia, A. Forman, H. K. Shim, D. J. Simpson, K. M. Smith, J. Fajer, *J. Am. Chem. Soc.* **1991**, *113*, 6891–6898.
29. G. K. Lahiri, L. J. Schussel, A. M. Stolzenberg, *Inorg. Chem.* **1992**, *31*, 4991–5000.
30. L. Signor, C. Knappe, R. Hug, B. Schweizer, A. Pfaltz, B. Jaun, *Chem. Eur. J.* **2000**, *6*, 3508–3516.
31. J. Nishigaki, T. Matsumoto, K. Tatsumi, *Inorg. Chem.* **2012**, *51*, 5173–5187.
32. C. Brenig, L. Prieto, R. Oetterli, F. Zelder, *Angew. Chem. Int. Ed.* **2018**, *57*, 16308–16312.
33. K. Oohora, Y. Miyazaki, T. Hayashi, *Angew. Chem. Int. Ed.* **2019**, *58*, 13813–13817.
34. Y. Murakami, Y. Aoyama, K. Tokunaga, *J. Am. Chem. Soc.* **1980**, *102*, 6736–6744.
35. Y. Morita, K. Oohora, A. Sawada, T. Kamachi, K. Yoshizawa, T. Hayashi, *Inorg. Chem.* **2017**, *56*, 1950–1955.
36. F. S. Mathews, P. H. Bethge, E. W. Czerwinski, *J. Biol. Chem.* **1979**, *254*, 1699–1706.
37. T. Hayashi, Y. Morita, E. Mizohata, K. Oohora, J. Ohbayashi, T. Inoue, Y. Hisaeda, *Chem. Commun.* **2014**, *50*, 12560–12563.
38. K. Oohora, T. Hayashi, *Methods in Enzymology* **2016**, *580*, 439–454.
39. The peak consistent with rCyt *b*<sub>562</sub>(Ni<sup>II</sup>(DDHC)) was obtained as a minor peak due to the low binding affinity of Ni<sup>II</sup>(DDHC) to apoCyt *b*<sub>562</sub> and shallow binding pocket of Cyt *b*<sub>562</sub> protein matrix. Most of Ni<sup>II</sup>(DDHC) appears to be released from Cyt *b*<sub>562</sub> protein matrix during ionization, which is also often observed in the reconstituted Cyt *b*<sub>562</sub> with other artificial heme.
40. I. Hara, T. Ueno, S. Ozaki, S. Itoh, K. Lee, N. Ueyama, Y. Watanabe, *J. Biol. Chem.* **2001**, *276*, 36067–36070.
41. T. D. Pfister, T. Ohki, T. Ueno, I. Hara, S. Adachi, Y. Makino, N. Ueyama, Y. Lu, Y. Watanabe, *J. Biol. Chem.* **2005**, *280*, 12858–12866.

42. Y. Morita, K. Oohora, A. Sawada, K. Doitomi, J. Ohbayashi, T. Kamachi, K. Yoshizawa, Y. Hisaeda, T. Hayashi, *Dalton Trans.* **2016**, 45, 3277–3284.
43. F. W. J. Teale, *Biochim. Biophys. Acta* **1959**, 35, 543.
44. C.-A. Yu, I. C. Gunsalus, *J. Bio. Chem.* **1974**, 249, 107–110.
45. H. Kitagishi, K. Oohora, H. Yamaguchi, H. Sato, T. Matsuo, A. Harada, T. Hayashi, *J. Am. Chem. Soc.* **2007**, 129, 10326–10327.

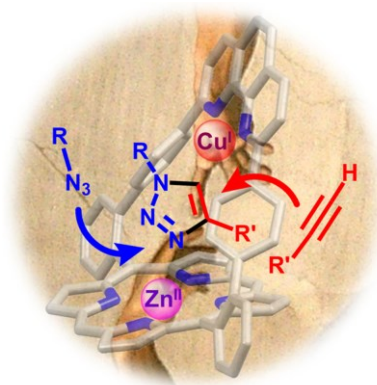
## Chapter 3

### Synthesis of rotaxane using the ditopic strapped porphyrin based on the active metal template method

Reproduced in part with permission from [*Chem. Eur. J.* **2017**, *23*, 13579–13582.]

DOI:10.1002/chem.201702553

License number: 4733440608972



#### 3-1. Introduction

In modern supramolecular chemistry, the copper-catalysed alkyne–azide cycloaddition (CuAAC),<sup>1</sup> better known as the click reaction, has provided access to a large variety of elaborate, but otherwise difficult to prepare molecular structures.<sup>2-5</sup> According to several investigations of the role of copper ion in the mechanism of the cycloaddition, two metal ions are expected to be involved in the cycloaddition step.<sup>7-10</sup> Experimental evidences for the cooperative process have been recently reported.<sup>3,9,11</sup> The exact role of the second metal ion is not completely elucidated and it can range from  $\pi$ -activation, due to Lewis acidic character, to coordination of the zwitterionic form of the azide reagent. The cooperative and simultaneous activation of both the azide and alkyne by two distinct metal centers is compatible with both a catalytic or stoichiometric use of copper in click reactions.<sup>6</sup> Several groups have developed rotaxane synthesis using copper-catalysed click reaction based on the active metal template approach.<sup>12-15</sup> In such the approach, the participation of two metal centers in the mechanism of the click reaction was also indicated by the use of copper-copper<sup>12</sup> or copper-nickel<sup>13</sup> in the formation of rotaxanes. In this context, the author demonstrates that the use of a ditopic ligand able to bind both an active copper ion and a coordinatively unsaturated metal ion induces both active and organising template effects, providing access to mechanically interlocked porphyrin architectures.

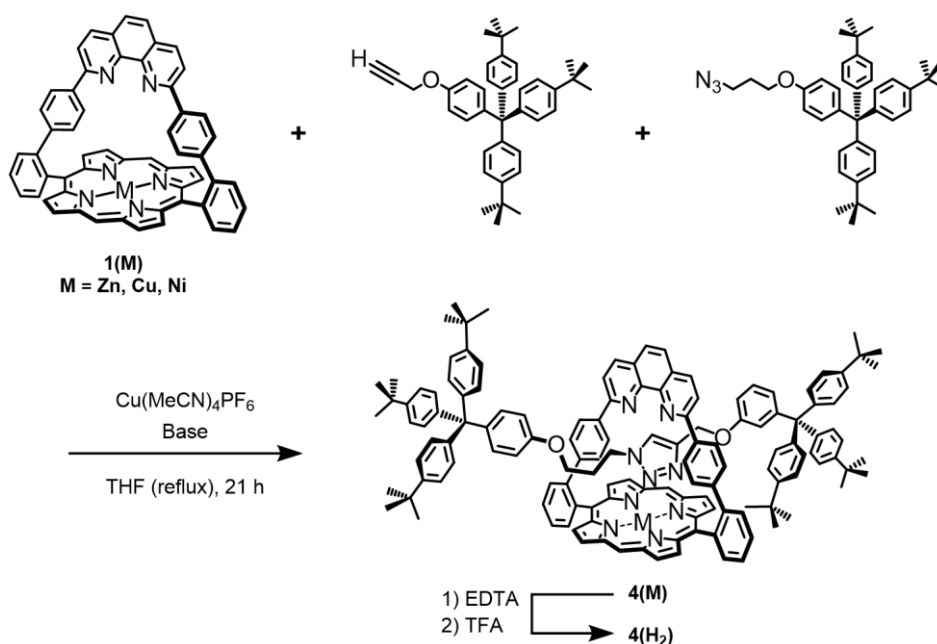
Phenanthroline (phen)-strapped porphyrin **1(H<sub>2</sub>)**, which is a ditopic ligand, has been employed for the construction of supramolecular architectures by Weiss group. This ditopic ligand has led to several species in which the phen binds and stabilizes a Cu(I) ion,<sup>16,17</sup> whereas the porphyrin binds various coordinatively unsaturated metal ions, thus offering the possibility of coordinating an exogenic substrate on either the open face, opposite to the strap, or within the phen pocket.<sup>18,19</sup> For instance, imidazole derivatives perfectly fit and are included within the cavity of

the zinc porphyrin **1(Zn)** by coordination and hydrogen bonding interaction with zinc center and phen moiety, respectively, which were confirmed by both NMR and X-ray studies.<sup>16</sup> Thus, the possible occurrence of a click reaction within the phen strap of **1(Zn)** is anticipated due to the isomorphous character of 1,2,3-triazole and imidazole, and an assistance by the coordination of an azide reagent to the zinc of the porphyrin is also expected.

### 3-2. Results and discussion

#### Synthesis of strapped porphyrin [2]rotaxane

Addition of a slightly sub-stoichiometric amount of  $\text{Cu}(\text{MeCN})_4\text{PF}_6$  to **1(Zn)** provided the zinc-copper complex in situ. As shown in Scheme 3-1, reaction in basic medium of the alkyne **2**<sup>12a</sup> and azide **3**,<sup>20</sup> bearing bulky stoppers commonly used in mechanically interlocked structures,<sup>21</sup> yielded mixtures of rotaxane structures still containing either copper, zinc or both metals. A part of the copper ion is extruded from binding moieties due to sterically demanding scaffoldings after the formation of triazole ring according to previous works for rotaxane synthesis based on the active metal template method.<sup>12-15</sup> To fully remove the copper ion, treatment with ethylenediaminetetraacetate (EDTA) was performed. Because this treatment initiated a partial demetallation of the zinc, complete removal of zinc was carried out upon trifluoroacetic acid (TFA) treatment. Finally, only the free base rotaxane species **4(H<sub>2</sub>)** was isolated in various yields and characterized (Entries 1-7). The corresponding nickel and zinc rotaxanes **4(Ni)** and **4(Zn)** were later obtained by metalation of **4(H<sub>2</sub>)** with nickel and zinc salts, respectively.



**Scheme 3-1.** Synthesis of **4(H<sub>2</sub>)**. Reactions were performed in the presence of 0.96 eq of Cu(I) and subsequently treated with EDTA and TFA.

**Table 3-1.** Yields of rotaxane **4(H<sub>2</sub>)** obtained by click-reaction of **2** and **3** in the presence of **1(M)** and 0.96 eq of Cu(MeCN)<sub>4</sub>PF<sub>6</sub>.

Entry	M	Base <sup>[a]</sup>	Yield (%) <sup>[b]</sup>
1	Zn	None	n.d.
2	Zn	4-picoline	11
3	Zn	2,6-lutidine	18
4	Zn	DIPEA (0.5 eq)	23
5	Zn	DIPEA (1 eq)	50
6	Zn	DIPEA (5 eq)	20
7	Zn	DBU (1 eq), DIPEA (0.5 eq)	45
8	Cu	DIPEA (1 eq)	16
9	Ni	4-picoline	n.d.
10	Ni	2,6-lutidine	n.d.
11	Ni	DIPEA (1 eq)	n.d.

[a] DIPEA: *N,N*-diisopropylethylamine, DBU: diazabicycloundecene.

[b] n.d.: not detected.

### Investigation of effects of metal ions and bases on rotaxane synthesis

To demonstrate the essential role played by the metal ion in the porphyrin core, the nature of the metal in the porphyrin was investigated (Table 3-1). Due to the previously reported fast disproportionation of a Cu(I) phen-strapped porphyrin and its rapid conversion to the Cu(II) porphyrin, synthetic attempts involving the free base porphyrin **1(H<sub>2</sub>)** and the Cu(I) phen strap complex were precluded.<sup>17</sup> Although Zn(II) salts have been reported to catalyze azide–alkyne cycloadditions,<sup>22</sup> the use of **1(Zn)** alone in the absence of Cu(MeCN)<sub>4</sub>PF<sub>6</sub> did not afford rotaxane or the free dumbbell under the same reaction conditions, emphasising the expected role of Cu(I) ion as the active metal template.

The use of **1(Cu)**, which weakly binds an axial ligand, resulted in a significantly lower yield of rotaxane (Entry 8) compared to that obtained with **1(Zn)**. This result shows that the coordination on the metalloporphyrin is the most important for a productive dual template effect. Indeed, the 16% yield obtained in the presence of **1(Cu)** is representative of the oxophilic nature of hard porphyrin-Cu(II) complexes,<sup>23</sup> whereas the soft porphyrin-Zn(II) complex has a clearly enhanced affinity for nitrogen-containing axial ligands and affords up to 50% yield of rotaxane (Entry 5). Finally, when the nickel porphyrin **1(Ni)**, which is inert towards the axial binding of exogenic ligands, was employed, no rotaxane was detected (Entries 9-11). Therefore, the presence of a second, coordinatively unsaturated metal in the porphyrin core is necessary for the success of the click reaction.

The coordination of the azide on the zinc center in the porphyrin core of **1(Zn)** is in agreement with the observed influence of the base on the efficacy of the CuAAC reaction (Entries 1-7). Thus, the nature of the base used in the click reaction was also studied. The yield of the rotaxane increased with increasing basicity, from picoline to 2,6-lutidine and DIPEA, emphasizing the role of the base in the deprotonation of the terminal alkyne and stressing

the necessary weak binding of a nitrogen ligand on the open face of the porphyrin (Entries 1-7). The azide group coordinates to zinc center and forms the zwitterionic intermediate on the open face (Fig. 3-1A) or on the strapped-side (Figure 1 C or D). An assistance of the click reaction by coordination of the azide to a second metal requires binding of the azide on the strapped-side of the porphyrin, as proposed in Fig. 3-1C or D. Azide binding can be oriented to the strapped-side if a fifth ligand, in fast exchange, is already present on the open face of the zinc porphyrin. Picoline strongly binds to zinc but only on the open face of the porphyrin due to steric hinderance; therefore, this base is in slow exchange and clearly competes with the binding of azide on the strapped-side (Entry 2). With DIPEA, which is a stronger yet non-nucleophilic base that weakly binds to zinc, the temporary binding of this base on the open face of the zinc porphyrin favours the insertion of the azide on the strapped-side (Entry 5). In the case of 2,6-lutidine, the steric hindrance in the vicinity of the nitrogen atom prevents binding on either side of the porphyrin, thus resulting in the productive binding of the azide on the strapped-side and the non-productive binding on the open face (Entry 3). Although stoichiometric amounts of both diazabicycloundecene (DBU) and DIPEA were employed to try to take advantage of the reactivity of a strong base and the weak binding of a bulky base on the open face, the yield was slightly lower than when using only DIPEA (Entry 7).

To rule out geometric effects influencing the efficacy of the cycloaddition, the dimensions of the strapped porphyrin scaffolds of **1(Zn-Cu)**,<sup>18</sup> **1(Ni)**, **4(Ni)**, and **4(H<sub>2</sub>)** were compared in their respective crystal structures (Fig. 3-2). The dimensions of the hollow pyramidal space between the porphyrin plane and the phen strap are nearly identical in all four structures; therefore, geometric effects cannot explain the difference observed in the reactivity of **1(Zn)** and **1(Ni)** in the presence of Cu(I) for the templated 1,3-cycloaddition of the azide and alkyne stoppers. Thus, only the nature of the metal in the porphyrin and its ability to assist the templated process *via* azide binding are responsible for the formation of the rotaxane. In this regard, the classical Sauvage macrocycle, derived from 2,9-diphenylphenanthroline pentaethylene-glycol, did not produce a rotaxane<sup>12b</sup> by the active metal template method, confirming the essential assistance of the metal in the porphyrin core observed in this work.

Thus, two distinct and complementary roles are played by each metal. Copper is the active metal template, as previously described in works by Leigh<sup>12,13</sup> and Goldup.<sup>14</sup> Zinc plays the role of an organising template according to Sauvage's definition<sup>24</sup> and is responsible for a productive positioning of the azide in the cavity defined by the phen strap, probably as shown in Fig. 3-1D. At this stage, the competing and temporary binding of a base on the open face of the porphyrin, which favours the productive binding of the azide in the strap side, restricts the efficiency of the zinc organising template effect, resulting in moderate yield of rotaxane synthesis (~50%). Current work is in progress to explore variation of the base or the ditopic nature of the macrocycle to enhance the productive binding of the azide in the strap.

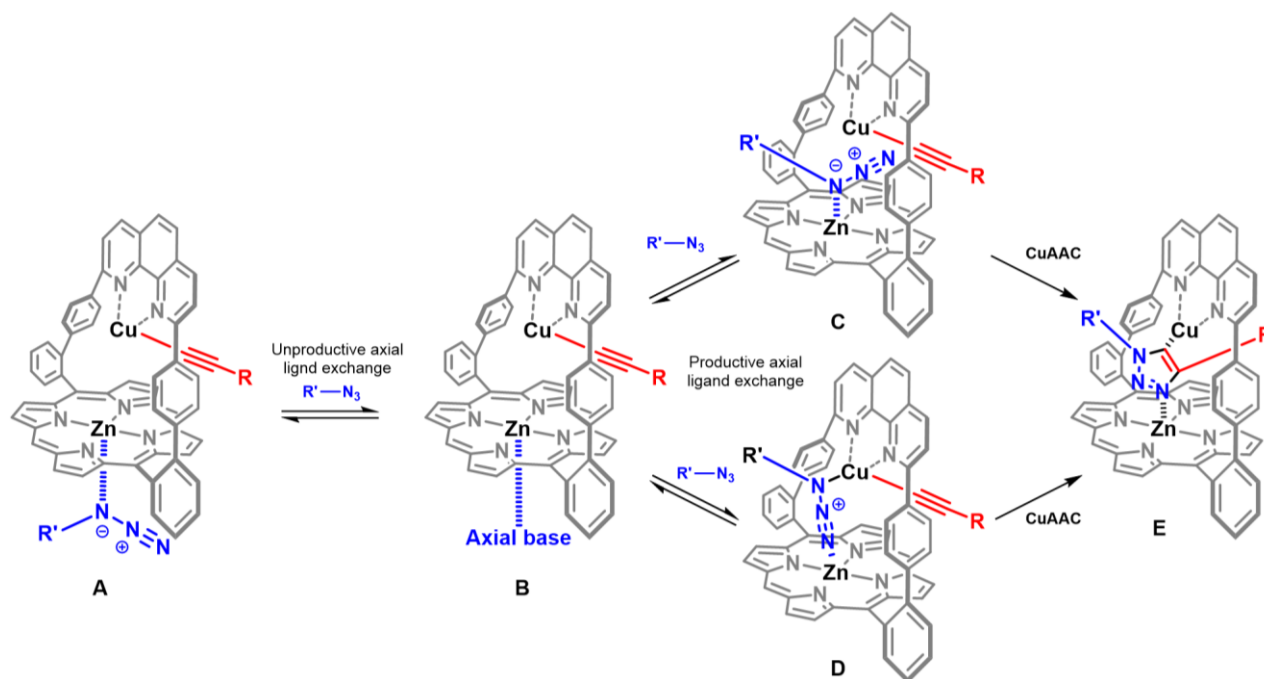


**Figure 3-1.** Proposed tandem actions of a Zn organizing template and a Cu active metal template: The competitive binding of the azide on the metallic porphyrin core and the axial base is ruled by their respective affinities for the central metal.

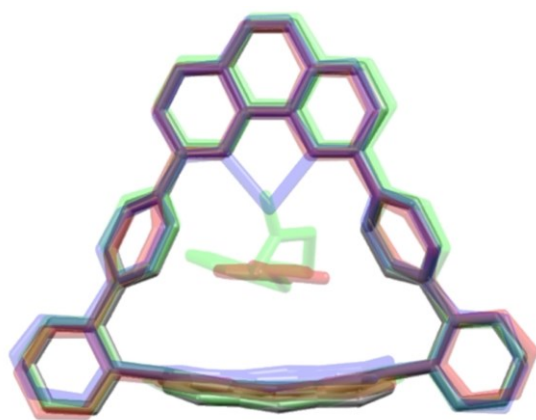


**Figure 3-2.** Overlay of the solid state structures of  $[1(\text{Zn-Cu})]^+$  (blue),  $1(\text{Ni})$  (grey),  $4(\text{Ni})$  (green), and  $4(\text{H}_2)$  (red). Other colors (purple and brown) denote major overlaps between several structures.

### Structural investigation of strapped porphyrin rotaxanes

Single crystals of  $4(\text{H}_2)$  and  $4(\text{Ni})$  suitable for X-ray diffraction analyses were obtained by vapour diffusion of acetonitrile into a saturated solution of  $4(\text{H}_2)$  in dichloroethane/acetonitrile ( $v/v = 1:1$ ) and vapour diffusion of acetonitrile into a saturated  $\text{CH}_2\text{Cl}_2$  solution of  $4(\text{Ni})$ . In the solid state structure of  $4(\text{H}_2)$  the propyl chain's carbon atoms and the porphyrin plane are separated by distances ranging from 3.3 to 3.6 Å, which are close to van der Waals distances (Fig. 3-3a). Weaker C–H/ $\pi$  interactions probably contribute to the additional stabilization of the propylene chain threaded through the phen strap. The triazole develops  $\pi$ - $\pi$  stacking interactions with the porphyrin ring at a distance of approximately 3.7 Å and the dumbbell's phenyl group on the left-hand side in Fig. 3-3a is stacked above the edge of the porphyrin ring at a distance of approximately 3.3 Å. The latter stabilizing interaction was previously observed for an inclusion complex of 2-phenylimidazole in  $1(\text{Zn})$ .<sup>25</sup>

In the crystal structure of **4(Ni)** in Fig. 3-3b, the weak oxophilic interaction, denoted by the 3.0 Å distance between the nickel center and the phenol ether, is assisted by two additional noncovalent interactions. The stacking of the left-hand phenyl group and the porphyrin edge occurs again, with distances ranging from 3.6 to 3.9 Å, in spite of the slight distortion of the porphyrin macrocycle. Furthermore, the protons located on the first and third carbons of the propylene chain are at rather short distances (2.3 and 2.7 Å) from the phen's nitrogen atoms.

These structural features are preserved in solution, as confirmed by 2D <sup>1</sup>H NMR experiments. In all three rotaxanes, displacements of chemical shifts observed for different segments of the dumbbell's signals indicated the location of each dumbbell segment in the phen-strapped porphyrin (Fig. 3-4). In **4(Zn)**, the triazole was clearly located in the phenanthroline-porphyrin pocket, as shown by the deshielding of the triazole proton that is hydrogen bonded to the phenanthroline.<sup>14e</sup> The binding of the triazole to zinc was also detected in the UV-vis spectrum of **4(Zn)** where the Soret and Q bands appeared at 428 and 559 nm compared to those of **1(Zn)** at 418 and 546 nm (Fig. 3-5). The red-shifted absorptions of **4(Zn)** are consistent with reported observations of triazole coordinated to a zinc porphyrin.<sup>26</sup>

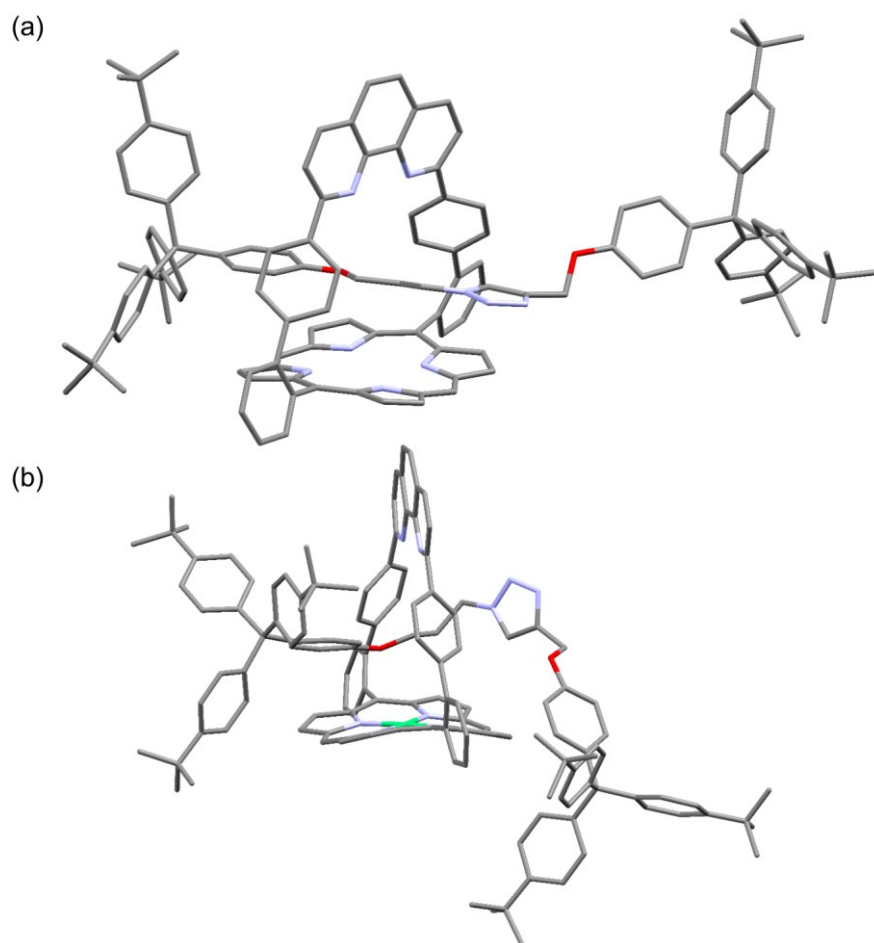


**Figure 3-3.** Solid state structures of rotaxanes (a) **4(H<sub>2</sub>)** and (b) **4(Ni)**. Hydrogen atoms and solvent molecules are omitted for clarity. Significant distances are discussed in the text.

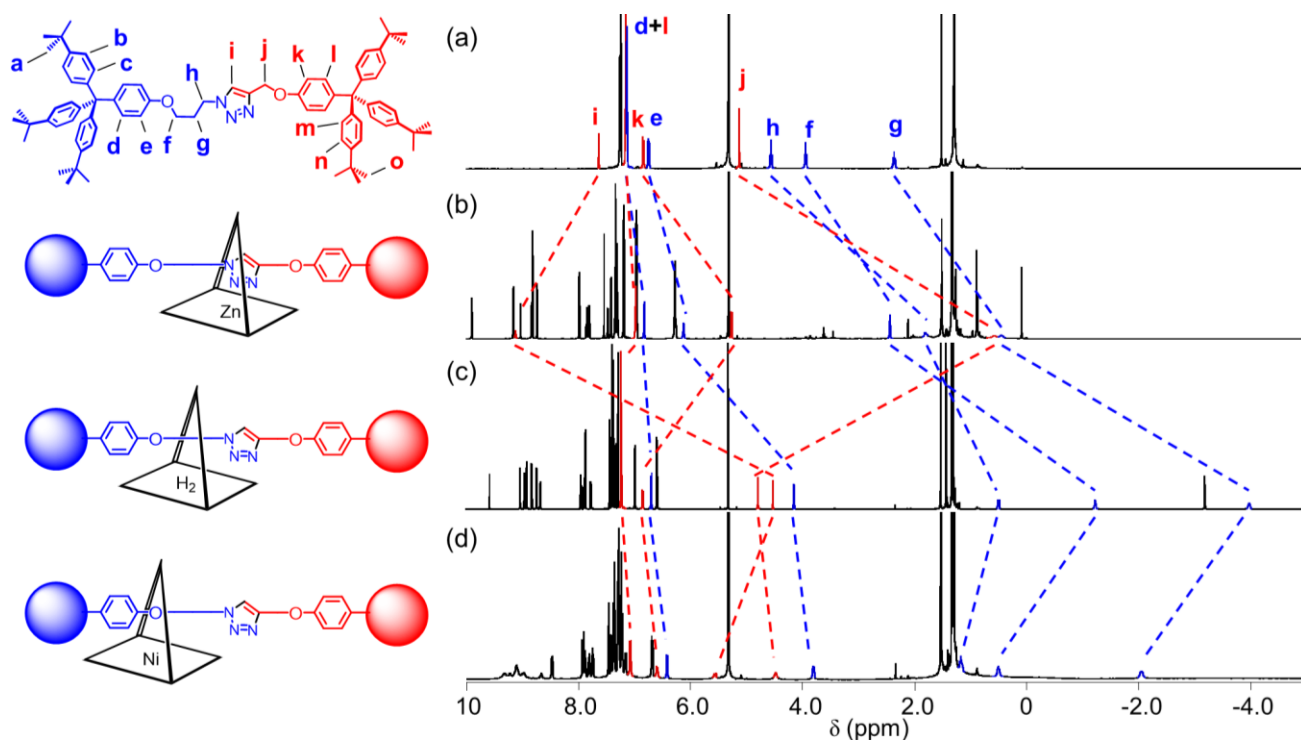


**Figure 3-4.**  $^1\text{H}$  NMR comparison of the dumbbell protons' chemical shifts in (a) the absence of strapped porphyrin, (b)  $4(\text{Zn})$ , (c) the free base rotaxane  $4(\text{H}_2)$ , and (d)  $4(\text{Ni})$ . All spectra were recorded in  $\text{CD}_2\text{Cl}_2$  (298 K) at 600 MHz.

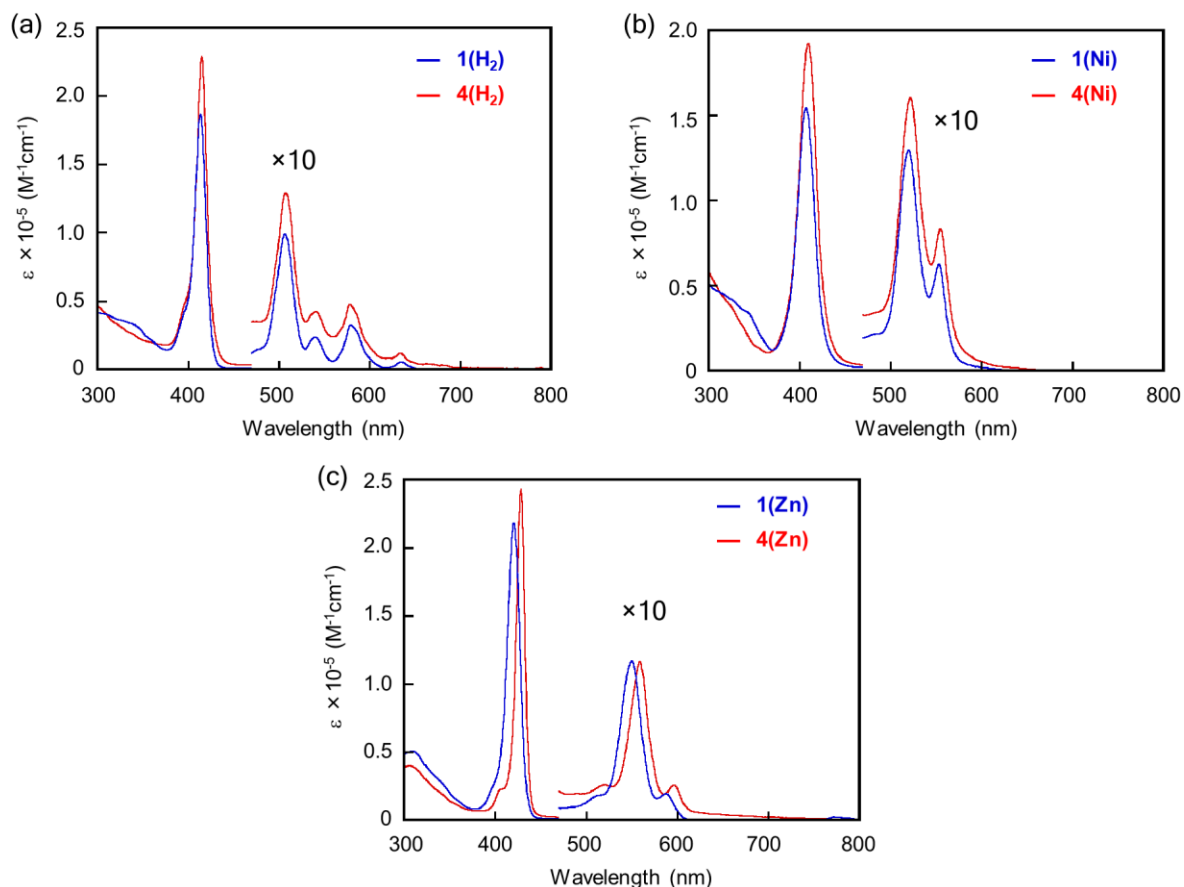


**Figure 3-5.** UV-vis spectra of (a) **1(H<sub>2</sub>)** (blue line) and **4(H<sub>2</sub>)** (red line) in CH<sub>2</sub>Cl<sub>2</sub>, (b) **1(Ni)** (blue line) and **4(Ni)** (red line) in CH<sub>2</sub>Cl<sub>2</sub>, (c) **1(Zn)** (blue line) and **4(Zn)** (red line) in CH<sub>2</sub>Cl<sub>2</sub>. All measurements were carried out at 25 °C. Enlarged spectra are employed in Q-band region.

### 3-3. Summary

In conclusion, this work confirms the role played by a second metal ion, Zn(II), in the copper-catalysed alkyne–azide cycloaddition mechanism and opens the way to a “tandem active metal template” approach to rotaxanes that cannot be obtained by a “single active metal template” method. Although this example uses a ditopic porphyrin ligand, the approach could be extended to a wide range of ditopic ligands. In the particular case of easily accessible phenanthroline-strapped porphyrins, this strategy is currently being explored for the straightforward preparation of mechanically interlocked multi-porphyrin scaffolds such as photochemical dyads and triads.

### 3-4. Experimental section

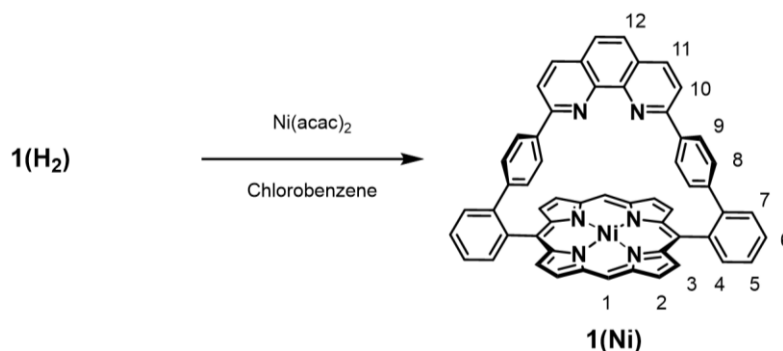
#### Instruments

UV-vis spectral measurements were carried out with a JASCO V-670 spectrophotometer. ESI-TOF MS analyses were performed with a Bruker Daltonics microTOF II mass spectrometer.  $^1\text{H}$  NMR spectra were collected on a Bruker BioSpin Avance III HD (400 MHz) spectrometer or an Avance III (600 MHz) spectrometer. The  $^1\text{H}$  chemical shift values are reported in ppm relative to a residual solvent peak. Coupling constants ( $J$ ) are reported in Hertz (Hz). Standard abbreviations indicating multiplicity were used as follows: m = multiplet, t = triplet, d = doublet, dd = double doublet, s = singlet, br = broad. Signal assignments were carried out using 2D NMR methods (COSY, NOESY, HSQC, HMBC) where necessary

#### Materials and methods

Unless otherwise stated, all reagents were purchased from commercial sources and used without further purification. Saturated  $\text{EDTA}_{\text{aq}}$  and 1 M  $\text{NaOH}_{\text{aq}}$  were prepared before the experiment. 0.10 M solutions of base in THF were prepared under inert atmosphere before the experiment. The following compounds were synthesized according to literature procedures: free base strapped porphyrin **1(H<sub>2</sub>)**,<sup>27</sup> Zn(II) strapped porphyrin **1(Zn)**,<sup>28</sup> 1-(prop-3-ynoxy)-4-(tris-(4-tert-butyl-phenyl)methyl)-benzene **2**,<sup>12a</sup> and 1-(3-azido-propoxy)-4-(tris-(4-tert-butyl-phenyl)methyl)benzene **3**.<sup>20</sup>

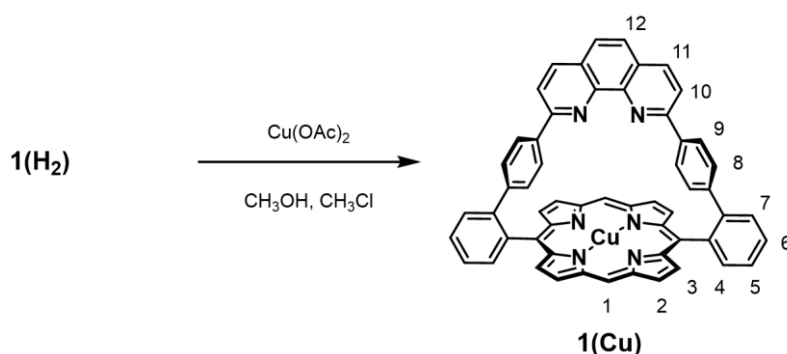
#### Synthesis of nickel(II) strapped porphyrin (**1(Ni)**)



**Scheme 3-2.** Synthesis of **1(Ni)**.

To a solution of strapped porphyrin **1(H<sub>2</sub>)** (150 mg, 190  $\mu\text{mol}$ ) in chlorobenzene (30 mL) was added nickel acetylacetonate (490 mg, 1.9 mmol, 10eq). The solution was refluxed for 2 h. After cooling, the solution was passed through an  $\text{Al}_2\text{O}_3$  (neutral, grade 1) column (eluent: THF) and the collected fraction was dried over  $\text{Na}_2\text{SO}_4$ . After removal of solvents, the product was re-precipitated from *n*-hexane/ $\text{CH}_2\text{Cl}_2$  to yield purple crystalline needles (150 mg, 180  $\mu\text{mol}$ ) of **1(Ni)** in 95% yield.  $^1\text{H}$  NMR (600 MHz,  $\text{THF}-d_8$ , 298 K)  $\delta$ : 9.88 (s, 2H, H<sub>1</sub>), 9.14 (d, 4H,  $J = 4.7$  Hz, H<sub>2</sub>), 8.84 (d, 4H,  $J = 4.7$  Hz, H<sub>3</sub>), 8.57 (d, 2H,  $J = 7.2$  Hz, H<sub>4</sub>), 8.07 (d, 2H,  $J = 8.6$  Hz, H<sub>11</sub>), 7.96-7.91 (m, 4H, H<sub>6</sub>, H<sub>7</sub>), 7.83 (dd, 2H,  $J = 7.2$  Hz,  $J = 7.2$  Hz, H<sub>5</sub>), 7.71 (d, 2H,  $J = 8.6$  Hz, H<sub>10</sub>), 7.56 (s, 2H, H<sub>12</sub>), 7.12 (d, 4H,  $J = 8.5$  Hz, H<sub>9</sub>), 6.63 (d, 4H,  $J = 8.5$  Hz, H<sub>8</sub>). HRMS (ESI, positive mode,  $m/z$ ):  $[\text{M}+\text{H}]^+$  calcd. for  $\text{C}_{56}\text{H}_{33}\text{N}_6\text{Ni}$ , 847.2115; found, 847.2114. UV-vis ( $\text{CH}_2\text{Cl}_2$ , (nm)  $\epsilon$  ( $\text{M}^{-1}\cdot\text{cm}^{-1}$ )):  $\lambda_{\text{max}} = 407.5$  (154000), 520 (13400), 553 (6450).

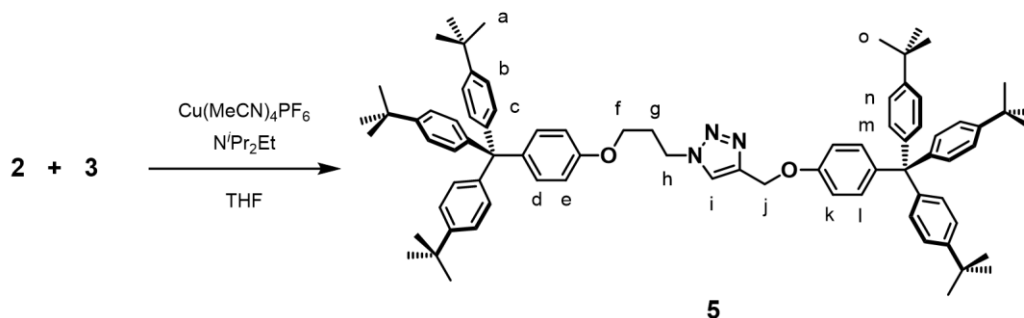
### Synthesis of copper(II) strapped porphyrin (**1(Cu)**)



**Scheme 3-3.** Synthesis of **1(Cu)**.

A solution of strapped porphyrin **1(H<sub>2</sub>)** (34 mg, 63  $\mu$ mol) in  $\text{CHCl}_3$  (8 mL) was added to a solution of copper acetate (34 mg, 190  $\mu$ mol, 3.0 eq) in  $\text{CH}_3\text{OH}$  (8 mL). The solution was warmed to reflux and stirred for 20 h. After cooling down to room temperature, the solution was washed with water and dried over  $\text{Na}_2\text{SO}_4$ . After removal of solvents, **1(Cu)** was obtained as a red solid (45 mg, 53  $\mu$ mol, 84% yield). MS (ESI, positive mode,  $m/z$ ):  $[M+H]^+$  calcd. for  $\text{C}_{56}\text{H}_{33}\text{CuN}_6$ , 852.21; found, 852.20.

### Synthesis of dumbbell molecule (**5**)



**Scheme 3-4.** Synthesis of **5**.

To a solution of  $\text{Cu}(\text{MeCN})_4\text{PF}_6$  (21 mg, 56  $\mu$ mol, 0.96 eq) in THF (5.9 mL) were added the azide **2** (41 mg, 70  $\mu$ mol, 1.2 eq), alkyne **3** (32 mg, 59  $\mu$ mol, 1.0 eq), and diisopropylethylamine (0.10 M in THF, 0.59 mL, 59  $\mu$ mol, 1.0 eq). The reaction solution was stirred at 65  $^\circ\text{C}$  for 3 h under an  $\text{N}_2$  atmosphere. After confirmation of consumption of the alkyne by  $^1\text{H}$  NMR spectroscopy, the reaction solution was diluted with  $\text{CH}_2\text{Cl}_2$  (20 mL), washed with saturated  $\text{EDTA}_{\text{aq}}$  and saturated  $\text{NaCl}_{\text{aq}}$  and dried over  $\text{Na}_2\text{SO}_4$ . After removal of the solvents under reduced pressure, the product was purified by  $\text{SiO}_2$  column chromatography (eluent: *n*-hexane then a gradient from 20 to 50% AcOEt in *n*-hexane) to yield the dumbbell molecule **5** as a white solid (61 mg, 54  $\mu$ mol, 92% yield).  $^1\text{H}$ NMR data were identical to those previously reported for **5**.<sup>12a</sup>

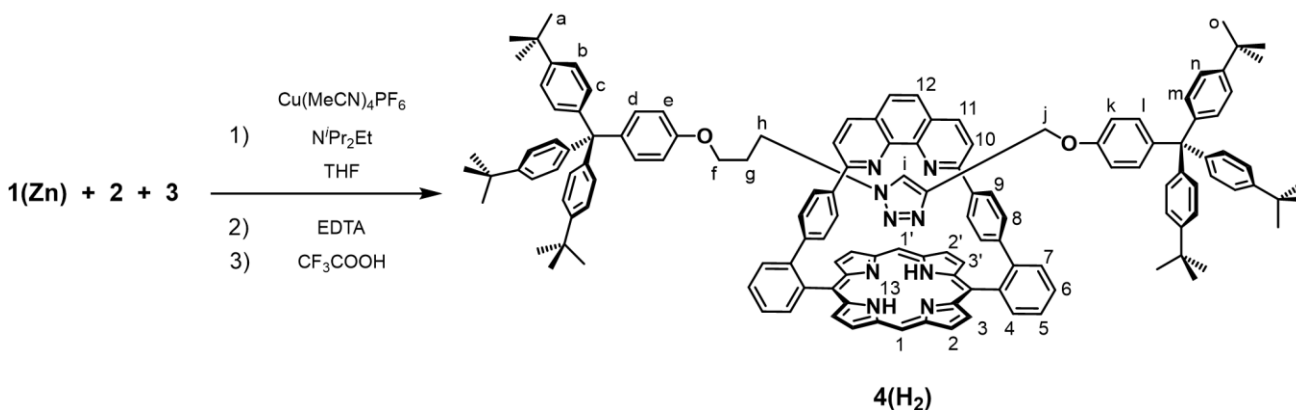
### General procedure for the click reaction with 1(Zn) (general procedure A)

To a solution of Zn(II) strapped porphyrin **1(Zn)** (50 mg, 59  $\mu\text{mol}$ ) in THF (5.9 mL) was added  $\text{Cu}(\text{MeCN})_4\text{PF}_6$  (21 mg, 56  $\mu\text{mol}$ , 0.96 eq) and the solution was stirred at room temperature for 30 min under inert atmosphere. The azide **2** (41 mg, 70  $\mu\text{mol}$ , 1.2 eq), alkyne **3** (32 mg, 59  $\mu\text{mol}$ , 1.0 eq), and base (0.10 M in THF, 0.59 mL, 59  $\mu\text{mol}$ , 1.0 eq) were added and the solution was stirred at 65  $^\circ\text{C}$  for 21 h. After confirmation of consumption of the alkyne by  $^1\text{H}$  NMR spectroscopy, the reaction solution was diluted with  $\text{CH}_2\text{Cl}_2$  (5.0 mL) and washed with saturated  $\text{EDTA}_{\text{aq}}$ . To the organic layer was added trifluoroacetic acid (2.0 mL) and the solution was stirred at room temperature for 1 h. The solution was washed with 1 M  $\text{NaOH}_{\text{aq}}$  and then with saturated  $\text{NaCl}_{\text{aq}}$  and dried over  $\text{Na}_2\text{SO}_4$ . After removal of the solvents under reduced pressure, the product was purified by  $\text{SiO}_2$  column chromatography (eluent:  $\text{CH}_2\text{Cl}_2$  then a gradient from 0.1 to 10% MeOH in  $\text{CH}_2\text{Cl}_2$ ) to yield the freebase rotaxane **4(H<sub>2</sub>)**.

### General procedure for the click reaction with 1(Ni) (general procedure B)

To a solution of Ni(II) strapped porphyrin **1(Ni)** (50 mg, 59  $\mu\text{mol}$ ) in THF (5.9 mL) was added  $\text{Cu}(\text{MeCN})_4\text{PF}_6$  (21 mg, 56  $\mu\text{mol}$ , 0.96 eq) and the solution was stirred at room temperature for 30 min under inert atmosphere. The azide **2** (41 mg, 70  $\mu\text{mol}$ , 1.2 eq), alkyne **3** (32 mg, 59  $\mu\text{mol}$ , 1.0 eq), and base (0.10 M in THF, 0.59 mL, 59  $\mu\text{mol}$ , 1.0 eq) were added and the solution was stirred at 65  $^\circ\text{C}$  for 21 h. After confirmation of consumption of the alkyne by  $^1\text{H}$  NMR spectroscopy, the solution was diluted with  $\text{CH}_2\text{Cl}_2$  (50 mL), washed with saturated  $\text{EDTA}_{\text{aq}}$  and dried over  $\text{Na}_2\text{SO}_4$ . After removal of the solvents under reduced pressure, the crude product was analyzed for the formation of rotaxane by  $^1\text{H}$  NMR spectrometry.

### Synthesis of free base rotaxane (4(H<sub>2</sub>))



Scheme 3-5. Synthesis of **4(H<sub>2</sub>)**.

Following the general procedure A, Zn(II) strapped porphyrin **1(Zn)** (50 mg, 59  $\mu\text{mol}$ ) was reacted with azide **2**, alkyne **3**, and diisopropylethylamine as a base to yield the crude reaction solution. Demetallation with saturated  $\text{EDTA}_{\text{aq}}$  and trifluoroacetic acid and purification by  $\text{SiO}_2$  column chromatography gave the freebase rotaxane **4(H<sub>2</sub>)** as a red solid (56 mg, 29  $\mu\text{mol}$ , 50% yield).  $^1\text{H}$  NMR (600 MHz,  $\text{CD}_2\text{Cl}_2$ , 298 K)  $\delta$ : 9.58 (s, 1H, H<sub>1</sub>), 9.03 (d, 2H,  $J = 4.5$  Hz, H<sub>2</sub>), 8.96 (s, 1H, H<sub>1</sub>), 8.92 (d, 2H,  $J = 4.5$  Hz, H<sub>2</sub>), 8.83 (d, 2H,  $J = 4.5$  Hz, H<sub>3</sub>), 8.73 (d, 2H,  $J = 4.5$  Hz, H<sub>3</sub>), 8.67 (d, 2H,  $J = 7.4$  Hz, H<sub>4</sub>), 7.95 (dd, 2H,  $J = 7.7$  Hz,  $J = 7.7$  Hz, H<sub>6</sub>), 7.90-7.87 (m, 4H, H<sub>5</sub>, H<sub>11</sub>), 7.77 (d, 2H,

$J = 7.7$  Hz,  $H_7$ ), 7.44 (s, 2H,  $H_{12}$ ), 7.40 (d, 6H,  $J = 8.8$  Hz,  $H_b$ ), 7.36 (d, 6H,  $J = 8.8$  Hz,  $H_c$ ), 7.33 (d, 2H,  $J = 8.4$  Hz,  $H_{10}$ ), 7.29 (d, 6H,  $J = 8.8$  Hz,  $H_n$ ), 7.23-7.22 (m, 8H,  $H_m, H_i$ ), 6.99 (d, 4H,  $J = 8.5$  Hz,  $H_9$ ), 6.85 (d, 2H,  $J = 8.8$  Hz,  $H_k$ ), 6.69 (d, 2H,  $J = 8.8$  Hz,  $H_d$ ), 6.59 (d, 4H,  $J = 8.5$  Hz,  $H_8$ ), 4.79 (s, 2H,  $H_j$ ), 4.52 (s, 1H,  $H_i$ ), 4.14 (d, 2H,  $J = 8.8$  Hz,  $H_e$ ), 1.33 (s, 27H,  $H_a$ ), 1.30 (s, 27H,  $H_o$ ), 0.50 (br, 2H,  $H_h$ ), -1.23 (br, 2H,  $H_f$ ), -3.18 (s, 2H,  $H_{13}$ ), -3.97 (br, 2H,  $H_g$ ). HRMS (ESI, positive mode,  $m/z$ ):  $[M+H]^+$  calcd. for  $C_{136}H_{130}N_9O_2$ , 1922.0374; found, 1922.0375. UV-vis ( $CH_2Cl_2$ , (nm)  $\epsilon$  ( $M^{-1}\cdot cm^{-1}$ )):  $\lambda_{max} = 415$  (229000), 507.5 (12900), 540.5 (4200), 578.5 (4750), 634.5 (1180).

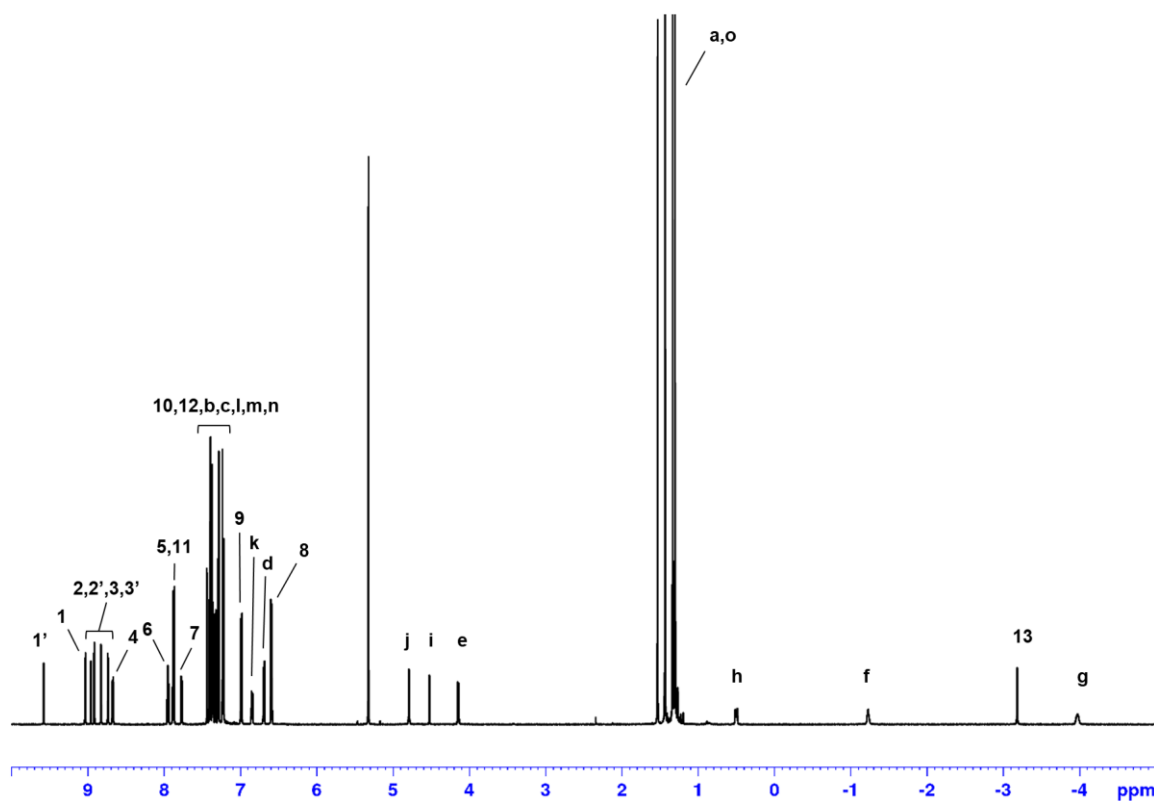
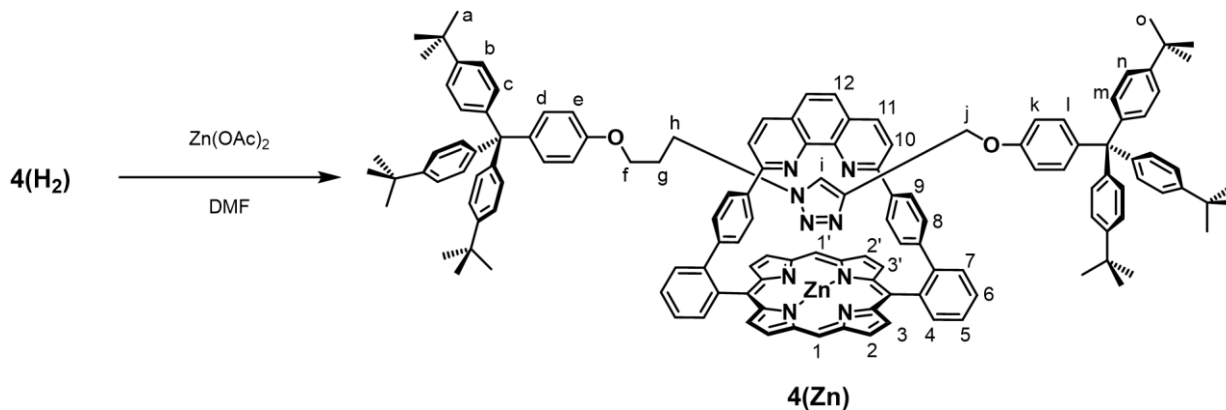


Figure 3-6.  $^1H$  NMR spectrum ( $CD_2Cl_2$ , 600 MHz) of  $4(H_2)$ .

### Synthesis of zinc(II) rotaxane ( $4(Zn)$ )



Scheme 3-6. Synthesis of  $4(Zn)$ .

To a solution of free base rotaxane **4(H<sub>2</sub>)** (8.6 mg, 4.5 μmol) in DMF (1.5 mL) was added Zn(II) acetate dihydrate (9.8 mg, 45 μmol, 10 eq). The solution was refluxed for 16 h under inert atmosphere. After cooling, the solution was poured into water (20 mL). The red precipitate was collected by filtration, and washed with water and methanol. The crude product was purified by SiO<sub>2</sub> column chromatography (eluent: CH<sub>2</sub>Cl<sub>2</sub>) to afford **4(Zn)** as a red solid (6.3 mg, 3.2 μmol, 71% yield). <sup>1</sup>H NMR (600 MHz, CD<sub>2</sub>Cl<sub>2</sub>, 298 K) δ: 9.90 (s, 1H, H<sub>1</sub>), 9.16 (d, 2H, *J* = 4.2 Hz, H<sub>2</sub>), 9.12 (s, 1H, H<sub>i</sub>), 9.03 (s, 1H, H<sub>1'</sub>), 8.84-8.82 (m, 6H, H<sub>2'</sub>, H<sub>3</sub>, H<sub>4</sub>), 8.74 (d, 2H, *J* = 4.2 Hz, H<sub>3'</sub>), 7.99 (d, 2H, *J* = 8.5 Hz, H<sub>11</sub>), 7.85 (dd, 2H, *J* = 7.7 Hz, *J* = 7.7 Hz, H<sub>5</sub>), 7.81 (dd, 2H, *J* = 7.7 Hz, *J* = 7.7 Hz, H<sub>6</sub>), 7.54 (s, 2H, H<sub>12</sub>), 7.48 (d, 2H, *J* = 7.7 Hz, H<sub>7</sub>), 7.42 (d, 2H, *J* = 8.5 Hz, H<sub>10</sub>), 7.34 (d, 6H, *J* = 8.7 Hz, H<sub>n</sub>), 7.31 (d, 6H, *J* = 8.7 Hz, H<sub>m</sub>), 7.19 (d, 6H, *J* = 8.7 Hz, H<sub>b</sub>), 6.99-6.95 (m, 8H, H<sub>c</sub>, H<sub>i</sub>), 6.83 (d, 2H, *J* = 8.8 Hz, H<sub>d</sub>), 6.29-6.26 (m, 8H, H<sub>8</sub>, H<sub>9</sub>), 6.12 (d, 2H, *J* = 8.8 Hz, H<sub>e</sub>), 5.27 (d, 2H, *J* = 8.8 Hz, H<sub>k</sub>), 2.44 (t, 2H, *J* = 5.6 Hz, H<sub>f</sub>), 1.81 (br, 2H, H<sub>h</sub>), 1.34 (s, 27H, H<sub>a</sub>), 1.32 (s, 27H, H<sub>o</sub>), 0.58 (br, 2H, H<sub>j</sub>), 0.45 (br, 2H, H<sub>g</sub>). HRMS (ESI, positive mode, *m/z*): [*M*+H]<sup>+</sup> calcd. for C<sub>136</sub>H<sub>128</sub>N<sub>9</sub>O<sub>2</sub>Zn, 1984.9538; found, 1984.9539. UV-vis (CH<sub>2</sub>Cl<sub>2</sub>, (nm) ε (M<sup>-1</sup>·cm<sup>-1</sup>)): λ<sub>max</sub> = 428.5 (242000), 521 (2610), 559 (11600), 596.5 (2580).

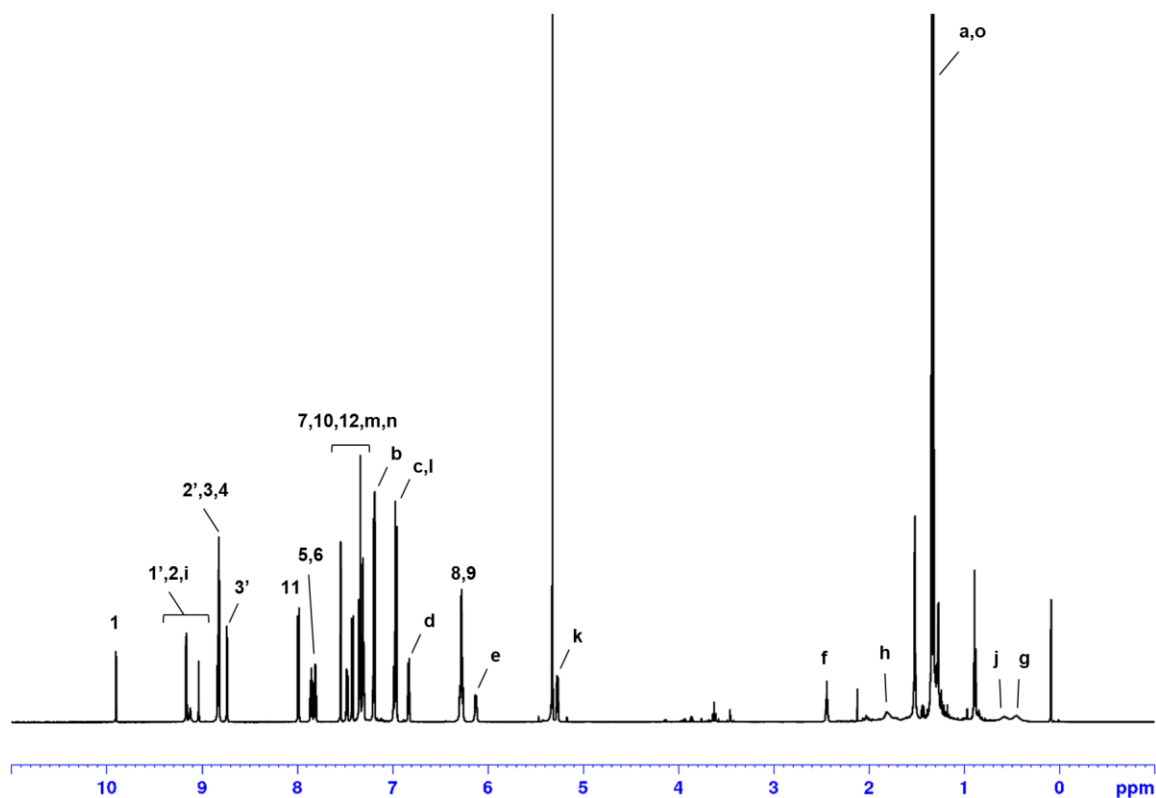
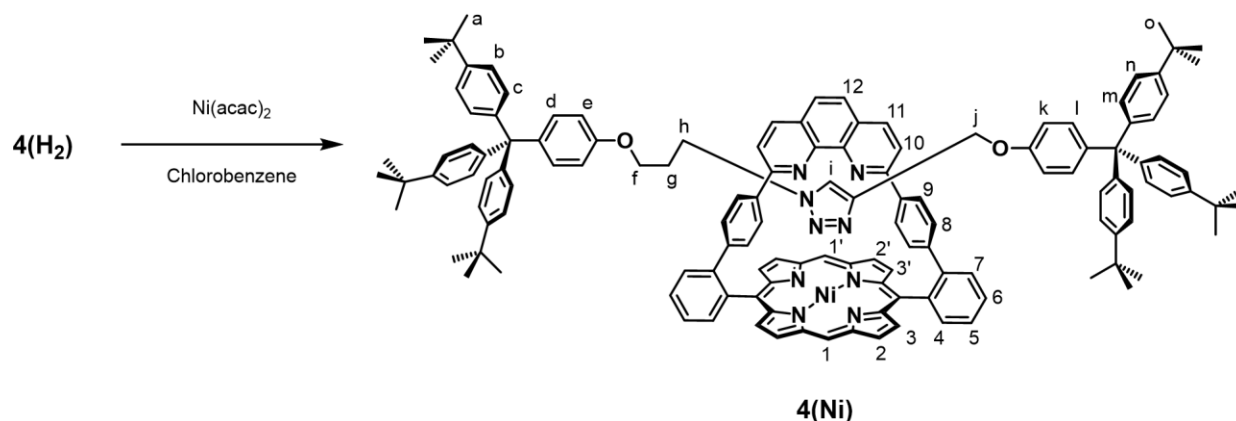


Figure 3-7. <sup>1</sup>H NMR spectrum (CD<sub>2</sub>Cl<sub>2</sub>, 600 MHz) of **4(Zn)**.

### Synthesis of Nickel(II) rotaxane (**4(Ni)**)



Scheme 3-7. Synthesis of **4(Ni)**.

To a solution of freebase rotaxane **4(H<sub>2</sub>)** (8.6 mg, 4.5  $\mu\text{mol}$ ) in chlorobenzene (1.5 mL) was added Ni(II) acetylacetonate (23 mg, 90  $\mu\text{mol}$ , 20 eq). The solution was refluxed for 4 h under air. After cooling, the solution was passed through an  $\text{Al}_2\text{O}_3$  (neutral, grade 1) column (eluent:  $\text{CH}_2\text{Cl}_2$ ) and the collected fraction was dried over  $\text{Na}_2\text{SO}_4$ . The crude product was purified by  $\text{SiO}_2$  column chromatography (eluent:  $\text{CH}_2\text{Cl}_2$  then a gradient from 0.1 to 10% MeOH in  $\text{CH}_2\text{Cl}_2$ ). After removal of solvents, the product was re-precipitated from *n*-hexane/ $\text{CH}_2\text{Cl}_2$  to yield **4(Ni)** as a red solid (6.3 mg, 3.2  $\mu\text{mol}$ , 71% yield).  $^1\text{H}$  NMR (600 MHz,  $\text{CD}_2\text{Cl}_2$ , 298 K)  $\delta$ : 9.31-8.98 (m, 9H,  $\text{H}_{1/1'}$ ,  $\text{H}_2$ ,  $\text{H}_2'$ ,  $\text{H}_3$ ,  $\text{H}_3'$ ), 8.66 (s, 1H,  $\text{H}_{1/1'}$ ), 8.47 (d, 2H,  $J = 7.7$  Hz,  $\text{H}_4$ ), 7.92 (d, 2H,  $J = 8.5$  Hz,  $\text{H}_{11}$ ), 7.89 (dd, 2H,  $J = 7.7$  Hz,  $J = 7.7$  Hz,  $\text{H}_6$ ), 7.81 (dd, 2H,  $J = 7.7$  Hz,  $J = 7.7$  Hz,  $\text{H}_5$ ), 7.74 (d, 2H,  $J = 7.7$  Hz,  $\text{H}_7$ ), 7.46 (s, 2H,  $\text{H}_{12}$ ), 7.42 (d, 2H,  $J = 8.5$  Hz,  $\text{H}_{10}$ ), 7.37 (d, 6H,  $J = 8.8$  Hz,  $\text{H}_n$ ), 7.30-7.27 (m, 12H,  $\text{H}_b$ ,  $\text{H}_c$ ), 7.22 (d, 6H,  $J = 8.8$  Hz,  $\text{H}_m$ ), 7.16 (d, 2H,  $J = 8.5$  Hz,  $\text{H}_i$ ), 7.07 (d, 4H,  $J = 7.9$  Hz,  $\text{H}_8$ ), 6.68 (d, 4H,  $J = 7.9$  Hz,  $\text{H}_9$ ), 6.60 (br, 2H,  $\text{H}_k$ ), 6.42 (d, 2H,  $J = 8.6$  Hz,  $\text{H}_d$ ), 5.57 (s, 1H,  $\text{H}_j$ ), 4.48 (s, 2H,  $\text{H}_j$ ), 3.81 (br, 2H,  $\text{H}_e$ ), 1.33 (s, 27H,  $\text{H}_a$ ), 1.30 (s, 27H,  $\text{H}_o$ ), 1.17 (br, 2H,  $\text{H}_h$ ), 0.50 (br, 2H,  $\text{H}_f$ ), -2.05 (br, 2H,  $\text{H}_g$ ). HRMS (ESI, positive mode,  $m/z$ ):  $[M+H]^+$  calcd. for  $\text{C}_{136}\text{H}_{128}\text{N}_9\text{O}_2\text{Ni}$ , 1978.9599; found, 1978.9588. UV-vis ( $\text{CH}_2\text{Cl}_2$ , (nm)  $\epsilon$  ( $\text{M}^{-1}\cdot\text{cm}^{-1}$ )):  $\lambda_{\text{max}} = 409.5$  (192000), 522 (16000), 555 (8320).

Note: The absolute assignment of some protons of **4(Ni)** was not possible due to broadened peaks. Therefore indicative "either/or" assignments (e.g.  $\text{H}_{1/1'}$  for  $\text{H}_1$  or  $\text{H}_{1'}$ ) were provided.

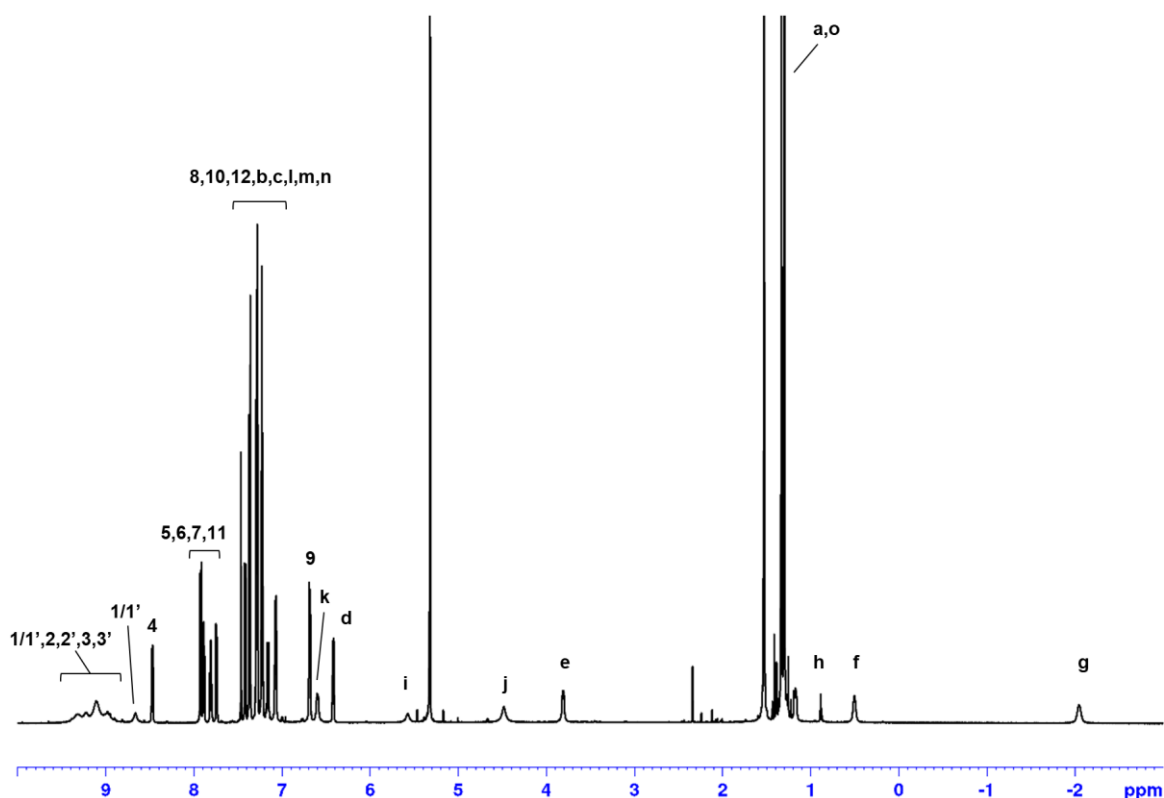


Figure 3-8.  $^1\text{H}$  NMR spectrum ( $\text{CD}_2\text{Cl}_2$ , 600 MHz) of **4(Ni)**.

### X-ray crystal structural analysis

**1(Ni)**: Crystals of **1(Ni)** suitable for x-ray crystallography were grown by vapor diffusion of *n*-hexane into a saturated  $\text{CH}_2\text{Cl}_2$  solution containing small amount of methanol. The crystals were mounted on the CryoLoop (Hampton Research Corp.) with a light mineral oil and placed in a nitrogen stream at 160(1) K. All measurements were carried out on a Rigaku XtaLAB P200 diffractometer, which is equipped with a rotating anode X-ray source (Mo  $K\alpha$  radiation) and a hybrid photon counting detector (PILATUS 200K).

**4(H<sub>2</sub>)**: Crystals of **4(H<sub>2</sub>)** suitable for x-ray crystallography were grown by vapor diffusion of acetonitrile into a saturated dichloroethane/acetonitrile ( $v/v = 1:1$ ) solution. X-ray diffraction data were collected at Rigaku Corp. (Akishima, Japan). The crystals were mounted on the MicroMount (MiTeGen Corp.) with the Fomblin<sup>®</sup> Y (Sigma-Aldrich Corp.) and placed in a nitrogen stream at 100(1) K. All measurements were carried out on a Rigaku XtaLAB Synergy-S diffractometer, which is equipped with a microfocus sealed-tube source (Cu- $K\alpha$  radiation) and a hybrid photon counting detector (HyPix-6000HE).

**4(Ni)**: Crystals of **4(Ni)** suitable for x-ray crystallography were grown by vapor diffusion of acetonitrile into a saturated  $\text{CH}_2\text{Cl}_2$  solution. The crystals were mounted on the MicroMount (MiTeGen Corp.) with the Fomblin<sup>®</sup> Y (Sigma-Aldrich Corp.) and placed in a nitrogen stream at 100(1) K. All measurements were carried out on a Rigaku

XtaLAB P200 diffractometer, which is equipped with a rotating anode X-ray source (Mo  $K\alpha$  radiation) and a hybrid photon counting detector (PILATUS 200K).

The cell refinements were performed with a software CrystalClear and CrysAlis<sup>Pro</sup> <sup>29</sup> software package (Data Collection and Processing Software Package, Rigaku Corp.). All of the crystallographic calculations were performed using the CrystalStructure software package (Crystal Structure Analysis Software Package, Version 4.1, 4.2.4 and 5.0rc2, Rigaku Corp.). The structures were solved by direct method (SIR92, SHELXT Version 2014/5).<sup>30</sup> Non-hydrogen atoms were refined anisotropically by full-matrix least-squares on  $F^2$  using SHELXL2013 and SHELXL Version 2014/7.<sup>31</sup> Refined models of **4(H<sub>2</sub>)** and **4(Ni)** in which the solvent contribution was removed using SQUEEZE <sup>32</sup> procedure of PLATON.<sup>33</sup> The structure in the final stage of refinement showed no movement in the atom position. Hydrogen atoms were attached at idealized positions on carbon atoms and not refined. Crystal data and structural refinement parameters were listed below (Table 3-2). The CCDC numbers for strapped porphyrin and rotaxanes are 1526878 (**1(Ni)**), 1532039 (**4(H<sub>2</sub>)**), and 1532040 (**4(Ni)**), respectively. This data can be obtained from The Cambridge Crystallographic Data Centre via [www.ccdc.cam.ac.uk/data\\_request/cif](http://www.ccdc.cam.ac.uk/data_request/cif).

**Table 3-2.** Crystal data and data collection parameters

Compounds	<b>1(Ni)</b>	<b>4(H<sub>2</sub>)</b>	<b>4(Ni)</b>
CCDC Number	1526878	1532039	1532040
Empirical formula	C <sub>58</sub> H <sub>36</sub> Cl <sub>4</sub> N <sub>6</sub> Ni	C <sub>138.33</sub> H <sub>132.98</sub> Cl <sub>0.95</sub> N <sub>9.69</sub> O <sub>4.41</sub>	C <sub>138</sub> H <sub>130</sub> N <sub>10</sub> NiO <sub>2</sub>
Formula weight	1017.47	2035.49	2019.31
Temperature (K)	113(1)	100(1)	100(1)
Wavelength (Å)	0.71075	1.54184	0.71073
Crystal system	Triclinic	Triclinic	Triclinic
Space group	P-1 (#2)	P-1 (#2)	P-1 (#2)
a (Å)	9.7748(5)	15.6262(2)	15.8666(5)
b (Å)	15.0932(8)	16.5446(2)	19.9870(6)
c (Å)	17.4610(8)	25.6864(2)	21.0229(6)
α (deg.)	96.0310(7)	85.7596(9)	89.677(3)
β (deg.)	106.6480(7)	89.8608(9)	75.072(3)
γ (deg.)	109.7107(6)	77.9221(11)	84.870(2)
Volume (Å <sup>3</sup> )	2264.6458(3)	6475.33(13)	6415.0(3)
Z	2	2	2
Density (calculated) (g/cm <sup>3</sup> )	1.492	1.044	1.045
μ[Mo-Kα], (/cm)	7.141	6.635	2.026
Crystal size (mm)	0.270 x 0.190 x 0.080	0.450 x 0.310 x 0.020	0.230 x 0.160 x 0.030
Theta range for data collection	3.018-27.508	2.739-68.253	1.712-25.351
No. of reflections measured	37264	75408	104820
Unique data ( <i>R</i> <sub>int</sub> )	9863 (0.0209)	23709 (0.0386)	23410 (0.1095)
Data/restraints/parameters	9863/0/622	23709/3072/1581	23410/2538/1438
<i>R</i> 1 <sup>a</sup> ( <i>I</i> >2.0σ( <i>I</i> ))	0.0317	0.0770	0.0752
<i>wR</i> 2 <sup>b</sup> ( <i>I</i> >2.0σ( <i>I</i> ))	0.0891	0.2208	0.1778
<i>R</i> 1 <sup>a</sup> (all data)	0.0366	0.0853	0.1671
<i>wR</i> 2 <sup>b</sup> (all data)	0.0911	0.2296	0.2149
GOF on <i>F</i> <sup>2</sup>	1.081	1.036	0.957
Δρ, e/Å <sup>3</sup>	0.81, -0.63	1.28, -0.70	0.79, -0.34

[a]  $R1 = (\sum ||F_o| - |F_c||) / (\sum |F_o|)$ , [b]  $wR2 = [\{\sum w(F_o^2 - F_c^2)^2\} / \{\sum w(F_o^4)\}]^{1/2}$

## Reference and notes

1. R. Huisgen, *Angew. Chem.* **1963**, *75*, 604–637.
2. K. D. Hänni, D. A. Leigh, *Chem. Soc. Rev.* **2010**, *39*, 1240–1251.
3. C. Wang, D. Ikhlef, S. Kahlal, J.-Y. Saillard, D. Astruc, *Coord. Chem. Rev.* **2016**, *316*, 1–20.
4. P. G. Clark, E. N. Guidry, W. Y. Chan, W. E. Steinmetz, R. H. Grubbs, *J. Am. Chem. Soc.* **2010**, *132*, 3405–3412.
5. A. Tăbăcaru, B. Furdui, I. O. Ghinea, G. Cârâc, R. M. Dinică, *Inorg. Chim. Acta* **2017**, *455*, 329–349.
6. H. C. Kolb, M. G. Finn, K. B. Sharpless, *Angew. Chem. Int. Ed.* **2001**, *40*, 2004–2021.
7. B. Schulze, U. S. Schubert, *Chem. Soc. Rev.* **2014**, *43*, 2522–2571.
8. K. Ladomenou, V. Nikolaou, G. Charalambidis, A. G. Coutsolelos, *Coord. Chem. Rev.* **2016**, *306*, 1–42.
9. V. O. Rodionov, S. I. Presolski, D. D. Diaz, V. V. Fokin, M. G. Finn, *J. Am. Chem. Soc.* **2007**, *129*, 12705–12712 and references therein.
10. B. T. Worrell, J. A. Malik, V. V. Fokin, *Science* **2013**, *340*, 457–460.
11. L. Jin, D. R. Tolentino, M. Melaimi, G. Bertrand, *Sci. Adv.* **2015**, *1*, e1500304.
12. (a) V. Aucagne, K. D. Hänni, D. A. Leigh, P. J. Lusby, D. B. Walker, *J. Am. Chem. Soc.* **2006**, *128*, 2186–2187. (b) V. Aucagne, J. Berná, J. D. Crowley, S. M. Goldup, K. D. Hänni, D. A. Leigh, P. J. Lusby, V. E. Ronaldson, A. M. Z. Slawin, A. Viterisi, D. B. Walker, *J. Am. Chem. Soc.* **2007**, *129*, 11950–11963. (c) E. A. Neal, S. M. Goldup, *Angew. Chem. Int. Ed.* **2016**, *55*, 12488–12493.
13. J. D. Crowley, S. M. Goldup, N. D. Gowans, D. A. Leigh, V. E. Ronaldson, A. M. Z. Slawin, *J. Am. Chem. Soc.* **2010**, *132*, 6243–6248.
14. (a) E. A. Neal, S. M. Goldup, *Chem. Sci.* **2015**, *6*, 2398–2404. (b) J. Winn, A. Pinczewska, S. M. Goldup, *J. Am. Chem. Soc.* **2013**, *135*, 13318–13321. (c) A. Tron, P. J. Thornton, B. Kauffmann, J. H. R. Tucker, N. D. McClenaghan, *Supramol. Chem.* **2016**, *28*, 733–741. (d) A. Noor, S. C. Moratti, J. D. Crowley, *Chem. Sci.* **2014**, *5*, 4283–4290. (e) H. Lahlali, K. Jobe, M. Watkinson, S. M. Goldup, *Angew. Chem. Int. Ed.* **2011**, *50*, 4151–4155.
15. J. E. M. Lewis, J. Winn, L. Cera, S. M. Goldup, *J. Am. Chem. Soc.* **2016**, *138*, 16329–16336.
16. C. Kahlfuss, J. A. Wytko, J. Weiss, *ChemPlusChem* **2017**, *82*, 584–594.
17. A. Giraudeau, J. P. Gisselbrecht, M. Gross, J. Weiss, *J. Chem. Soc., Chem. Commun.* **1993**, 1103–1105.
18. F. Melin, C. Boudon, M. Lo, K. J. Schenk, M. Bonin, P. Ochsenbein, M. Gross, J. Weiss, *J. Porph. Phthalocyanines* **2007**, *11*, 212–221.
19. J. Froidevaux, P. Ochsenbein, M. Bonin, K. Schenk, P. Maltese, J.-P. Gisselbrecht, J. Weiss, *J. Am. Chem. Soc.* **1997**, *119*, 12362–12363.
20. H. Zheng, W. Zhou, J. Lv, X. Yin, Y. Li, H. Liu, Y. Li, *Chem. Eur. J.* **2009**, *15*, 13253–13262.
21. H. W. Gibson, S.-H. Lee, P. T. Engen, P. Lecavalier, J. Sze, Y. X. Shen, M. Bheda, *J. Org. Chem.* **1993**, *58*, 3748–3756.
22. (a) M. A. Morozova, M. S. Yusubov, B. Kratochvil, V. Eigner, A. A. Bondarev, A. Yoshimura, A. Saito, V. V. Zhdankin, M. E. Trusovad, P. S. Postnikov, *Org. Chem. Front.* **2017**, DOI: 10.1039/c6qo00787b. (b) C. D. Smith, M. F. Greaney, *Org. Lett.* **2013**, *15*, 4826–4829.
23. For the quantification of Cu-pyridine interaction ( $\Delta G \sim 0$ ) see: J. Cremers, S. Richert, D. V. Kondratuk, T. D. W.

- Claridge, C. R. Timmel, H. L. Anderson, *Chem. Sci.* **2016**, *7*, 6961–6968; for axial oxygenated ligands on Cu(II) porphyrins see for example: F. R. Kooriyaden, S. Sujatha, C. Arunkumar, *Polyhedron* **2015**, *97*, 66–74.
24. J.-P. Sauvage, *Acc. Chem. Res.* **1990**, *23*, 319–327.
  25. D. Paul, F. Melin, C. Hirtz, J. Wytko, P. Ochsenbein, M. Bonin, K. Schenk, P. Maltese, J. Weiss, *Inorg. Chem.* **2003**, *42*, 3779–3787.
  26. C. Maeda, S. Yamaguchi, C. Ikeda, H. Shinokubo, A. Osuka, *Org. Lett.* **2008**, *10*, 549–552.
  27. J. Wytko, E. Graf, J. Weiss, *J. Org. Chem.* **1992**, *57*, 1015–1018.
  28. P. Ochsenbein, M. Bonin, K. Schenk, J. Froidevaux, J. Wytko, E. Graf, J. Weiss, *Eur. J. Inorg. Chem.* **1999**, *7*, 1175–1180.
  29. Rigaku Oxford Diffraction (2015), CrysAlisPro, Rigaku Corporation, Tokyo, Japan.
  30. (a) A. Altomare, G. Cascarano, C. Giacovazzo, A. Guagliardi, *J. Appl. Cryst.* **1993**, *26*, 343–350. (b) G. M. Sheldrick, *Acta Cryst.* **2014**, *A70*, C1437.
  31. (a) G. M. Sheldrick, *Acta Cryst.* **2008**, *A64*, 112–122. (b) G. M. Sheldrick, *Acta Cryst.* **2015**, *C71*, 3–8.
  32. A. L. Spek, *Acta Cryst.* **2015**, *C71*, 9–18.
  33. A. L. Spek, *Acta Cryst.* **2009**, *D65*, 148–155.

## Conclusion

In natural systems in which metalloproteins regulate functions of metalloporphyrinoid cofactors, protein matrices provide axial ligands and specific secondary coordination spheres as “reaction scaffolds” to active centers. In this context, the author constructed reaction scaffolds to metal porphyrinoids by biological and synthetic approaches to regulate and expand their functions.

In Chapter 1, myoglobin (Mb) reconstituted with nickel(I) tetrahydrocorrin ( $\text{Ni}^{\text{I}}(\text{TDHC})$ ) was investigated as a protein-based functional model of methyl-coenzyme M reductase, MCR. Nickel(II) tetrahydrocorrin ( $\text{Ni}^{\text{II}}(\text{TDHC})$ ), which has a monoanionic tetrapyrrole ligand, was synthesized as a model complex of F430. In contrast to previously reported model complexes and F430 requiring strong reductants such as Ti(III) citrate and NaHg,  $\text{Ni}^{\text{II}}(\text{TDHC})$  was successfully reduced by dithionite, a mild reductant, because of the relatively positive redox potential for the  $\text{Ni}^{\text{II}}/\text{Ni}^{\text{I}}$  process. Insertion of  $\text{Ni}^{\text{I}}(\text{TDHC})$  into apoMb provided reconstituted Mb which catalyzes methane generation from methyl iodide, an external methyl donor, meanwhile the bare  $\text{Ni}^{\text{I}}(\text{TDHC})$  complex does not show this activity. The protein matrix conferring the histidine ligation and the hydrophobic environment as a specific reaction scaffold appears to play an important role in shifting the redox potential, resulting in increase of the reactivity of the Ni(I) species to promote methane generation.

In Chapter 2, methane generation *via* intraprotein C–S bond cleavage using cytochrome  $b_{562}$  (Cyt  $b_{562}$ ) reconstituted with nickel(II) didehydrocorrin ( $\text{Ni}^{\text{II}}(\text{DDHC})$ ) was demonstrated.  $\text{Ni}^{\text{II}}(\text{DDHC})$ , which has a reduced tetrapyrrole framework, was synthesized as a model complex of F430 and found to provide a highly reactive Ni(I) species because of the negative redox potential of the  $\text{Ni}^{\text{II}}/\text{Ni}^{\text{I}}$  couple. Photoirradiation of reconstituted Cyt  $b_{562}$  transiently reduced the nickel center *in situ* in the presence of a photosensitizer and a sacrificial reagent, followed by activation of the  $\text{H}_3\text{C}-\text{S}$  group of the methionine by the Ni(I) species to generate methane gas. The proximity effect appears to promote the reaction between the cofactor and the closely located amino acid residue as expected from the hexa-coordinated native heme in the protein matrix. Further experiment using a Cyt  $b_{562}$  mutant, which contains a cysteine residue mimicking the native another substrate close to the reaction center, indicated enhanced methane generation activity, suggesting the importance of precise and close arrangements of the active center and substrates in the protein matrix for the MCR-catalyzing reaction.

In Chapter 3, synthesis of rotaxane was developed using a metal complex of strapped porphyrin as a reaction platform to perform molecular recognition and mechanical bond formation based on the active metal template method. The phenanthroline-strapped porphyrin, which functions as a ditopic ligand to form a bimetallic complex, recognized alkyne and azide units *via* a Cu(I) ion in the phenanthroline moiety and a coordinatively unsaturated metal ion, especially a Zn(II) ion, in the porphyrin moiety, respectively. The following copper-catalyzed azide–alkyne cycloaddition provided a porphyrin-based rotaxane structure. This result suggests the assistance of a second metal ion in the porphyrin moiety for templating azide unit and following reaction because the phenanthroline ligand does not support rotaxane synthesis in the original active template method using single metal ion according to the previous report. Further structural investigation on the obtained rotaxane with metalation of the porphyrin moiety showed the possibility of structural control depending on metal ions. This approach based on the bimetallic system opens the way to prepare interlocked molecules including rotaxanes that cannot be obtained by the original active

metal template method.

In conclusion, the author demonstrated significant expansion of physicochemical properties and reactivities of metal porphyrinoids by construction of appropriate reaction scaffolds around metal porphyrinoids as seen in native metalloproteins. The present findings in this thesis will facilitate the investigation of various physiological functions of natural systems in biochemistry as well as the construction of highly complexed architectures in supramolecular chemistry. Furthermore, the author believes that fusion of wide-range insights of porphyrinoids leads useful molecular systems to realize sustainable development of the world.

### **List of Publication**

1. Myoglobin Reconstituted with Ni Tetrahydrocorrin as a Methane-Generating Model of Methyl-coenzyme M Reductase  
Koji Oohora, Yuta Miyazaki and Takashi Hayashi  
*Angew. Chem. Int. Ed.* **2019**, *58*, 13813–13817.  
DOI: 10.1002/anie.201907584
2. Methane generation via intraprotein C–S bond cleavage in cytochrome *b*<sub>562</sub> reconstituted with nickel didehydrocorrin  
Yuta Miyazaki, Koji Oohora and Takashi Hayashi  
*J. Organomet. Chem.* **2019**, *901*, 120945.  
DOI: 10.1016/j.jorganchem.2019.120945
3. CuAAC in a Distal Pocket: Metal Active-Template Synthesis of Strapped-Porphyrin [2]Rotaxanes  
Yuta Miyazaki, Christophe Kahlfuss, Ayumu Ogawa, Takashi Matsumoto, Jennifer A. Wytko, Koji Oohora, Takashi Hayashi and Jean Weiss  
*Chem. Eur. J.* **2017**, *23*, 13579–13582. (selected as a front cover)  
DOI:10.1002/chem.201702553

### **Supplementary Publication**

1. Reactivity of Myoglobin Reconstituted with Ni Tetrahydrocorrin for Model Substrates of a Methane-producing Enzyme  
Yuta Miyazaki, Koji Oohora and Takashi Hayashi  
*in preparation.*

## Acknowledgements

The study presented in this thesis has been carried out at Department of Applied Chemistry, Graduate School of Engineering, Osaka University from April 2014 to March 2020 and at institute de Chimie, UMR 7177 CNRS-Université de Strasbourg from April 2016 to July 2016. The author would like to express his best gratitude to the supervisor, Professor Takashi Hayashi, for his continuous guidance, constant discussions, and warm encouragement throughout this research. The author would like to deeply thank Assistant Professor Koji Oohora for his kind and continuous guidance and valuable discussions. The author would like to deeply thank Associate Professor Akira Onoda for his helpful and insightful suggestion. The author also acknowledges Professors Hiroshi Uyama and Susumu Kuwabata for reviewing this thesis and their valuable suggestions.

The author is very grateful to Dr. Jean Weiss and Dr. Jennifer A. Wytoko at institute de Chimie, UMR 7177 CNRS-Université de Strasbourg for their kind guidance and the warm welcome during my stay in Strasbourg. The author would like to thank all the Weiss group members for all the help in the laboratory and meaningful discussion as well as introducing all the awesome places and foods, especially wine and cheese. The author believes that the collaboration work in Chapter 3 shows the great friendship between Hayashi group and Weiss group.

Acknowledgements are also made to Professor Kazushi Mashima and Assistant Professor Haruki Nagae at Department of Applied Chemistry, Graduate School of Engineering, Osaka University for their technical support and valuable discussions on X-ray crystal structural analysis in Chapters 1 and 3. The author would like to express his gratitude to Dr. Takashi Matsumoto at Application Laboratories Rigaku Corporation for his technical support and guidance on X-ray crystal structural analysis in Chapter 3. The author would like to thank Dr. Kyoko Inoue at Analytical Instrument Facility, Osaka University for her kind support and insightful comments for NMR measurements.

The author would like to express his gratitude to Ms. Kiyomi Lee for her kind help in laboratory life, and Dr. Yoshitsugu Morita for fundamental guidance of all laboratory work and showing eager attitude for research, and all members at Hayashi group, especially Nozomu Inoue and Shota Hirayama, for their discussions, encouragements and friendship.

The author expresses his great gratitude to his family, Shinji, Emiko, and Ayumi for their heartfelt assistance and encouragements.

Finally, the author is grateful for financial supports by JSPS Research Fellowship for Young Scientists and Incoming International Master program of IdEx of the Université de Strasbourg.

Yuta Miyazaki

January 2020